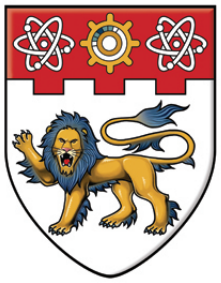

NANYANG TECHNOLOGICAL UNIVERSITY

THE PINCH-OFF PROCESS OF THE LEADING VORTEX RING IN A STARTING CIRCULAR JET

GAO LEI

SCHOOL OF MECHANICAL & AEROSPACE ENGINEERING

2011

THE PINCH-OFF PROCESS OF THE LEADING VORTEX RING IN A STARTING CIRCULAR JET

GAO LEI

School of Mechanical & Aerospace Engineering

A thesis submitted to the Nanyang Technological University
in partial fulfillment of the requirement for the degree of
Doctor of Philosophy

2011

Acknowledgements

First and foremost, I wish to express my sincere gratitude to my supervisor, Assoc. Professor Yu Ching Man, Simon. His constant guidance and advice are essential for carrying on this study. It is under his tutelage that I have gained the academic perspective and the confidence to solve problems confronted. His warm personality has also won my highest respect.

Special thanks to my senior, Dr. Ai Jiao Jian, for his experimental results, from which the Chapter 4 has been derived, as well as his suggestion on data analysis. I would like to thank Mr. Eric Yap in Fluid Mechanics Lab and Mr. Yuan Kee Hock in Thermal & Fluid Research Lab, whose help in designing and constructing the experimental rig is appreciated. My junior, Mr. Lim Yau Shiang, also deserves recognition for his assistance in conducting the experiments.

Last but not least, I owe my deepest gratitude and love to my parents for their dedication and the many years of support in my life.

Contents

Abstract

The pinch-off of the leading vortex ring at a critical time scale, defined as the formation number (Gharib et al., 1998), has been identified as an important phenomenon for vortex ring formation in a starting jet. Previous researchers have also demonstrated the effect of non-impulsive velocity program on delaying the onset of pinch-off process and generating thicker vortex ring. Thus, experiments in present study focus on starting jets with different velocity programs and Reynolds numbers (Re = 2600, 4100, 5600) so as to determine the detailed characteristics of the pinch-off process. Digital Particle Image Velocimetry (DPIV) has been used to measure the velocity field, from which vorticity, circulation, impulse, kinetic energy and vortex ring trajectories can be derived. Based on the prediction on the dynamic fluxes fed into the leading vortex ring, an analytical model for the pinch-off process is subsequently developed.

The properties of the leading vortex ring in a gravity-driven starting circular jet with converging nozzle are first analyzed based on the experimental results of Ai (2006), as a comparison to those generated by the piston-cylinder arrangement. It is proven that the properties of the pinched-off vortex ring in a gravity-driven jet are consistent with those for the piston-cylinder arrangement. The dimensionless circulation γ and energy α are found to be around 1.85 and 0.33 respectively. The result suggests that the leading vortex rings in the gravity-driven starting circular jet can also be approximated as the Norbury-Fraenkel family of vortex rings, which is of great importance in modelling the

pinch-off process.

The results from the present experiments show that the secondary vortices are formed in the trailing shear layer only after the formation number, $F = 4.2 \sim 4.6$, is achieved. Subsequently, the formation of trailing vortices leads to a rapid decrease in the vorticity and momentum fluxes being fed into the leading vortex ring. When the vorticity flux vanish, the leading vortex ring physically separates from the trailing jet, indicating the completion of the pinch-off process. Therefore, it suggests that the roll-up and further development of the trailing vortices due to the Kelvin-Helmholtz instability constrain the growth of leading vortex ring with larger circulation. The development of trailing jet instability is found to be associated with the velocity induced by the leading vortex ring. According to the instability analysis for axisymmetric shear flow, the thicker shear layer, which results from the negative radial velocity gradient $\partial v/\partial r$ induced by the leading vortex ring, is less unstable than the shear layer without any external influence. A dimensionless parameter 'A', defined as $\Gamma_{ring}/(x_{core}\Delta U)$, is subsequently proposed to characterize the effect of the leading vortex ring on the instability of the shear layer near the nozzle exit. Experimental results reveal that A decreases as formation time progresses, and a critical value $A_c = 1.0 \sim 1.2$ indicates the initiation of trailing vortex development and the onset of pinch-off process.

Finally, an analytical model is proposed for the vortex ring formation and pinch-off process in a starting jet by considering the fluxes of dynamic quantities fed into the leading vortex ring. The model distinguishes the leading vortex ring from its trailing jet so as to consider the details of the dynamics of the leading vortex ring during the pinch-off process. A two-stage process is identified before the complete separation of the leading vortex ring from its trailing jet. The first stage involves the growth of the leading vortex ring by absorbing all the ejected fluid from the nozzle until certain size is achieved. The second stage

is characterized by the appreciable translational velocity of the leading vortex ring followed by a trailing jet. The leading vortex ring is approximated as a member of the Norbury-Fraenkel vortex rings with growing dimensionless core radius ϵ, such that dimensionless energy α, as well as its translational velocity can be estimated. The pinch-off process is signified by two time scales, i.e., the formation number, which indicates the onset of the pinch-off process, and the separation time, which corresponds to the time when the leading vortex ring becomes physically separated from the trailing jet and is therefore referred to as the end of pinch-off process. The prediction of the formation number and the characteristics of the vortex ring are found to be in good agreement with previous experimental results on starting jets.

List of Tables

List of Figures

List of Symbols

A	$= \Gamma_{ring}/x_{core}\Delta U$, Dimensionless parameter for the trailing jet instability; Cross-section area at the jet exit plane
A_c	Critical value of A corresponding to the onset of pinch-off
C	Constant in the formula of jet tip penetration
C_e	Constant in the formula of random errors in DPIV
d_a	Actual displacement of the seeding particle
d_i	$i = 1, 2, 3, \ldots, n$, Estimated displacement of the seeding particles
d_m	Spatial mean of d_i
d_p	Effective particle image diameter
D	Nozzle or orifice diameter
D_b	Diameter of the vortex ring bubble, i.e., the radial extent of the vortex ring
D_p	Piston diameter
D_{ring}	Vortex ring diameter
e_{mean}	Mean bias errors
e_{rms}	Random errors
e_{total}	$= e_{mean} + e_{rms}$, Total uncertainty in velocity measurement
e_ω	Uncertainty in vorticity measurement
E	Kinetic energy
E_{total}	Total kinetic energy added to the flow by the apparatus
F	Formation number
I	Impulse

k	Ratio between the highest peak and the second highest peak in the cross-correlation plane for validating DPIV measurement
L	Stroke length of a starting jet, as a function of time t
$L_{\max}$	Maximum stroke length of a starting jet
L_p	Piston stroke length corresponding to L
M	Momentum of the fluid
n	Azimuthal wavenumber of the disturbance in instability analysis
P	$= \overline{U_0^2}/\bar{U_0}^2$, Velocity program factor
Q_0	Volumetric flow rate
r	Radial distance from the jet centerline axis; $\lvert\mathbf{r}\rvert$
$\mathbf{r}$	$= \mathbf{x} - \mathbf{x}'$, Displacement vector
R_{core}	Radius of the vortex ring core
R_r	Radius of the vortex ring
R_{tj}	Radius of the trailing jet stem near the leading vortex ring
R_v	U_∞/U_0, Ratio of the background flow velocity to the jet velocity
Re_D	$= U_0 D/\nu$ or $= U_{\max} D/\nu$, Reynolds number based on D
Re_Γ	$= \Gamma/\nu$, Reynolds number based on circulation
t	Physical time
t^*	Dimensionless formation time
T	Duration of the starting jet
$U(r)$	Velocity profile of the basic shear flow in instability analysis
$U_0(t)$	Spatially averaged jet velocity (x-component) at the exit plane
U_{co}	Velocity of the uniform background co-flow
U_{ct}	Velocity of the uniform background counter-flow
$U_{\max}$	Maximum piston velocity during jet ejection
U_p	Piston velocity
U_{tj}	Velocity of the trailing jet near the leading vortex ring

U_{tr}	Translational velocity of the vortex ring
U_∞	Velocity of the ambient fluid
ΔU	$= U_0 - U_\infty$, Strength of the shear layer
u, v, w	Velocity components in the axial, radial, and azimuthal direction, respectively
$\mathbf{u}$	$= (u,\ v,\ w)$, Velocity Vector
v_i	Radial component of the induce velocity of the leading vortex ring
V_c	Volume of the irrotational fluid in the vortex ring bubble
V_r	Volume of the leading vortex ring core
V_{total}	Total volume discharged by the starting jet
x, r, θ	Coordinates of a cylindrical coordinate system with the origin a the nozzle center line and nozzle exit plane
$\mathbf{x}$	$= (r,\ x)$, Position vector
x_{core}	Axial location of the vortex ring core
x_{tip}	Jet tip penetration in axial direction
α	Dimensionless energy used in the Norbury-Fraenkel vortex rings; Axial wavenumber of the disturbance in instability analysis
$\alpha_{\lim}$	Limiting value of the dimensionless energy for the pinched-off vortex ring
α_{ring}	Dimensionless energy of the leading vortex ring
α_{total}	Dimensionless energy of the total ejected fluid
γ	Dimensionless circulation used in the Norbury-Fraenkel vortex rings
γ'	Dimensionless circulation defined by (Shusser and Gharib, 2000a)
Γ	Circulation
Γ_{nd}	$= \Gamma / U_{max} D$, dimensionless circulation
Γ_{op}	Circulation added to the flow by the over-pressure effect
δ	Shear layer thickness
ϵ	Dimensionless mean core radius of the Norbury-Fraenkel vortex rings
ν	Kinematic viscosity [1.004^{-6} m^2/s for water]
ρ	Density of the fluid

Ψ	Stokes stream function
ω	Local azimuthal component of vorticity

Chapter 1

Introduction and Background

1.1 Introduction

In general, a starting jet is commonly referred to the initial development of a jet in which a single burst of fluid is issued from a nozzle or orifice into the quiescent ambient fluid. The starting jet exhibits different features from a continuous jet which behaves quasi-steadily. After the initiation of a starting jet, the cylindrical shear layer which separates at the edge of the nozzle or orifice would roll up into a leading vortex ring. The generation, formation and evolution of the leading vortex ring are the fundamental features of a starting jet. Among these features, the disconnection of the vorticity field of the leading vortex ring from that of the trailing jet, which was first observed experimentally and termed as 'vortex ring pinch-off' by Gharib et al. (1998), is of great interest since it imposes an upper limit to the growth of the leading vortex ring. As the dimensionless time increases beyond a critical value, the leading vortex ring would start separating from the trailing jet and additional circulation ejected by the jet would no longer be entrained into the leading vortex ring. The critical time scale for vortex ring formation was defined by Gharib et al. (1998) as the 'formation number' and its value was found to be in the range of 3.6 to 4.5 for a variety of exit

plane geometries, Reynolds numbers, and velocity programs. Physically, the formation number indicates the onset of the pinch-off process when the starting jet discharges circulation equal to what the final vortex ring can attain. At the end of the pinch-off process the leading vortex ring completely separates from the trailing jet and attains its maximum circulation.

The pinch-off process in starting jets characterized by the formation number represents an optimal vortex ring formation process which is believed to provide a utilitarian strategy in a variety of starting or pulsed flows in nature and engineering fields, such as cardiac flows, the pulsatile propulsion of certain aquatic creatures and synthetic jets. Due to the fundamental role of the pinch-off process in these practical applications of staring jets, a number of investigations have been conducted on the dependence of the formation number to various generation conditions of the starting jets, as well as on the theoretical explanation of the pinch-off process. It has also been found that the formation number would vary among different configurations of the starting jet. However, the existing theoretical models for the formation number mainly focused on vortex rings generated by the impulsively starting jets with classical piston-cylinder mechanism, and are inadequate to provide a general criterion for the limiting process of vortex ring formation. Therefore, it is of fundamental interest to develop a theory which has the potential to generalize the effect of different generation mechanisms on the formation number for the pinch-off process, as well as the kinematic and dynamic properties of the leading vortex ring. In addition, although there were extensive researches undertaken to predict the formation number analytically in starting jets, the theoretical model for the entire pinch-off process, from the formation number to complete separation of vorticity fields, is still lacking. It is partially attributed to the difficulty in distinguishing the leading vortex ring from the trailing jet during the vortex ring formation and pinch-off process.

It is evident that the growth of the leading vortex ring is supported by the

thin shear layer in the trailing jet at a specific rate of fluxes of the dynamic properties, namely circulation Γ, impulse I and kinetic energy E. According to previous experimental results, the trailing shear layer would roll up into a series of secondary vortices similar to those induced by the Kelvin-Helmholtz instability, which in turn affect the fluxes being fed into the leading vortex ring. Given this observation, it is reasonable to speculate that the development of the trailing jet instability might be a fundamental factor responsible for the vortex ring pinch-off in a starting jet. Although the previous studies have highlighted the effect of the instability of the trailing jet on the the formation number and vortex ring circulation, the problem of how the instability of the trailing shear layer develops in a starting jet has remained essentially unexplored. Moreover, in light of the ubiquity of the shear layer in various starting flows, a theoretical explanation that is capable of providing a unifying perspective for the pinch-off process and the properties of vortex ring in diverse jet generation mechanisms may be proposed in terms of the characteristics of the trailing jet instability. These questions are the prime focus of the present thesis.

1.2 Background

In this section, some fundamental concepts on vortex ring formation in starting jets will be introduced.

1.2.1 Vortex ring formation and pinch-off

The research on the topic of vortex ring dates back to the time of Helmholtz and Reynolds, and had attracted great attention in further researches, as can been seen in the reviews of Shariff and Leonard (1992) and Lim and Nickels (1995). The most commonly used mechanism for the vortex ring generation is by the motion of a piston pushing a column of fluid of length L through an orifice

or nozzle of diameter D. The piston-cylinder mechanism has been extensively used in many experimental studies of the vortex ring formation and evolution. Because the focus of previous studies was mainly on the dynamic and kinematic properties of the vortex ring, the vortex rings studied in the past were usually generated with small stroke length to nozzle diameter ratio, by which only a single vortex ring could be produced. When studying the vortex ring formation in starting jets, it is natural to consider an important question that how much circulation can be delivered to the leading vortex ring by the apparatus and whether there is any limit on the growth of the leading vortex ring.

This problem was first addressed systematically by Gharib et al. (1998) through an investigation on the vortex ring behaviour over a wide range of piston stroke to diameter ratio L/D. They discovered that the leading vortex ring would start to disconnect from the trailing jet when the piston had discharged the column of fluid at stroke length $L(t)$ approximately equal to four jet exit diameters. The dimensionless stroke length $L(t)/D = U_p t/D$ is defined as the *formation time* t^*, where U_p is the time-averaged piston velocity. If the piston stops before $L(t)/D = 4.0$ (i.e., in the cases with maximum stroke ratio $L_{\max}/D < 4.0$), all the discharged fluids would be absorbed into the final leading vortex ring. This critical formation time scale is commonly referred to as the *formation number* 'F'. It is noted that by changing the exit geometry, velocity program of the piston U_p and Reynolds number of the starting jet, Gharib et al. (1998) found the formation number to be in the narrow range of 3.6 to 4.5 for the piston-cylinder apparatus. Due to the disconnection of their vorticity fields, the maximum circulation that the leading vortex ring can achieve should be equal to those emanated from the generating jet up to the formation number. The pinched-off vortex ring then approaches its steady state that can be characterized by the Norbury-Fraenkel family of vortex rings (Fraenkel, 1972; Norbury, 1973).

Existence of the formation number was demonstrated to be the outcome of the Kelvin-Benjamin variational principle, which states that for a steady, symmetry-axis-touching vortex ring, the kinetic energy of impulse-preserving rearrangements of the vorticity field by an arbitrary solenoidal velocity field is maximum. Based on this principle, Gharib et al. (1998) suggested that the pinch-off occurs when the apparatus is no longer able to deliver energy at a rate compatible with the requirement that a steady translating vortex ring has maximum energy with respect to impulse-preserving iso-vortical perturbations. Several theoretical models were subsequently developed to predict the formation number, by considering the pinch-off as a relaxational process to its equilibrium state (Mohseni and Gharib, 1998; Linden and Turner, 2001) or by considering the kinematic relation of the leading vortex ring and the trailing jet (Shusser and Gharib, 2000a; Shusser et al., 2006).

1.2.2 Instability in the trailing shear layer

The instability in the trailing jet, i.e., the formation of secondary vortices, was observed previously in many experimental and numerical studies, However, its effect was usually ignored in the theoretical models of the formation number owing to the difficulty about the nonlinear dynamics of the trailing shear layer. For example, in the kinematic model of Shusser and Gharib (2000a) the trailing jet was approximated as a one-dimensional round jet of variable cross section, oversimplifying the dynamics of the trailing jet. In starting jet, the mechanisms for the formation of the leading vortex ring and the formation of the secondary vortices are fundamentally different. The leading vortex ring is formed by rolling-up of the separated shear layer at the nozzle edge according to the Kutta condition, while the secondary vortices (or trailing vortices) are the consequence of Kelvin-Helmholtz instability occurring in the shear layer. Once the trailing vortices are formed, its growth would affect the dynamic quantities being fed into the

leading vortex ring. Therefore, it is necessary to take into account of the trailing jet instability for a better understanding of the pinch-off process.

This topic has not been considered by researchers previously, except for the investigations by Zhao et al. (2000) and Marugan-Cruz et al. (2008). From a sequence of vorticity contours and the axial distribution of maximum vorticity during the pinch-off process, Zhao et al. (2000) suggested that the interaction between the leading vortex ring formation and the instabilities of the trailing jet would accelerate the process of pinch-off and introduced at least a 20% variation in vortex ring circulation and the value of the formation number. In the study of Marugan-Cruz et al. (2008), a small oscillation was superimposed on the piston velocity U_p so as to simulate the disturbance in the trailing jet. They only observed that if the secondary vortices appear, the radial vortex position will be affected most, while the axial position, stagnation point and total circulation will be less influenced. However, it is noted that both researchers considered the instability by assuming the instability has already taken place and then examining its effect consequently, rather than studying the characteristics of the instability of the trailing shear layer itself. Therefore it is still open to question what factors determine the instability of the trailing shear layer in starting jets (or similar flows) and how the growth of the leading vortex ring is limited by the appearance of trailing vortices.

1.3 Scope and objectives

To establish a generalized model for the pinch-off process, the universal properties of the leading vortex ring will firstly be examined. Mohseni et al. (2001) demonstrated that the properties of the leading vortex ring generated by piston-cylinder mechanism are consistent with those of the Norbury-Fraenkel family of vortex rings. The Norbury-Fraenkel vortices served as input to the models for

the formation number as mentioned above. To extend the validity of Norbury-Fraenkel vortices in describing the pinched-off vortex ring to other starting jet configurations, the vortex ring formation in a gravity-driven jet will be investigated, which are basically different from that generated by the piston-cylinder arrangement.

Motivated by Zhao et al. (2000), it is also of interest to investigate development of the trailing shear layer instability, and the effect of secondary vortices formation on the dynamic fluxes that support the growth of the leading vortex ring. Based on the experimental results, the criterion for identifying the pinch-off in terms of the trailing jet instability will be proposed. More importantly, the author intend to develop a framework in which the dynamics of the pinch-off process and observed variation of the formation number among different vortex generation mechanisms can be elucidated, in terms of fluxes of the dynamic properties into the leading ring and the invariant properties of the leading vortex ring.

Finally, a theoretical model will be proposed as a modification to the model of Shusser and Gharib (2000b) for starting plume, to predict the properties of the leading vortex ring during the entire vortex ring formation and pinch-off process. As inspired by the model for starting plume, the dynamic properties of the leading vortex ring and the trailing jet are considered separately via the fluxes of dynamic properties between them. This approach obviates the difficulty in distinguishing the leading vortex ring from the trailing jet before the distinct separation of their vorticity fields. Special emphasis will be placed on predicting the values of the formation number and separation time for starting jets with various generation configurations.

The above objectives are mainly addressed by discussion on the experimental results of vortex ring formation in starting jet generated under different mechanism and flow conditions, as well as theoretical analysis on the instability of the

trailing shear layer and the dynamic aspect of the pinch-off process. Experimental results of the leading vortex ring and the trailing jet in both gravity-driven starting jets and starting jets with piston-cylinder mechanism are obtained by digital particle image velocimetry (DPIV). After the brief introduction on the background and objectives of the present study, a thorough review of previous investigation on related topics is presented in Chapter 2. The experimental apparatus, and experimental techniques and procedure are described in Chapter 3. Chapter 4 discusses the invariant of the leading vortex ring in terms of the its dimensionless energy and circulation in gravity-driven starting jets and Chapter 5 devotes to the experimental and analytical study of the development of the trailing shear layer in the piston-cylinder mechanism. An theoretical model accounting for the entire pinch-off process is developed in Chapter 6. The results are summarized and recommendation for future work is given in Chapter 7.

Chapter 2

Literature Review

2.1 General description of vortex ring formation in starting jets

Starting jet can be regarded as a sudden ejection of fluid into the surrounding media. Although it has long been utilized as an approach to produce vortex ring, recent interest in the starting jet mainly stemmed from its special role as a basic component in a wide variety of flows in nature, ranging from jet pulse entering the human left ventricle to the pulsatile propulsion of aquatic creatures such as squids and salps.

In laboratory, starting jets generated by piston-cylinder mechanism have been extensively used to address the problem of vortex ring formation. The basic configuration of piston-cylinder mechanism for starting jet generation is schematically shown in figure 2.1, for both nozzle and orifice type of exit conditions. A piston initially at rest in a cylinder of diameter D_p moves through a length of L, ejecting fluid through exit with diameter D into the ambient quiescent fluid of the same density. The boundary layer separates at the edge of the orifice or nozzle and subsequently rolls up into a vortex ring. The vortex ring formation and evolution dominate the dynamics of the starting jets. It is noted

that some modifications of these two basic configurations were also utilized in previous experimental studies in order to simulate actual starting jet applications, such as temporally exit diameter $D = D(t)$ (Allen and Naitoh, 2005; Dabiri and Gharib, 2005), nozzles with vertical wall at exit plane (Gharib et al., 1998), and converging nozzle (i.e. $0° < \beta < 90°$ in figure 2.1(b)) (Ai, 2006). In studies of starting jets, dimensionless time of the flow is usually defined as

$$t^* = \frac{\bar{U_0}t}{D}, \quad \bar{U_0} = \frac{L}{t} = \frac{1}{t}\int_0^t U_0(\tau)d\tau. \tag{2.1}$$

t^* is equivalent to the ratio of stroke length to diameter of the jet exit (stroke ratio), and is referred to as the 'formation time' of the jet flow.

The evolution of the size, position, and circulation of vortex rings generated by piston-cylinder mechanism have been studied by numerous researchers in the past. Maxworthy (1977), Didden (1979), Auerbach (1987), Glezer (1988), and Glezer and Coles (1990) studied some of the fundamental aspects of vortex ring formation, such as the initial roll-up of separated shear layer into the vortical structure, the evolution of the vortex ring's size, trajectory and circulation. Glezer (1988) considered a few different piston velocity variation as a function of time and they are known as the 'velocity program'. By using dimensional arguments and experimental observation, he identified and classified some significant parameters of generation conditions for the production of a particular kind of vortex ring, e.g. Reynolds number $Re_\Gamma = \Gamma/\nu$, velocity program factor $P = \overline{U_0^2}/\bar{U_0}^2$ and stroke to diameter ratio L/D. The results verified that the two dimensionless parameters, Re_Γ and L/D, are often sufficient to characterize the behavior of a particular vortex ring during its formation. A transition map has also been developed to identify the conditions leading to the generation of vortex rings that are initially either laminar or turbulent. Based on Glezer (1988)'s observation, the present investigation mainly focuses on the generation

of laminar vortex rings.

2.2 Initial roll-up of vortex ring from vortex sheet

A great number of investigations has been dedicated to address the problem of the initial roll-up of vortex sheet into the ring. Didden (1979)'s experimental study provided a clear picture of the role of internal and external boundary layers in the vorticity flux at nozzle exit plane and demonstrated the important effect of boundary layer dynamics on the development of starting flows, especially in relation to leading vortex ring formation. Models of initial vortex ring formation have been considered analytically by Saffman (1975), who considered the roll-up of a cylindrical vortex sheet, and Saffman (1978) and Pullin (1979), who modeled the initial roll-up process using planar similarity theory. Nitsche (1996) showed numerically that planar similarity theory correctly predict the initial motion of a rolling-up vortex sheet issuing form a circular tube. Weigand and Gharib (1997) revisited the vortex ring problem using digital particle image velocimetry (DPIV) technique. They showed that vortex rings generated by a piston-cylinder mechanism possess a Gaussian vorticity distribution in their core region. James and Madnia (1996) presented a numerical study of vortex ring formation of different generator configurations and concluded that the total circulation and impulse in the flow field of the ring are approximately the same for nozzle with and without a vertical wall at the nozzle exit plane.

In terms of the dynamic properties, the vortex ring is usually described by its kinetic energy, impulse and circulation. Among these three quantities, circulation is the simplest to measure experimentally and, perhaps, the easiest to relate to the formation process. Several models have been proposed for determining Γ, but the most common model used for vortex rings formed by a piston-cylinder

mechanism is the so-called 'slug model'. In slug model, the ejected fluid is viewed as having a uniform velocity U_0 which is related to the piston velocity U_p and pressure equal to the ambient pressure, resulting in the vorticity flux at the jet exit plane as $d\Gamma/dt = 0.5U_0^2$. The model has been commonly used to estimate the circulation of the resulting vortex ring. However, numerous experimental and numerical studies have found that the slug model generally under-predicts the jet circulation. The difference between the actual circulation and slug model prediction should be attributed to the non-uniform velocity profile at the jet nozzle owing to the over-pressure effect during the initiation of the jet (Didden, 1979; Krueger, 2005) and the boundary-layer growth inside the nozzle at large formation time (Shusser et al., 2002). Despite the obvious oversimplification of the model and its deficiencies in determining accurately vortex ring circulation, its simplicity is appealing and it has been widely used in vortex ring research.

2.3 The limiting process of vortex ring formation

The evolution of the leading vortex ring generated by the piston-cylinder mechanism with small maximum stroke ratio ($L_{\max}/D < 4$) dominated the major body of vortex ring research for a long period of time. While for large stroke ratio, a striking feature about the limit on the growth of the vortex ring was first observed and explained by Gharib et al. (1998), and attracted a great deal of attention of researchers thereafter.

2.3.1 Pinch-off and formation number

In investigation on vortex ring formation from a piston-cylinder mechanism for large maximum stroke ratios ($L_{\max}/D > 4$), Gharib et al. (1998) discovered that after the time-dependent stroke ratio $L(t)/D$ had passed a certain value, no

additional circulation from the jet could be absorbed by the leading vortex ring and the ring gradually separated from the trailing jet. The additional vorticity in the trailing jet formed a wake of Kelvin-Helmholtz-type vortices instead. Equivalently, this phenomenon can be described in terms of the maximum stroke ratio of a given starting jet. If the piston stops before the stroke ratio reaches the critical value (small $L_{\max}/D$), only a single isolated vortex ring would be formed as time progresses. For large $L_{\max}/D$, however, the flow field consists of a leading vortex ring followed by a trailing jet. The vorticity field of the leading vortex ring is disconnected from that of the trailing jet. The phenomenon of disconnection was referred to as 'pinch-off'. The flow field of starting jets with and without pinch-off are illustrated in figure 2.2, by the planar laser induced fluorescence (PLIF) flow visualization for three cases with different $L_{\max}/D$.

Gharib et al. (1998) defined the critical value of t^*, at which pinch-off process was initiated, as the formation number F. Based on the criterion that only the vorticity that had emanated from the nozzle before the onset of pinch-off could accumulate in the vortex ring, the formation number was determined by finding the value of t^* at which the circulation of the pinched off vortex ring became equal to the total circulation discharged by the piston-cylinder apparatus. For all cases tested in their experiments with different piston velocity programs and nozzle geometries, F was found to be between 3.6 and 4.5. Due to the small variation in its value, the formation number was regarded as a universal time scale for vortex ring formation in starting jets in their study. However, subsequent investigations have found that this universal value may vary depending on some other flow conditions of the starting jet, such as exit velocity profile and Reynolds number. Rosenfeld et al. (1998) found that the formation number could be reduced by as much as 75% or increased by 35% by manipulating the temporal and spatial profiles of the cylinder exit velocity. For Reynolds number $Re_\Gamma = \Gamma_{ring}/\nu$ as low as 320 and 800, Mohseni et al. (2001) found that the vortex formation process

was highly viscous and the leading vortex ring never separated from its trailing jet. It is noted that the method of Gharib et al. (1998) faces challenges in more complex starting flows where the distortion or breakdown of the leading vortex ring makes it difficult to determine its final circulation. A criterion for identifying vortex ring pinch-off based on the Lagrangian Coherent Structures (LCSs) in the flow was proposed recently by O'Farrell and Dabiri (2010), in which the appearance of a new disconnected LCS and the termination of the original LCS were indicative of the onset of the pinch-off process. The formation number found by the criterion based on LCSs was found to be in good agreement with the results of the circulation criterion.

In addition to the existence of the formation number, another important result about the vortex ring formation in starting jets was that the pinched-off vortex ring can be approximated as a member of the Norbury-Fraenkel family of vortex rings (Fraenkel, 1972; Norbury, 1973). The Norbury-Fraenkel family of vortex rings are the solutions to the steady axisymmetric Euler equations with the assumption that the vorticity density ω/r in the vortex ring core is a constant. They are characterized by the dimensionless mean core radius ϵ, which ranges from about zero for vortex rings of small cross section to $\sqrt{2}$ for Hill's spherical vortex. The leading vortex ring, therefore, can be compared with those in the vortex rings in the Norbury-Fraenkel family in term of two dimensionless parameters, normalized energy α and normalized circulation γ, defined as

$$\alpha = \frac{E}{\sqrt{\rho I \Gamma^3}}, \tag{2.2a}$$

and

$$\gamma = \Gamma\Big(\frac{\rho}{I U_{tr}^2}\Big)^{\frac{1}{3}}, \tag{2.2b}$$

respectively. Here E is the kinetic energy, I is the impulse, Γ is the circulation, ρ is the density of the fluid and U_{tr} is the translational velocity of the vortex ring.

For Norbury-Fraenkel vortices, α and γ are only the function of the mean core radius ϵ. The studies of Mohseni et al. (2001) and Allen and Naitoh (2005) have demonstrated that the values of α and γ of the steady vortex rings generated by diverse starting jet configurations are relatively close to those of the Norbury-Fraenkel vortices with different ϵ. Thus, the properties of the theoretical results of the Norbury-Fraenkel vortices were adopted in the study on the vortex ring formation in starting jet, especially in the analytical models for the formation number (as introduced in section 2.3.3).

The physical mechanism for existence of the limiting dimensionless time scale in vortex ring formation was first discussed by Gharib et al. (1998) in terms of the energetics of the formation process. Based on the Kelvin-Benjamin variational principle (Kelvin, 1880; Benjamin, 1976), a steadily translating vortex ring has maximum energy with respect to the equivalent rearrangements of its vorticity that maintain the same total impulse. Therefore, a forming vortex ring can only accept additional vorticity and subsequently relax to a new configuration if the impulse-normalized energy of the new configuration is greater than the impulse-normalized energy of an alternative vortex ring/shear layer configuration in which the additional vorticity is not accepted by the vortex ring. As such, Gharib et al. (1998) suggested that the formation number could be determined as the time when the starting jet is no longer able to supply energy at the rate compatible with this energy requirement. In practice, the energy requirement for the steady vortex ring was considered in terms of a limiting value of the dimensionless energy α_{lim} of the leading vortex ring.

Besides the relaxation approach given by Kelvin-Benjamin variational principle, Mohseni et al. (2001) explained the pinch-off mechanism based on the translational dynamics of the leading vortex ring and its trailing shear layer. According to the fact that the leading vortex ring gains its strength from the trailing shear layer, they suggested a dynamic explanation as that the pinch-off

occurs when the maximum translational velocity of the ring equals the maximum axial velocity of the trailing shear layer. This explanation leads to further insight about the vortex formation process, and indicates way to modify the properties of the vortex ring by manipulating the characteristics of the generating shear layer. It is, however, rather cumbersome for modelling due to the nonlinear dynamics of the shear layer. On the other hand, the relaxation approach appears to obviate the need for such nonlinear modelling and thus is capable of offering an elegant theory for the existence of a limiting process. Manipulation of the pinch-off process and analytical models for the formation number will be reviewed in the following sections respectively.

2.3.2 Manipulation of the vortex ring formation

In many natural and engineering applications of starting jets, it is usually desirable to obtain a stronger vortex ring by delaying its pinch-off from the trailing jet. According to the dynamic explanation proposed by Mohseni et al. (2001), there are two possible mechanisms capable of extending the vortex ring growth process in starting jets generated by piston-cylinder mechanism. The first method is to accelerate the trailing shear layer relative to the forming vortex ring so that the shear layer energy and circulation was sufficient to be accepted by the forming vortex ring, and to achieve consequently a new steady vortex ring configuration. This approach could be realized by using acceleration program of the piston velocity during the formation stage. As verified by experiments of Gharib et al. (1998), non-impulsive velocity program could delay the pinch-off to occur at $4.2 \sim 4.5$ compared with the value of $F \approx 4.0$ for the impulsive starting velocity program. The results of Allen and Naitoh (2005) indicated the effectiveness of an accelerating source flow for generating thicker vortex rings with lower normalized energy α, possibly indicative of delayed vortex ring pinch-off.

Mohseni et al. (2001)'s second method to delay the formation number was to increase the radial extent of the trailing shear layer. Their simulation suggested that this would delay the onset of the symmetry-axis-touching state of the shear layer, which they correlated with vortex ring pinch-off. This method has been examined by experimental studies of Dabiri and Gharib (2005) (nozzle-type) and Allen and Naitoh (2005) (orifice-type). But they did not observe a significant delay in vortex ring pinch-off and generation of stronger vortex ring for the cases with temporally increasing exit diameter. Dabiri and Gharib (2005) suggested that the discrepancy between their results and theoretical analysis may be attributed in part to the thickness of the shear layer and the relative low Reynolds numbers of their experiments (refer to table 2.1). In contrast, it has been demonstrated by Dabiri and Gharib (2005) and Allen and Naitoh (2005) that growth of the leading vortex ring could be substantially augmented by temporally decreasing the exit diameter during fluid ejection. In these cases, vortex ring circulation was increased by 35%, and the normalized energy was found equivalent to that of Hill's spherical vortex. In Dabiri and Gharib (2005), this effect was related to changes in the vorticity distribution of the forming leading vortex ring that are induced by the nozzle motion. Allen and Naitoh (2005) explained the successful production of a vortex ring of low α as that, by closing the orifice during jet ejection, the leading vortex ring continues to be supplied with circulation, impulse and kinetic energy via a trailing jet with increasing velocity. Therefore, it is reasonable to conclude that increasing the jet piston velocity during the formation stage is more effective to produce strong vortex ring than expanding the radial extent of the trailing shear layer.

Besides the two methods mentioned above, other piston-cylinder configurations have also been used experimentally in recent years to manipulate the pinch-off of vortex ring. Dabiri and Gharib (2004) realized a modest pinch-off delay of approximately 10% in the limiting vortex ring formation time by immersing a

piston-cylinder apparatus in a uniform bulk counter-flow. Krueger et al. (2006) demonstrated the opposite effect, i.e., a reduction in the vortex ring formation number in the case of uniform bulk co-flow around a piston-cylinder apparatus. For co-flow velocity ratios $U_{co}/U_p > 0.6$, vortex ring pinch-off occurred almost immediately following the initiation of the vortex ring's formation, resulting in a much lower circulation and high normalized energy of the pinched-off vortex ring. The change of pinch-off process by imposing a counter-flow or co-flow to the basic starting jet was explained in terms of the kinematic mechanism proposed by Shusser and Gharib (2000a) and Mohseni et al. (2001).

As a reference to above discussion, the results of recent experimental investigations on the vortex ring pinch-off in starting flows are summarized in table 2.1.

2.3.3 Analytical models for the formation number

Based on the understanding of the mechanism of vortex ring pinch-off, several analytical models had been developed, mainly to predict the value of formation number. A model developed by Mohseni and Gharib (1998) predicted the formation number by determining the formation time when the dynamic quantities (kinetic energy, impulse, and circulation) discharged by the starting jet become equal to those quantities of the final vortex ring. They utilized the slug model for the discharge process of the total jet, and approximated the pinched-off leading vortex ring as the Norbury-Fraenkel family of vortex ring. An estimation of the translational velocity of the leading vortex ring after pinch-off was also introduced as an extra condition for closure of the model. It is noted that since characteristics of the leading vortex ring are in their steady state (i.e., after pinch-off), the dynamic process of the vortex ring pinch-off is not considered. The value of formation number was found to be between 3 and 4.5, consistent with results obtained from experiments (Gharib et al., 1998; Pawlak et al.,

2007) and simulations (Rosenfeld et al., 1998; Zhao et al., 2000) for the starting jet with piston-cylinder arrangement. However, the prediction of this model was strongly dependent on the accuracy of the translational velocity estimation. This method of matching the properties of the total jet with those of the vortex ring family was also adopted by Linden and Turner (2001), except that they introduced volume conservation relation as the extra condition instead of the translational velocity.

Shusser and Gharib (2000a) modeled the vortex ring formation by using a kinematic hypothesis that the vortex ring completes its formation and pinches off from its trailing jet when the translational velocity of the vortex ring becomes equal to the jet flow velocity near the ring. The translational velocity of the leading vortex ring was estimated by the properties of Norbury-Fraenkel vortices, and the local trailing jet velocity was related to the piston velocity via conservation of mass. The dynamic properties of the vortex ring were also approximated by those of the total jet using the slug model. By comparing the vortex ring velocity with the trailing jet velocity near the ring, they derived the limiting value of the dimensionless energy $\alpha_{\text{lim}} = 0.31$, which matched well the experimental value $\alpha_{\text{lim}} = 0.33$. Thus, they suggested that the dynamical (based on Kelvin-Benjamin variational principle) and kinematic approaches (based on comparison of the velocities) are equivalent. In a later publication, Shusser et al. (2006) have extended the model to cases of time varying piston velocity programs and have clearly demonstrated the mechanism that increases formation number when the piston velocity increases with time.

Subsequently, models based on statistical physics (Mohseni, 2001), and more complex vortex ring families (Kaplanski and Rudi, 2005) predicted the existence of the process that limits the maximum growth of vortex rings in starting jets. Although the basic perspectives of these models are different, all bear an assumption that before the onset of the pinch-off process, all the fluids discharged

from nozzle exit were regarded as the leading vortex ring so that the properties of the vortex ring could be estimated by the slug model. In other words, models that consider the dynamics of the vortex ring formation process did not distinguish the leading vortex ring and the trailing jet before the pinch-off.

2.3.4 Implication of pinch-off in optimal vortex ring formation

Since the vortex ring growth in starting jets is limited by the Kelvin-Benjamin variational principle, one may ask whether the vortex rings generated according to the critical time scale is optimal in terms of its kinematic and dynamic properties. The pinch-off phenomenon in starting jets may provide a fundamental perspective in the mechanism of optimal vortex ring formation in various configurations of starting flows, in which the formation and shedding of coherent vortices are predominant, such as biological propulsion and starting or oscillating motion of circular cylinder. The concept of optimal vortex formation was precisely defined and discussed recently in the review by Dabiri (2009). Only a few ideas of the optimal vortex formation and its relation to the pinch-off process will be discussed here.

The relation between the optimal properties of vortex ring formation and the pinch-off process was first demonstrated by Krueger and Gharib (2003). They found experimentally that the normalized time-averaged thrust per jet pulse reached its maximum value just before the limiting dimensionless vortex formation time $t^* \approx 4$. In other words, by maximizing the size of the vortex rings formed during propulsion, the efficiency of momentum transport is also optimized. Physically, the benefit of vortex ring formation for propulsion arises mainly due to the entrainment of ambient fluid by the forming vortex ring, as well as the added mass of non-entrained fluid surrounding the vortex that will be accelerated with the vortex ring. Thus the propulsive reaction force experienced

by the vortex generator is proportional to the sum of the shear layer source fluid, entrained fluid, and the added mass of the fluid surrounding the vortex ring before the pinch-off. This benefit on pulsed jet thrust disappears as the leading vortex ring disconnects with the trailing jet.

For some biological flows similar to the starting jet generated by piston-cylinder mechanism, optimal vortex ring formation has also been identified. Gharib et al. (2006) used the optimal vortex formation concept to quantify vortex formation in the left heart of patients measured using echocardiography. In a blind study of 120 normal volunteers, they observed that vortex formation in the left ventricle occurred in a dimensionless time $t^* \approx 4$, similar to the result of previous laboratory studies of vortex ring formation. Furthermore, patients with abnormal left heart function (i.e., dilated cardiomyopathy) exhibited significantly lower vortex formation times, indicating suboptimal fluid transport.

The direct relation of the pinch-off and optimal vortex formation explains the strong interest of researcher on modelling and manipulating the formation number, when the ejected fluid starts to separate from the vortex generator. After the formation number, the reaction force exerted on the leading vortex ring bubble cannot be experienced by the vortex generator any longer because the shear layer connecting them disappears.

2.4 Instability of axisymmetric parallel flows

As the instability of the trailing jet will be considered in our study, it is necessary to review briefly the current understanding of the linear instability of axisymmetric shear flows.

The instability characteristics of many classical velocity profiles have been studied by previous researchers. Due to the relevance to this study, only the study in the axisymmetric parallel flows of inviscid fluid will be introduced here.

There are many calculations of the stability characteristics of axisymmetric flows of an inviscid fluid, ranging from Rayleigh (1880) to Batchelor and Gill (1962) to the present day. Rayleigh (1892) determined that the necessary (but not sufficient) condition for the existence of amplified disturbance in the inviscid axisymmetric parallel flows is that

$$Q(r) = \frac{rU'}{n^2 + \alpha^2 r^2} \tag{2.3}$$

has a numerical maximum somewhere in the fluid. This condition is analogue of the requirement of a maximum of mean vorticity for plane parallel flows, In Rayleigh's work, α and n are respectively the axial and azimuthal wavenumber of the Fourier component of the disturbance, $U(r)$ is the mean flow velocity and r is the radial co-ordinate. This necessary condition defines the range of the parameters α and n for which the flow can be unstable. The condition for the jump of the perturbation across the critical layer in the limit of zero viscosity has been given by Tollmien (1935) and it follows the general results given for the two dimensional system.

The theoretical analysis of the stability of steady axisymmetric parallel flows was conducted thoroughly by Batchelor and Gill (1962). They, using an even more restrictive condition than equation 2.3, showed that there is one and only one neutral disturbance ($\alpha \neq 0$) for the far jet profile ($U = 1/(1+r^2)^2$) and that it is possible only when $n = 1$. A numerical investigation showed that for this profile the wavenumber of the neutral disturbance with $n = 1$ is $\alpha = 1.46$. They also showed that when the azimuthal wavenumber n is large, complete stability occurs, regardless of the jet velocity profile $U(r)$. The wave phase velocity c_r of a neutral disturbance is equal to the value of U either at the point where equation 2.3 is satisfied or at $r = 0$. In addition, a complete solution of the disturbance equation can only be obtained for the cylindrical vortex sheet ('top-

hat' velocity profile). The result showed that the flow is unstable to a small disturbance for all value of n and α. Given the shear layer in actual viscous flow has finite thickness δ, one may expect that the maximum growth rate occurs when α is of order $1/\delta$. For the jet with parabolic velocity profile, Kambe (1969) studied its stability by asymptotic methods in the limits of small αRe and large αRe and calculated a critical Reynolds number of 32.8 for the sinuous mode, i.e, the non-axisymmetric disturbance. His examination showed that the amplified disturbance did not exist for the rotationally symmetric ($n = 0$) mode and that the $n = 1$ mode was more unstable than the $n = 2$ mode. By studying the stability of laminar axisymmetric jets and wakes and comparing with prior results, Lessen and Singh (1973) suggested that the axisymmetric shear layer flows appears to be more stable than the corresponding plane shear layer flows. On the basis of the results of the above and other axisymmetric flow stability analysis, it seems most likely that the $n = 1$ mode will be most unstable. By comparing the stability characteristics of 'top-hat' profile and parabolic profile, one may also expect that the slowly varying profile is more likely subject to unstable disturbance than the profile with steep gradient at some finite r, especially for axisymmetric disturbance.

Besides the studies on the instability on axisymmetric free shear layer, the influence of an external flow velocity on the instability of a circular jet has been investigated by Michalke and Hermann (1982), by means of inviscid linearized stability theory. The instability properties of spatially growing axisymmetric ($n = 0$) and first-order ($n = 1$) azimuthal disturbances showed that the external co-flow ($U_\infty > 0$) inhibits the instability of the circular jet (reduces their spatial growth rate), but the range of unstable frequencies and the phase velocity are increased. Their results can be applicable to the discussion of the important contribution of the shear layer instability to starting-flow dynamics with external co-flow Dabiri and Gharib (2005) or counter-flow Krueger et al. (2006).

Table 2.1: Summary of previous experimental investigation on vortex ring pinch-off in starting flows

Studies	Generator Config.	Velocity program	$\mathrm{Re}_D = U_0 D/\nu$	F	Leading vortex ring		
					ϵ	α_{ring}	U_{tr}
Gharib et al. (1998)	piston-cylinder	impulsive	1900	4.0			
	piston-cylinder	impulsive	3800	4.2		0.33 ± 0.01	$0.475U_0$
	piston-cylinder	non-impulsive	3800	4.5		0.33 ± 0.01	
Dabiri and Gharib (2005)	fast closing nozzle	impulsive	930	8.0		0.16 ± 0.02	
	slow closing nozzle	impulsive	930	6.9		≈ 0.19	
	static nozzle	impulsive	660	4.6		≈ 0.29	
Allen and Naitoh (2005)	closing orifice	impulsive			0.94 ± 0.07	0.19 ± 0.04	
	static orifice	impulsive	2500		0.80 ± 0.07	0.29 ± 0.04	$0.64U_0$
	static orifice	non-impulsive			0.90 ± 0.07	0.18 ± 0.04	
Krueger et al. (2006)	piston-cylinder	impulsive	1430	4 ± 0.5		0.23 ± 0.03	
	co-flow ($R_v < 0.6$)	impulsive		$3 \sim 4$		$0.2 \sim 0.34$	
	co-flow ($R_v > 0.6$)	impulsive		1 ± 0.3		$0.47 \sim 0.63$	
Pawlak et al. (2007)	piston-cylinder (with vertical wall)	non-impulsive	$1660 \sim 2500$	$3.5 \sim 5$			
O'Farrell and Dabiri (2010)	piston-cylinder	impulsive	≈ 1430	4.2 ± 0.2			

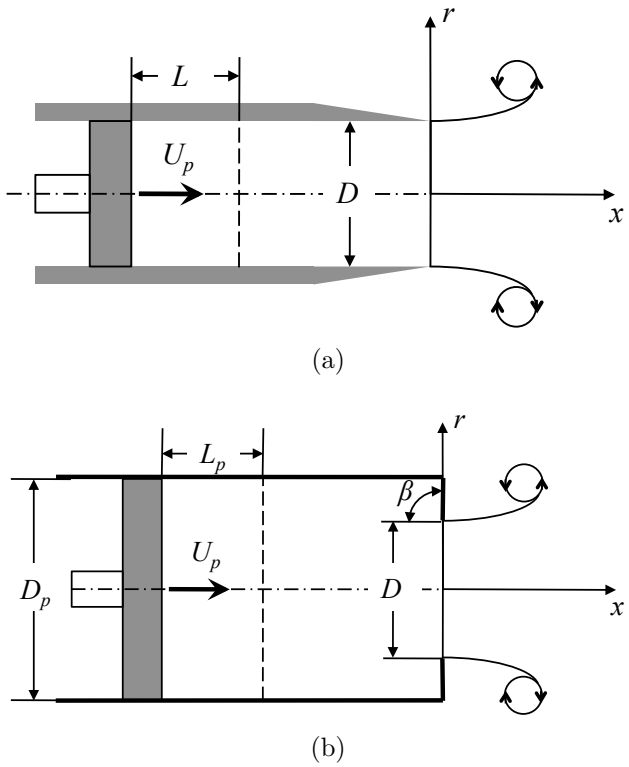

Figure 2.1: Schematic of (a) nozzle and (b) orifice type piston-cylinder vortex ring generators.

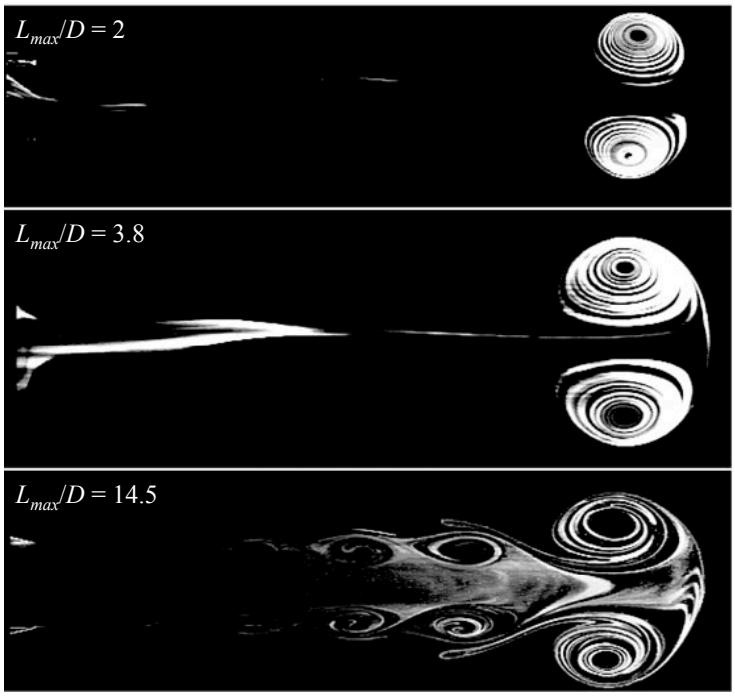

Figure 2.2: Flow fields of the starting jet with different maximum stroke ratio when leading vortex rings travel downstream to $x_{core}/D \approx 9$ (reproduced from Gharib et al. (1998))

Chapter 3

Experimental Setup and Techniques

3.1 General description of the experimental set up

Experiments have been designed and performed in this study so as to investigate the characteristics of the leading vortex ring and the trailing shear layer. Using digital particle image velocimetry (DPIV), velocity and corresponding vorticity fields of the starting jets can be obtained. Starting circular jets are generated by using the piston-cylinder mechanism, which has been extensively used in previous experimental studies on vortex ring formation. The experimental setup, similar to that of Gharib et al. (1998), is capable of controlling the motion of the piston so as to generate starting jets with different velocity program $U_p(t)$, Reynolds number Re, and maximum stroke lengths $L_{\max}$. Velocity fields on the azimuthal plane of symmetry of the starting jets are obtained by the DPIV system (FlowMap SystemHub, Dantec dynamics). Corresponding vorticity fields are calculated by using the integrated software FlowManager in the DPIV system. Post-processing is conducted using the MATLAB programs in order to

obtain other relevant information of the starting jets, such as the integrals of motion (circulation Γ, hydrodynamic impulse I and kinetic energy E) of the leading vortex ring and the total flow.

3.2 Experimental apparatus and its operation

3.2.1 Starting jet generation facility

Starting jets were generated by the motion of a piston of diameter D_p pushing a column of fluid of length L through a cylindrical nozzle into the quiescent ambient fluid. The starting jet generation facility basically consists of a test water tank, a constant-head tank, a cylindrical nozzle, and PVC (polyvinyl chloride) piping, as shown schematically in figure 3.1.

The experiments are conducted in the test water tank, by allowing the flow from the constant-head tank, which maintains the water level at about 1.5 m above the nozzle axis, to drive a piston which in turn pushes the water out of the nozzle horizontally into the surrounding fluid. The test tank is made by plexiglas to ensure optical access for laser sheet and camera. The test tank has the dimensions of 0.5 m $\times$ 0.6 m $\times$ 1.3 m. A nozzle with circular cross-section can be attached to a PVC coupling, which is fixed on the center of the test tank end wall and connected to the supplying pipe on the other side of the wall. Thus, the detachable nozzle can be refilled with fluid containing seeding particles before each run. The geometry of the circular nozzle and relevant parameters are shown in figure 3.2. Both the circular nozzle and the piston are also made by plexiglas. The moving piston ensures that the flow ejected out of the nozzle is free from any disturbances introduced when fluid passes through the piping connecting the constant-head tank and the cylindrical nozzle. The cylindrical nozzle has an inner diameter of 2.54 cm. The outer contours of nozzle near the exit is shaped to form a wedge with a tip angle of 20 $^\circ$ (figure 3.2) so as

to diminish the influence of the thickness of the edge of the nozzle exit on the circulation of the leading vortex ring. The length of the nozzle is 36 cm. So the maximum stroke length of the starting jet in this experiment can reach about $L_{\max} = 36$ cm/2.54 cm $\approx 14D$, which is sufficiently long to observe the entire formation and pinch-off process of the leading vortex ring. Figure 3.2 also defines the cylindrical coordinate system (r, θ, x) used in this investigation. The x axis is taken to coincide with the jet axis and u and v are used to represent the axial and radial components of the velocity $\mathbf{U}$.

3.2.2 Flow control section

The volumetric flow rate $Q_0(t)$ of the starting jet, as well as the duration of each pulse T, can be controlled accurately by a solenoid proportional valve and monitored by an ultrasonic flowmeter. The flow rate, in turn, controls the velocity program of the piston U_p, which, in combination with T, determined the maximum stroke length $L_{\max}$ of the starting jet. The instantaneous piston stroke length $L(t)$ is defined as

$$L(t) = \int_0^t U_p(t)dt = \frac{1}{A}\int_0^t Q_0(t)dt, \tag{3.1}$$

and the maximum stroke length is

$$L_{\max} = L(T) = \int_0^T U_p(t)dt. \tag{3.2}$$

A solenoid valve and a ultrasonic flowmeter, both connected to a PC via a data acquisition card, are used to control and monitor the flow rate, respectively. The valve used to regulate the volumetric flowrate is Burkert 6024 solenoid proportional valve in combination with the Burkert 8623-2 PI-controller. This direct-acting proportional valve works as an electromagnetically actuated control valve with relatively high flow rates at low operating pressures, which was just

the situation in present experiment where pressure difference between the inlet and outlet of the tubing system is generated by limited height difference of water level between the constant-head tank and the test tank. Together with the flow controller, the solenoid valve can keep the flowrate to track the designed variation against time corresponding to a external standard analog signal (0–10 V or 4–20 mA). Because of the unsteady nature of the starting jet and the short duration of the issuing, an ultrasonic flowmeter (Shenitech STUF-200F1G) with fast response time is selected to measure the instantaneously flowrate and also to generate a feedback signal to the valve controller. A multifunctional data acquisition card (NI USB-6251) is used to exchange signal and data between the valve controller, the flowmeter and a PC. A LabVIEW program is developed to provide the signal to operate the valve and store the flowrate data from the flowmeter in the PC. Control of the PC offers precise timing and synchronization of various events with a time resolution of approximately 10^{-3} s. These events include, for example, jet generation, start of flowrate measurement, as well as a trigger signal for DPIV system.

Overall, similar to the experimental configuration in Gharib et al. (1998), the piston-cylinder mechanism with the closed-loop control system, which consists of a solenoidal valve, a ultrasonic flowmeter and a LabVIEW program, is found to be able to generate the starting jet with a variety of velocity programs, Reynolds numbers and maximum stroke lengths.

3.3 DPIV measurement

The interest of this experiment includes the temporal evolution of the vortex ring and the trailing jet, their dynamical properties, and the full velocity field near the nozzle exit (i.e., $0 < x < 5D$). These measurements are mainly obtained using digital particle image velocimetry (DPIV). It is the digital counterpart

of conventional laser speckle velocimetry (LSV) and particle image velocimetry (PIV) techniques, for flow field measurement. Its principle and implementation have been introduced in the reviews of Willert and Gharib (1991) and Raffel et al. (2007), so only a general description of DPIV and its implementation in the present experiments will be described below.

3.3.1 Theory of DPIV

DPIV is based on the well known and simple equation of speed equal to distance traveled divided by time taken. The parameter measured is actually the distance traveled by a group of particles in the flow within a prescribed time interval. A pulsed laser is used to generate a light-sheet shining through the area of interest. A digital camera is positioned at right angles to the light-sheet and is used to capture the scattered light by the illuminated seeding particles.

During the measurement, the laser will generate two consecutive pulses at a very short time interval. With the help of optics, the laser pulses will spread into a flat sheet that shine into the area of interest. The scattered lights of the seeding particles in the flow are captured by a digital camera, which is capable of recording two single-exposed images separately. A standard procedure called spatial cross-correlation is applied to correlate the second image to the first image to obtain the map of displacement vectors.

The primary objective of cross-correlation is to derive the displacement of a group of particles in two sequential images. In two-dimensional cases, two sequential digital images are first subsampled into particular areas called interrogation areas (IA) or interrogation regions. For each of these interrogation areas, the program will move the first image and calculate the sum of products of every pixel with the second image to obtain the average spatial shift of particles. Performing this procedure for all interrogation regions produces a displacement vector map. Division of the displacement by the time interval Δt between the

capture of the images provides the average velocity of the sampled region. In order to speed up the process of correlations, Fast-Fourier-Transform (FFT) algorithm is usually used. The captured particle images may be regarded as two-dimensional signal field analogous to a digital time series in one-dimension. The Fast Fourier Transformations of the two images are first obtained and then multiplied by each other. The results are inversely transformed to determine the peaks of the coefficient of cross-correlation, from which the displacement vectors can then be obtained.

The cross-correlation will always produce results no matter what the initial input images are. Therefore, it is necessary to follow some rules of thumb to obtain meaningful results. The minimum number of particles within each interrogation area should be about 5. It is generally recommended to keep the maximum displacement of the particles below a quarter of the side of the interrogation area (Keane and Adrian, 1992). Based on this rule, the maximum velocities and the time interval between two consecutive pulses then can be calculated. In addition, the size of the particles should occupy 3 pixels in the recorded images. Sometimes, the camera is deliberately slightly de-focused to obtain the blurred particle images for this purpose.

The vector maps produced after cross-correlation are termed raw vector maps. Some vectors are incorrect due to the noise signal, which are also termed outliers. Therefore, a few techniques are implemented to validate the vectors on the raw vector maps. These include Peak-height validation, velocity-range validation, and moving-average validation. The outliers or incorrect vectors occur in almost any DPIV measurement. It is important to note that there will always be an outcome whether the input is meaningful or not.

The Peak-height validation verifies or rejects individual vectors based on the values of the peak heights in the correlation plane where the vector displacement is measured. In the correlation plane, there will always be the highest peak,

which is hopefully to be the signal peak. This highest peak should be greater than the second-highest peak by a certain factor k if it is considered valid. This is also known as detectability criterion. It is recommended to use 1.2 for the value of k for validation (Keane and Adrian, 1992). In the case of insufficient seeding particles in the images, it might be necessary to use a lower k value.

Velocity-range validation rejects vectors based on the maximum possible velocity vectors in the flow field provided by the user. The range can be calculated based on past experience, formulas provided by other researchers, the upstream conditions, criteria of displacement less than one-quarter of IA side, or any other methods. In this experiment, the IA is assumed to be 32×32 pixels. The time interval between two consecutive pulses is determined based on the maximum velocity estimated for the present experiments. About 80% to 90% of tolerance is allowed and the time interval between pulses is reduced to the nearest hundred micro-second. The maximum velocity is then back calculated from the time interval.

Moving-average validation is based on an implicit assumption of the continuity behavior of the flow field. It means that the velocity field is slowly changing so that there is not too much variation from one vector to its neighborhood vector. It rejects vectors by comparing them among the neighborhood vectors. Thus, if a vector deviates too much from its neighborhood vectors, it must be an erroneous vector.

The choice of the seeding particle depends on a number of parameters. Primarily the seeding material should be chosen considering the flow that is to be measured and the illumination system available. Seeding particles should be chosen as large as possible in order to scatter the most light, but the particle size is limited, since large particles may not track the flow properly. In general, the maximum allowable particle size decreases with increasing flow velocity, turbulence and velocity gradients. One should also be aware that the camera images

of seeding particles should have a diameter of at least 2 pixels, preferably 3 pixels or more. This will allow the system to estimate particle positions and displacements to subpixel accuracy, effectively increasing the resolution of the technique. Ideally the seeding material should also be chosen, so that the seeding particles are neutrally buoyant in the carrying fluid, but in many flow situations this is a secondary consideration.

3.3.2 Experimental Procedures for DPIV measurement

In the present experiment, Polyamide Seeding Particle (PSP) made by Dantec, which has a mean diameter of 50 μm and a density of 1.03 g/cm^3, is chosen as the seeding particle. The particles are illuminated by a dual-cavity pulsed Nd: YAG laser (NewWave Gemini) with a maximum repetition rate of 15 Hz for each cavity. The maximum energy level is 120 mJ per pulse and the pulse duration is about 10 ns. The emitted laser is green with a wavelength of 532 nm. A cylindrical lens is used to form a laser sheet with thickness of 3 mm and divergence angle of 32 °, which is positioned vertically and crossing the jet axis. The 12-bit digital camera (HiSense MkII), to which the AF Micro Nikkor 60 mm lens is attached, is positioned normal to the laser sheet plane and records the images of the particle field in the region of $0 < x/D < 5.5$ and $-2 < r/D < 2$ with a image resolution of $1,344 \times 1,024$ pixels. Although the laser could achieve higher frequency, the actual measurements are taken at the frequency of 5.5 Hz due to the limit of the camera frame rate (maximum 5.6 Hz for double-frame mode). The software, FlowManager from Dantec dynamics, employs the standard cross-correlation technique and the cross-correlation peak could be resolved with a sub-pixel accuracy of approximately 0.01 pixels. Using an interrogation area of 32×32 pixels and a step size for the moving average of 16×16 pixels (50% window overlap), the processing can construct a flow field of 83×63 velocity vectors. The spatial resolution of the resulting velocity vector

fields is $0.063D \times 0.063D$.

The procedures of DPIV measurement in this experiment can be summarized into four stages, e.g. (1) preparation, (2) laser alignment and calibration, (3) focusing of cameras, and (4) selecting measurement parameters. The implementation of these procedures in the present experiment is introduced as follows.

3.3.2.1 Preparation

The first step is to prepare the ambient and jet fluids with the seeding particles. Both the ambient and jet fluids are fresh tap water. The test tank is drained, cleaned thoroughly and then is filled up with ambient fluids. Seeding particles are subsequently added into the ambient fluid to enhance the velocity measurements in the vicinity of the starting jet flow. On the other hand, the nozzle is filled with the fresh tap water with higher particle density, and then submerges in the test tank and mounts to the PVC coupling, which is connected to the piping with high pressure fluid. The water in the test tank is then left to settle for a certain time to ascertain that the water in the test tank is sufficiently still.

3.3.2.2 Laser alignment and focusing of cameras

A string tied with a weight is hung along the vertical axisymmetric plane of the nozzle in the tank. The laser is then adjusted to align with the string to obtain a vertical illuminating plane to ensure the measurement conducted is on a two-dimensional $x - r$ plane as shown in figure 2.1(a). The distance between the laser and the area of measurement is kept to a minimum so as to obtain the maximum light intensity but yet wide enough to illuminate the whole imaging area evenly.

Next step is to adjust the focusing of the camera, as well as to determine the scale factor of the image. It is important to make sure that the camera axis is perpendicular to the plane of laser sheet and thus geometric distortion could be

minimized. This requirement is ascertained by placing a grid paper at the area of measurement. The grid paper is attached to a perspex sheet so as to ensure that it is hanging vertically downwards. The position of the camera, which is mounted on a tripod, is then adjusted so that the camera is able to capture the desired area of measurement, and the images captured are free from geometrical distortions. Once the position of the camera is fixed, it is necessary to determine the object to image scale factor of the image. A ruler is placed vertically in the laser sheet plane as an indicator of the physical length scale. From the image of the ruler in the area of interest the scale factor is calculated to be 15.58 (CCD sensor size is 8.669 mm $\times$ 6.605 mm). The scale factor is required by the DPIV system to calculate the velocity vectors in physical world. By doing so, the DPIV system is able to estimate the particles actual position and displacement to sub-pixel accuracy. This would effectively increase the spatial resolution of the technique.

3.3.2.3 Selection of measurement parameters

To obtain high quality DPIV measurements, it is important that the correct parameters are selected. These include the size of the IA, the thickness of the light sheet and the optimization of the time interval between the pulse pairs. In order to obtain the best combination of the experimental parameters, several trial runs with experimental conditions similar to that of the actual tests are conducted. For the present study, each IA used is made of 32 $\times$ 32 pixels with 50% overlapping. Then optimization of the time interval between pulse pairs in one recording is determined according to the requirement discussed in section 3.3.1. Typically, the larger the flow field displacements, the more accurate the measurements would be. However, the maximum displacement of the particles is suggested to be kept below a quarter of the side of the IA so as to reduce the effects of velocity biasing and signal drop out. This implies that the recommended

maximum displacement on the camera should be 8 pixels. Therefore, the time interval between two pulses would vary in terms of the maximum velocity in various cases. In addition, DPIV requires a certain thickness of the laser sheet to prevent seeding particles from moving out of illuminated plane during the pulse pair interval that may lead to significant bias in the velocity determination. In this study, the thickness of the laser sheet is 3 mm. Another important parameter influencing the quality of the results is the number of seeding particles within each interrogation area. With a large number of seeding particles, there will be many true correlations ensuring a high signal to noise ratio, and in this case, an average displacement exceeding one quarter of the side of the IA may be acceptable. Generally a minimum of 5 particles per interrogation area (32×32 pixel) is recommended to achieve reasonable results using correlation techniques.

3.3.3 Uncertainty analysis for DPIV measurements

In uncertainty analysis of the experimental results, we neglect the systematic biases related to technical details of the experimental arrangement like the alignment of the laser sheets, focusing of the camera and stability of the laser-camera synchronization, since these biases have been carefully checked and diminished to the lowest level. Thus, the sources of uncertainty mainly arise from DPIV measurement of the velocity field.

3.3.3.1 The uncertainty in velocity measurement

The velocity measured by DPIV contains errors arising from several sources: (1) Random error due to noise in the recorded images (i.e. quality of the particle images); (2) Bias error arising from the process of calculating the signal peak location to sub-pixel accuracy; (3) Gradient error resulting from rotation and deformation of the flow within an interrogation area leading to loss of correction;

(4) Tracking error owing to the inability of a particle to follow the flow without slip; and (5) Acceleration error caused by approximating the local Eulerian velocity from the Lagrangian motion of tracer particles.

Certain errors can be minimized by careful selection of experimental conditions (e.g., tracking error). However, other sources are inherent to the nature of the correlation in DPIV and cannot be eliminated. For example, even if the recorded images are free from noise, the location of the correlation peaks can be influenced by random correlations between particle images not belonging to the same pair (such random correlations are visible as small peaks). In addition, bias error results from a phenomenon called pixel-locking in which the signal peak location is biased towards the nearest pixel while using a curve-fit or centroiding scheme to locate the discretized signal with sub-pixel accuracy. Similarly, gradient errors will occur in turbulent flow. Finally, acceleration error cannot be eliminated because of the very principle of DPIV which uses the Lagrangian motion of particles to approximate the instantaneous Eulerian flow velocity.

In typical flows, particle streamlines are not straight, but curved. Consequently, error would be incurred when the Eulerian velocity is approximated using Lagrangian particle displacements. It is easy to understand that if the pulse separation Δt is greater, the displacement Δx becomes larger too and consequently, greater is the deviation of the measured velocity from the true velocity. This suggests that one must reduce Δt. On the other hand, if one reduces Δt too much, the measurement of small Δx becomes difficult; at very small values of Δt , it may become impossible to distinguish Δx from random error. Obviously, simple error considerations suggest that the fractional random error can be reduced only by increasing Δx , and corresponding Δt . So it is very important to properly select the value of Δt.

Errors associated with DPIV algorithms often are decomposed into two components: mean bias error and RMS (random) error (Huang et al., 1997).

Given the actual displacement, d_a, and the estimated DPIV displacements, d_i $(i = 1, 2, 3, \ldots, n)$, the mean bias error can be defined as

$$e_{mean} = d_m - d_a, \tag{3.3}$$

where d_m represents the spatial mean of the n estimated displacements. Mean bias errors arise when the actual correlation peak is not well represented by the peak-fitting curve or procedure (Huang et al., 1997). This is often the case when out-of-pattern effects are prominent, or when strong gradients within the sub-IA act to broaden and/or distort the symmetry of the correlation peak (McKenna and McGillis, 2002).

Bias errors arise during the process of calculating the particle displacement to sub-pixel accuracy. Essentially the correlation field is available on a discretized grid (typically 32×32 pixels). The location of the maximum value in the cross-correlation field will correspond to the particle displacement, but obviously such displacement will be an integer pixel value. In order to reduce measurement error, one attempts to locate the peak with sub-pixel accuracy using either a curve-fitting method or a centroiding scheme. The term bias error is coined to describe the phenomenon of pixel-locking, i.e. during the process of determining the displacement to sub-pixel accuracy, the resulting value is always biased toward the nearest integer-valued pixel (Prasad et al., 1992). Bias error is zero if the particle displaces exactly n or $n + 0.5$ pixels. If the displacement falls in $n < \Delta x < n + 0.5$ pixels, the measured displacement is biased towards n, and for $n + 0.5 < \Delta x < n + 1$ pixels displacement, the measured displacement is biased towards $n + 1$. The true and measured values coincide at integer or at half-pixel values. The bias error in DPIV occurs primarily at the time of calculating the centroid or curve-fit of the correlation signal peak (Prasad et al., 1992). The software used in the present DPIV measurement, FlowManager, em-

ploys the standard cross-correlation technique and the cross-correlation peaks can be resolved with a sub-pixel accuracy of approximately 0.01 pixel (Willert and Gharib, 1991).

By satisfying the constraints mentioned above, it is possible to make valid measurements in over $90 \sim 95\%$ of the interrogation areas with small bias errors. McKenna and McGillis (2002) reported that the maximum uncertainty based on FFT/correlation techniques for the local velocity and vorticity magnitude is $\pm 1\%$ and $\pm 3\%$, respectively. With the peak-compensation technique in the process of correlation peak detection (Huang et al., 1997), the mean bias error could be reduced to so small that it is negligible, i.e. one magnitude less, in comparison with the RMS error. Therefore, the RMS error becomes the only major error in the present DPIV measurement.

Previous studies show that random errors in DPIV may be affected by many factors, such as particle image size, the size of the interrogation window, local velocity gradients, the number of particles within the sampling window, camera performance characteristics and digital computational errors. Willert and Gharib (1991) found that as the displacements increase, the corresponding RMS errors, given in pixel values, increase as well, but not in a linear fashion. However, the relative errors actually decrease with increasing particle displacements. For the present DPIV processing with a 32 by 32 pixel IA size and displacements of less than 8 pixels, the RMS error in the velocity measurement should be about 0.08 pixels (see figure 6b in Willert and Gharib (1991)), resulting in the relative error of $0.08/8 = 1\%$.

Therefore, the overall relative error of the measured velocity components can be calculated as

$$e_{total} = e_{mean} + e_{rms} \approx e_{rms} = 1\%. \tag{3.4}$$

As demonstrated by Prasad et al. (1992), the variation of the DPIV bias error with respect to the actual displacement is sine-wave-like with a wavelength of

one pixel. When measuring turbulent flows, the velocity fluctuations cause both the negative and positive biasing to occur alternatively or intermittently. As such, the contribution of the bias errors to the measured mean velocity should be generally suppressed due to the neutralization of the negative and positive biasing.

3.3.3.2 The uncertainty in the velocity derivatives

A standard central difference scheme, accurate to the second order, is used to calculate the vorticity:

$$\omega_{i,j} = \frac{v_{i+1,j} - v_{i-1,j}}{2\Delta x} - \frac{u_{i,j+1} - u_{i,j-1}}{2\Delta y}. \tag{3.5}$$

Since the final window overlap is 50%, the velocity used in equation 3.5 are uncorrelated and the uncertainty in vorticity is given by the expression $e_\omega = 0.7e_{total}/\Delta x$ (Raffel et al., 1998). In the present experiments, the spatial step size is $32 \times 50\% = 16$ pixels and the error in velocity measurement is estimated at about 0.08 pixels, which results in

$$e_\omega = 0.7 \times 0.08 \text{ pixels}/16 \text{ pixels} = 3.5 \times 10^{-3} \text{ pixels per pixel} \tag{3.6}$$

In the core region, it is found that the maximum displacement gradient is about 0.12 pixels per pixel. There fore the uncertainty in the derived vorticity results is bounded to about $\pm 3\%$.

3.4 Experimental setup for gravity-driven generator with converging nozzle

Finally, setup of the experiment performed by Ai (2006) is briefly introduced since his data are employed by the author for discussion in Chapter 4. The

apparatus and configuration are shown in figure 3.3. The starting jet is generated in a test tank made of plexiglass with dimensions of 400 mm × 400 mm × 1000 mm. The water is discharged vertically downward through a converging nozzle attached to a constant head tank mounted at 800 mm above the level of nozzle exit plane in the test tank. The circular nozzle contracts from a round cross-section with a diameter of 260 mm smoothly and gradually to a diameter of $D = 36$ mm, with a wall thickness of 1 mm at the exit edge. The contraction ratio of the nozzle (A_{inlet}/A_{outlet}) was about 52 : 1. Flow is initiated by a sudden opening of solenoid valve (< 20 ms) to ensure an impulsive start for the jet. Another needle valve controlled the volumetric flow rate Q_0 at the nozzle exit, which was monitored by an electromagnetic flowmeter (model Endress+Eauser Promag 53).

Planar laser induced fluorescence (PLIF) is employed to visualize the flow field of the starting jets in the axisymmetric plane. 7-Dichlorofluorescein ($C_{20}H_{10}C_{l2}O_5$), MW = 401.21) is chosen as the dye tracer. A 5 W Argon laser coupled with a cylindrical lens forms a 3 mm thick light sheet as the source of illumination. A 12 bit high-resolution ($1,000 \times 1,000$) digital camera (COOKE Pixelfly) is placed perpendicular to the laser sheet to record the flow evolution at 12.5 Hz. The shutter speed of the camera is set at 1/125 seconds which should be sufficient to capture the instantaneous distribution of the jet fluid. .

Digital particle image velocimetry (DPIV) is used to measure the two-dimensional velocity field. The light source employs a dual-cavity pulsed mini Nd:YAG laser with a maximum repetition of 15 Hz for each cavity. The energy level is 50 mJ per pulse and the pulse duration is about 7 ns. The flow is seeded with neutrally buoyant Polyamid Seeding Particles (PSP) with average diameter of 50 μm and illuminated by a sheet of laser light with a thickness of approximately $2 \sim 3$ mm. Similar to the PLIF experiments, the digital camera (Kodak Megaplus ES1.0) is positioned perpendicular to the measurement plane and records an image se-

quence of the particle fields with a spatial resolution of $1,008 \times 1,016$ pixels. The time interval between two successive exposures is set properly in order to limit the maximum displacement of particles within a quarter of the side of the interrogation area. The measurements are performed and recorded in the axial range of $0 < x/D < 9$. Using an interrogation area (IA) of 32×32 pixels and a step size for the moving average of 8×8 pixels (75% window overlap), the processing results in a field measurement of 123×124 velocity vectors with a temporal resolution of 6.25 Hz. With a typical field of view of 31.9 cm $\times$ 32.1 cm, the spatial resolution of the IA is 1.01 cm $\times$ 1.01 cm. The software, FlowManager by Dantec, employed the advanced adaptive-cross-correlation technique and the cross-correction peak can be resolved with a sub-pixel accuracy of approximately 0.01 pixel. By satisfying the constraints of DPIV measurements and careful alignment, i.e. time interval, particle size and particle concentration, $\pm 1\%$ and $\pm 3\%$ accuracy for the velocity and vorticity measurements can be achieved.

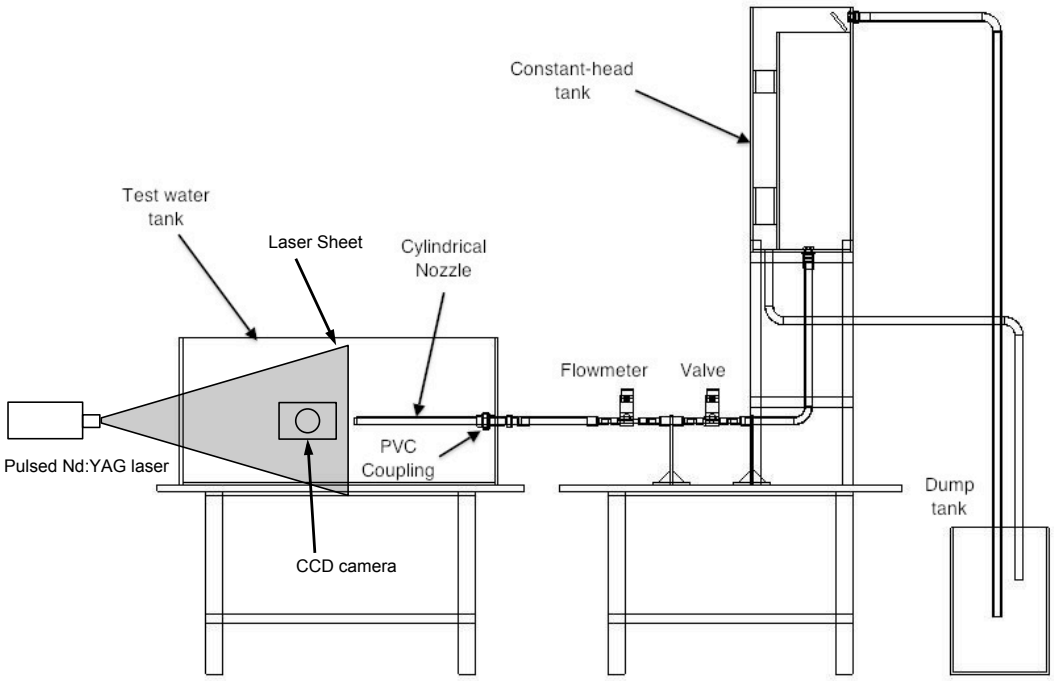

Figure 3.1: Schematic of the experimental apparatus for starting jets with piston-cylinder arrangement.

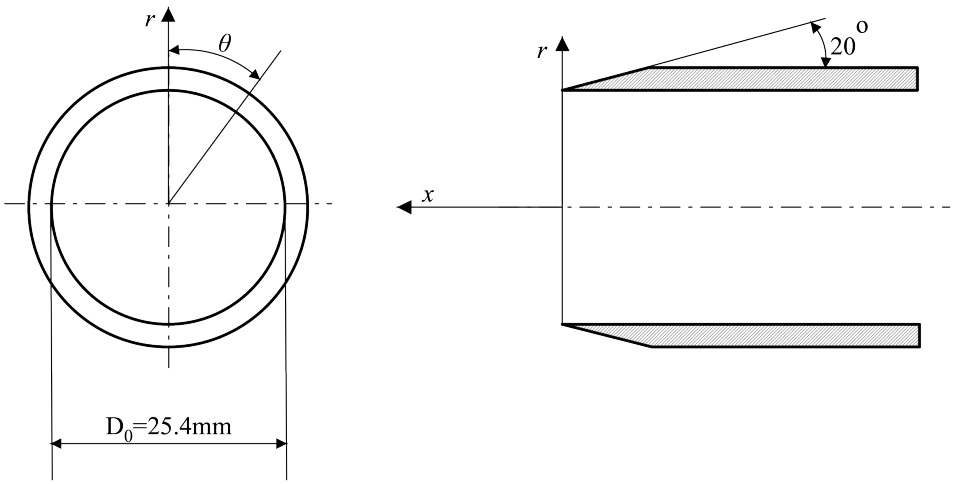

Figure 3.2: Nozzle geometry and the coordinate system

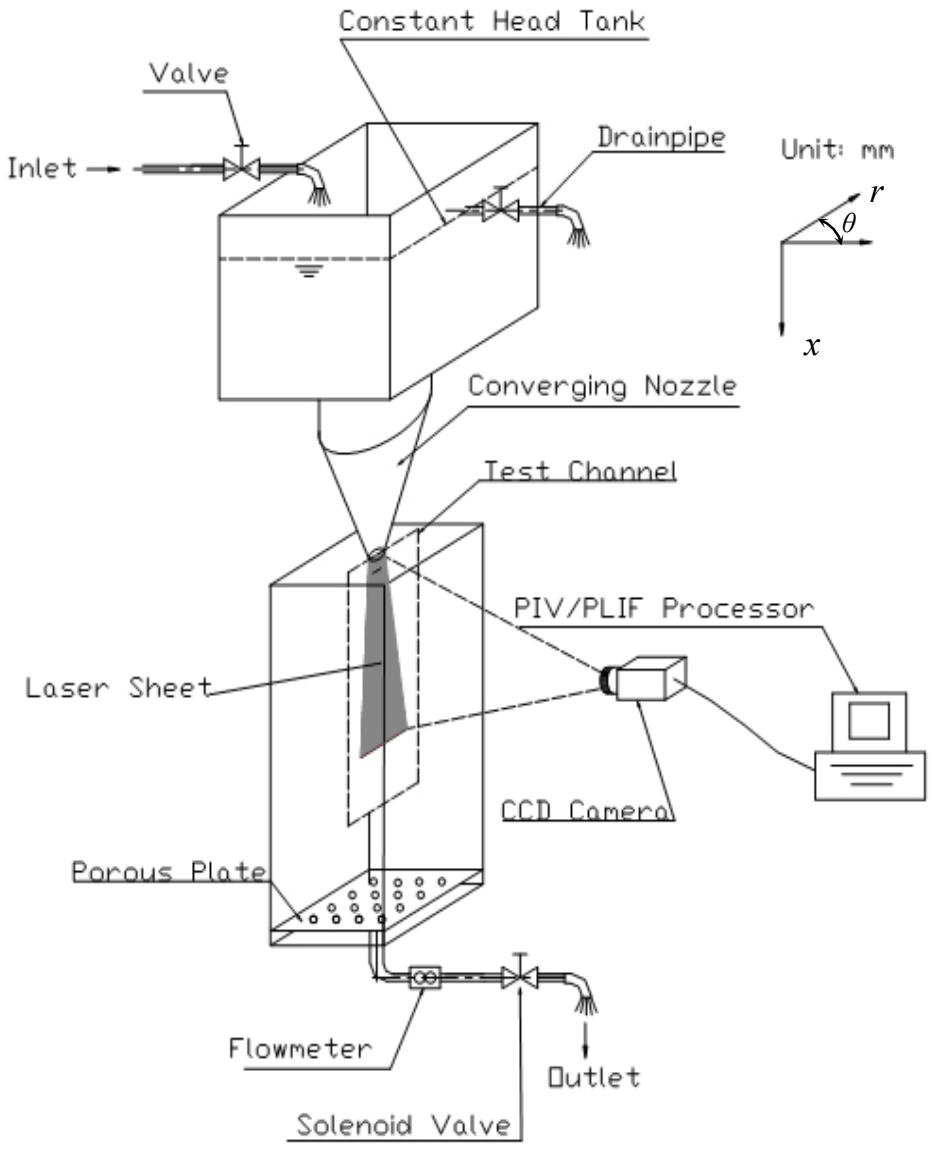

Figure 3.3: Schematic of the experimental apparatus for the gravity-driven starting jet. (reproduced from Ai (2006))

Chapter 4

Universal Characteristics of the Leading Vortex Ring

4.1 Introduction

It has been demonstrated by Mohseni et al. (2001) that properties of the leading vortex ring are basically determined by the rates of delivery of dynamic quantities, i.e., circulation Γ, impulse I and kinetic energy E by the trailing shear layer. These rates would appear to vary among different vortex generation mechanisms. However, invariant properties may exist for the pinched-off vortex rings, in terms of their dimensionless energy and circulation as defined in the Norbury-Fraenkel vortices. Previous experimental investigations on the pinch-off in starting jets usually utilized piston-cylinder arrangement with various piston velocity programs, exit diameters and generator configuration (nozzle or orifice). In contrast, gravity-driven starting jets with converging nozzle were found to produce larger flux of circulation and smaller formation number than the piston-driven jets. The formation number in gravity-driven starting jet was also observed to be smaller than piston-cylinder jets under similar flow conditions (Yu et al., 2007). Thus, the next question would be that whether the

vortex rings after pinch-off would have similar characteristics which are consistent with Norbury-Fraenkel family of vortex rings, even though variation in the formation number between piston-driven and gravity-driven starting jets existed. If the answer is positive, the characteristics of the pinched-off vortex ring may be independent of the generation mechanism of the starting jets. Therefore, in this chapter, we focus on examining the kinematic and dynamic properties of the leading vortex ring in gravity-driven starting jet with different Reynolds number.

This analysis is based on the experimental results of Ai (2006) on the gravity-driven starting jet, whose experimental setup and techniques have been described in Chapter 3. In the experiment, a total of 17 tests is performed on the starting circular jets with a wider range of Reynolds number from 1,179 to 10,611, as shown in table 4.1. It is noted that only three cases, as indicated in table 4.1, have been measured by the DPIV. The discussion in the following sections, therefore, will mainly concentrate on these three cases.

The azimuthal component of vorticity, ω, is calculated by the measured velocity data as,

$$\omega = \frac{\partial v}{\partial x} - \frac{\partial u}{\partial r}, \tag{4.1}$$

where u and v are the local axial and radial velocity, respectively, x and r are the streamwise distance from the nozzle exit and the radial distance from the axisymmetric centerline (see the cylindrical coordinates defined in figure 3.3), respectively. The total circulation is obtained by integrating the vorticity contained within the lowest detectable contours for either positive or negative values. This vorticity contour level is determined to be at 1.5 s^{-1} here. This is different from our earlier analysis presented in Yu et al. (2007) at which a higher level was used for computations. Sensitivity analysis has been conducted by selecting contour levels at 2.0 s^{-1}, 1.5 s^{-1} and 1.0 s^{-1} as the boundary of the vorticity field of the vortex ring. The circulation of the vortex ring is found to be

Table 4.1: Cases tested in the experiment; '*' indicates that DPIV measurements were obtained.

Case	$Re_D = U_0 D/\nu$	Average velocity U_0 (m/s)
C1	1179	0.0327
C2	1474	0.0409
C3	1768	0.0491
C4	2063	0.0573
C5*	2358	0.0655
C6	2653	0.0737
C7	2948	0.0819
C8	3242	0.0900
C9*	3528	0.0980
C10	3832	0.1064
C11	4127	0.1146
C12*	4716	0.1310
C13	5306	0.1473
C14	5895	0.1637
C15	7074	0.1965
C16	8253	0.2292
C17	10611	0.2947

sensitive to the choice of the cut-off level between 2.0 s^{-1} and 1.5 s^{-1}, especially at time after the leading vortex ring has pinched-off. In addition, at the limit of 1.5 s^{-1} level, the detachment of the leading vortex ring from the trailing jet can be clearly distinguished in the vorticity field. At 1.0 s^{-1} level or below, however, noise signal would become unacceptable. As such, the level of 1.5 s^{-1} is chosen as the lowest detectable counter of vorticity for the present analysis.

The three dynamic properties (or integrals of motion), i.e. circulation Γ, impulse I and kinetic energy E, which characterize the leading vortex ring, are calculated from the experimental results in cylindrical coordinates as,

$$\Gamma = \int_0^\infty \omega dx dr, \tag{4.2a}$$

$$I = \pi\rho \int_0^\infty \omega x^2 dx dr, \tag{4.2b}$$

$$E = \pi\rho \int_0^\infty \omega \Psi dx dr, \tag{4.2c}$$

where $\Psi(r, x)$ is the stream function. The dimensionless time t^*, also known as formation time, is defined by

$$t^* = tU_0/D, \tag{4.3}$$

where t is the physical time from the jet initiation and U_0 is the average velocity at nozzle exit.

4.2 Experimental results and discussion

4.2.1 Kinematic properties of the leading vortex ring

Figure 4.1 shows flow visualization results obtained at three selected cases within the range of Reynolds number investigated. At Reynolds number below 3,000, such as in case 5, vortex leapfrogging phenomenon for the first two vortex rings is observed (figure 4.1(a) and 4.1(b)). For cases 9 and 16 (figure 4.1(c) and 4.1(d)), the detachment of the leading vortex is found. As may have been expected, the vortex ring at higher Reynolds number ($Re_D = 8,253$) exhibits the typical turbulent ring characteristics.

Figure 4.2(a) shows the normalized penetration of the jet tip, which is defined as the most downstream position the ejected fluid could reach (see figure 4.1(a)), against the formation time t^* plotted in a log-log scale. The variations of the penetration rate of jet tip for all cases are nearly the same within the range of measurements, except at the beginning of the initiation phase. It should be noted that the slopes of the curves started to change at around $t^* = 2.0 \sim 3.0$ (i.e., also at axial position of about $2D$ to $3D$ from the nozzle exit plane). The results are similar to those found by Kouros et al. (1993) but somewhat different

from those found, for example by Lahbabi et al. (1993) and Cossali et al. (2001) where the change of the slopes appeared at around $6D$ and $10D$ respectively. Although there are some differences in the initial stage, all cases tested in our experiment seem to converge after $t^* = 3.0$.

The following linear expression may be used to fit the experimental data within the range of $t^* > 3.0$:

$$x_{tip}/D = C(tU_0/D)^{1/2} \tag{4.4}$$

where C is a constant within the range of 3.15 to 4.08 for the best fitted line. Table 4.2 summarizes the equations proposed for the tip penetration by previous researchers.

Table 4.2: Fitted expression for the jet tip penetration.

Johari et al. (1997) ($Re_D = 5 \times 10^3 \sim 2 \times 10^4$)	$x_{tip}/D = C(tU_0/D)^{1/2}$ $C = 2.14 \sim 2.58$
Lahbabi et al. (1993) ($Re_D = 2.6 \times 10^3$)	$x_{tip}/D = C(tU_0/D)^{1/2}$ $C = 2.9$
Cossali et al. (2001) ($Re_D = 1.26 \times 10^4 \sim 1.36 \times 10^4$)	$x_{tip}/D = C(tU_0/D)^{1/2}$ $C = 3.41$
Ai (2006) ($Re_D = 1474 \sim 10611$)	$x_{tip}/D = C(tU_0/D)^{1/2}$ $C = 3.15 \sim 4.08$

Figure 4.2(b) shows the growth of the diameter of the vortex ring bubble D_b, which is normalized by the jet exit diameter D, for various cases. The boundary of the vortex ring is defined at the level 1.5 s^{-1} in the azimuthal vorticity contours for respective cases. The overall growth rate is nearly the same for all cases considered. After the initial rapid growth up to about $t^* = 2.0 \sim 3.0$, the vortex bubble size actually shrinks slightly before increasing steadily again, albeit with a slower rate. The leading vortex ring attained its maximum size at about the same location where the slope of the jet tip penetration starts to change. The

initial rapid increase appears to be the effect of small translational velocity of the forming vortex ring. It is shown in Figure 11 of Gharib et al. (1998) that the vortex ring in starting jets accelerates gradually and moves much slower than the trailing jet feeding it during the initial stage. According to the mass conservation law, the fluids from the generating jet would be mostly absorbed into the forming vortex ring, resulting in the rapid growth rate for vortex ring size. Similar situation was also observed in the formation process of a two-dimensional vortex dipole (Afanasyev, 2006).

Attention will now be turned to the properties of the leading vortex ring that can be described by the Norbury-Fraenkel vortices, including the translational velocity of the vortex ring and its circulation, impulse, and kinetic energy. Translational velocity of the vortex ring describes the axial evolution of its core and is an important property. The dynamic mechanism of the pinch-off process suggests that a vortex completes its formation and pinches off from the trailing jet when the translational velocity of the ring becomes equal to the jet flow velocity near the ring. In addition, the experimental results of the gravity-driven starting jet will be compared to the results of Gharib et al. (1998), which are obtained from experiments by piston-cylinder mechanism, in order to examine the effect of generation mechanism on the final state of the leading vortex ring. According to the criteria for the state of the vortex rings in jet flow found by Glezer (1988), cases of both piston-driven and gravity-driven starting jets considered have Reynolds numbers less than 2×10^4, and thus they can be considered as laminar vortex rings. To make meaningful comparison between piston- and gravity-driven starting jets, all quantities, such as circulation Γ and kinetic energy E, are properly normalized in the analysis.

4.2.2 Translational velocity of the leading vortex ring

Based on theoretical results of the Norbury-Fraenkel family of vortex rings (Norbury, 1973; Fraenkel, 1972), the translational velocity U_{tr} can estimated as

$$U_{tr} = B\sqrt{\frac{\rho\Gamma^3}{\pi I}}, \tag{4.5}$$

where parameter B can be expressed as a function of ϵ as

$$B = \frac{1}{4}\sqrt{1+\frac{3}{4}\epsilon^2}\left[\ln\frac{8}{\epsilon} - \frac{1}{4} + \frac{3\epsilon^2}{8}\left(\frac{5}{4} - \ln\frac{8}{\epsilon}\right)\right], \tag{4.6}$$

where ϵ is defined as the dimensionless mean core radius of Norbury-Fraenkel family of vortices, ranging from 0 to $\sqrt{2}$. The translational velocity may be determined from the slope of the curve of the vortex ring's axial position against formation time from flow visualization results. After being normalized by the average exit velocities U_0 for different Reynolds numbers, they are plotted in figure 4.3. As shown, the ratios of the translational velocity to average exit velocity fall into a narrow range from 0.46 to 0.59. The velocities of vortex rings remain constant after they reach the steady state in Case 9 and 12, despite the fact that there is a slight decline with time due to the viscosity diffusion with ambient fluids. For smaller Reynolds number in Case 5, the translational velocity is initially close to the other two cases immediately after the pinch-off. However, because of the interaction with the subsequent vortex ring in the trailing jet which resulted in leapfrogging between them, the velocity of the leading vortex ring decreases markedly thereafter ($t^* > 3.0$).

Estimation for the translational velocity is crucial in the analytical models of vortex ring formation process. Mohseni and Gharib (1998) derived U_{tr} from the relation

$$\partial E/\partial I|_{\text{fixed }\Gamma\text{ and vol.}} = U_{tr}. \tag{4.7}$$

By applying the slug model, equation 4.7 leads to $U_{tr} = U_0/2$. But they also stated that the actual translational velocity of the real vortex rings should be more than $U_0/2$. Shusser and Gharib (2000a) predicted U_{tr} by using the mass conservation law to the trailing jet and the properties of Norbury-Fraenkel vortices. They found that U_{tr} is equal to $0.59U_0$ with core size $\epsilon = 0.5$. This value of ϵ corresponded to the experimental result of non-dimensional energy $\alpha_{\text{lim}} = 0.33$ (Its definition is given in Chapter 2). The translational velocity was also measured experimentally by Gharib et al. (1998). They found that the ratio of U_{tr} to U_0 was about 0.4575 for the steady translation vortex ring after pinch-off, which is a little smaller than the theoretical one as predicted above.

The values of U_{tr}/U_0 for Norbury-Fraenkel vortex rings at $\epsilon = 0.5$ and the previous experimental results are also plotted in figure 4.3. It is shown that the translation velocities for the gravity-driven starting jets with various Reynolds number are consistent with the theoretical prediction and are similar to that generated by the piston-cylinder arrangement, indicating that the leading vortex rings may belong to the Norbury-Fraenkel family of vortex rings with different but close mean core radius ϵ. However, further analysis is required to confirm the above statement based on other two dynamical invariants of vortex ring: normalized circulation and energy, which will be discussed in the next section.

4.2.3 Dimensionless circulation of the leading vortex ring

The dimensionless circulation γ is defined as

$$\gamma = \frac{\Gamma \rho^{1/3}}{I^{1/3} U_{tr}^{2/3}} = \frac{\Gamma_N}{\sqrt[3]{I_N U_N^2}} = f(\epsilon), \tag{4.8}$$

where subscript N indicates the dimensionless quantities of Norbury-Fraenkel family of vortex rings.

The γ in equation 4.8 is given in terms of the translational velocity of the

leading vortex ring U_{tr}. Shusser and Gharib (2000a) and Shusser et al. (2006) approximated the jet flow as a one-dimensional round jet of a variable cross section, whose diameter is equal to the jet diameter D near the jet exit and equal to the diameter of the vortex ring D_{ring} in the immediate vicinity of the ring. Therefore, according to the mass conservation law, the translational velocity of vortex at pinch off can be correlated to the jet velocity U_0. It gives another definition of dimensionless circulation,

$$\gamma' = \Gamma \left(\frac{\rho}{I U_0^2} \right)^{\frac{1}{3}}, \tag{4.9}$$

which is equivalent to the definition in equation 4.8 but avoids the difficulty of calculating the value of U_{tr}.

The comparison of theoretical value of γ' with the experimental results is presented in figure 4.4. As shown for Case 5, 9 and 12, the dimensionless circulation for the steady state vortex ring after pinch off are about 0.942, 1.147 and 1.263, respectively. For Cases 9 and 12, the dimensionless circulation correlated with the theoretical value well, with maximum deviation of about 9%. On the other hand, the obvious discrepancy for Case 5, as stated above, can be attributed to the interaction between the leading vortex rings and the first trailing vortex, by which the prediction of translational velocity by mass conservation is not valid any more. The value of this dimensionless circulation would be different for non-uniform exit velocity profile. This may be the reason for the difference in theoretical and experimental values presented above, since the time varying exit velocity profiles in gravity-driven starting jet are not uniform (Yu et al., 2007).

For these two different kinds of vortex ring generation mechanism discussed in this chapter, although there are no identical cases for comparison, Case 9 (Re = 3528) and one of the cases in Gharib et al. (1998) (referring to figure 10 in their paper) have similar Reynolds number for the final vortex ring (defined

as $\mathrm{Re}_\Gamma = \Gamma_{ring}/\nu \approx 6000$). The comparison of circulation for the two cases is plotted in figure 4.5 in dimensional form. The circulation of leading vortex rings for two cases are at the same level after the steady state has been reached. However, the total circulation of the gravity-driven starting jet is larger than that in the case of Gharib et al. (1998), although both increased almost linearly with the formation time t^*. Thus, it is conjectured that during the initial stage of starting jet, the over-pressure effect, which has been theoretically studied by Krueger (2005), on the rate of delivery of circulation and other integrals of motion would be different between the gravity-driven starting jet and the piston-cylinder arrangement. Because the over-pressure effect would shift the total circulation curve toward the left hand side in figure 4.5, the intersection point also moves toward the left. That is the reason why the gravity-driven starting jet has much smaller formation number at about 2.0 (Yu et al., 2007), in contrast to about 4.0 for the cases of Gharib et al. (1998).

4.2.4 Dimensionless energy of the leading vortex ring

The Kelvin-Benjamin variational principle states that the vortex ring pinches off at the instant when the apparatus is no longer able to supply energy at a level sufficient for ring growth. To apply this theory, the dimensionless kinetic energy defined as (the same as in equation 2.2a)

$$\alpha = \frac{E}{\sqrt{\rho I \Gamma^3}}. \tag{4.10}$$

is used to normalize the vortex ring energy. It is noted that Shusser and Gharib (2000a) defined the dimensionless energy in another form as

$$E_{nd} = \frac{4E}{\rho \pi D^3 U_0^2} \tag{4.11}$$

to illustrate the evolution of the jet and the leading vortex ring. Unlike the definition in equation 4.10, equation 4.11 is normalized by the quantities related to the generating jet (the jet exit diameter D and the average velocity at jet exit U_0) rather than to the vortex ring formation process (Γ and I).

First, the dimensionless energy E_{nd} of total flow and the leading vortex ring for Case 5, 9, and 12 are shown in figure 4.6. As shown, the energy delivered by the apparatus for all the three cases nearly collapses on the same line. However, the energy of the leading vortices does not. From the slug model, $E = 1/(8\pi D^2 \rho L U_0^2)$. Substituting this into the equation 4.11, we obtain $E_{nd} = L/(2D) = t^*/2$, which is only the function of the formation time t^*. The E_{nd} derived from the slug model is also shown in figure 4.6. As may have been expected, its value is smaller than the actual E_{nd} since the slug model neglects the effect of over-pressure during the onset of the jet development and underestimates the dynamic quantities of the total jet.

Figure 4.7 shows the results obtained using equation 4.10. The DPIV results show that the values of α for the steady vortex rings are within the range of 0.3 to 0.4, due to the scatter of the integrated quantities, for the three cases with different Reynolds number. The increase of α_{ring} in Case 5 indicates the leapfrogging phenomenon. Also shown in the figures are the prediction of α of the total jet flow by the slug model. Noting that α of total jet flow predicted by the slug model overestimates α of the apparatus because it mainly underrates the circulation delivered into flow due to uniform exit velocity profile assumption. For the case of Gharib et al. (1998), the formation number at 4.0 provided a value for α at about 0.33. However, for the present investigation, the limiting value of α within the range of 0.3 to 0.4 gives the approximately formation number roughly around 2. Similar to the dimensional circulation of the total jet and the leading vortex ring shown in figure 4.5, the effect of over-pressure is attributed to the fast drop in α_{total} compared to the results found in the

starting jet with piston-cylinder mechanism (Gharib et al., 1998). This effect is important only during the onset of the jet development. Despite the behaviors of the total energy α_{total} are different, the dimensionless energies of the leading vortex rings appear to converge to certain constant.

The finding of α for steady vortex rings provides us with the method to match their properties to those of Norbury-Fraenkel family of finite core vortex rings. For the axisymmetric steady vortex ring, the dimensionless energy is exclusively determined by the dimensionless mean core radius ϵ. Their γ_{ring} and α_{ring} range from about 1.71 and 0.557 ($\epsilon = 0.2$) to 2.7 and 0.16 ($\epsilon = \sqrt{2}$ for Hills spherical vortex), respectively. In figure 4.8, we compare the experimental results of γ_{ring} and α_{ring} to those inferred for the Norbury-Fraenkel vortices. It should be noted that the dimensionless circulation here is derived by equation 4.8 using translation velocity of the vortex ring. For all cases considered, it is shown that the dimensionless energy and circulation of leading vortex rings after pinch-off correspond to those of a member of the Norbury-Fraenkel vortex rings with ϵ in the range from 0.35 to 0.50. This value is close to $\epsilon = 0.5$ found in the piston-driven starting jets. It indicates that although the vorticity distribution of the leading vortex rings are different from that of Norbury-Fraenkel vortices which has the vorticity density $\omega/r = \text{const}$, the integrals of motion of the leading vortex ring α and γ are quite similar to those for the Norbury-Fraenkel vortices. Thus the leading vortex ring generated by the gravity-driven starting jet could also be approximated as a member of Norbury-Fraenkel vortices, and have comparable properties to those previously investigated for piston-driven arrangement (Mohseni et al., 2001).

4.3 Concluding remarks

Experimental results of Ai (2006) on the gravity-driven starting jets using Planar Laser Induced Fluorescence (PLIF) and Digital Particle Image Velocimetry (DPIV) over a range of Reynolds number from $1,179$ to $10,611$ are analyzed and discussed. The following remarks can be extracted from the preceding texts.

1. The penetration of jet tip beyond $t^* = 3.0$ may be expressed as $x_{tip}/D = C(tU_0/D)^{1/2}$ where the constant C is found to fall in the range of 3.15 to 4.08. This expression is found to be similar to the values obtained previously. The effects of vortex leapfrogging and over-pressure are important at the onset of the jet development but they dissipated away quickly.

2. The dimensionless circulation of leading vortex ring γ' (based on U_0) after pinch-off is found to be at around 1.26 which is in agreement with (to within 9%) the theoretical value obtained by Shusser et al. (2006).

3. The dimensionless energy of the leading vortex at the pinch-off is found to be within the range of 0.3 to 0.4 comparing to 0.33 obtained previously by Gharib et al. (1998) using a piston-cylinder arrangement. Again, the over-pressure effect causes a more rapid decrease in the dimensionless energy of the total jet, and as a consequence prompting a faster pinch-off.

4. The current investigation thus suggests that the final state of the pinch-off vortex may converge towards some sort of universal constants, i.e., the properties of the Norbury-Fraenkel family of vortex rings, which may also be independent of generation mechanism. In short,

$$\text{Formation number } F \approx 2.0;$$

$$0.3 < \alpha_{ring} < 0.4;$$

$$1.75 < \gamma_{ring} < 1.95;$$

$$0.35 < \epsilon < 0.50;$$

$$\gamma' \approx 1.26.$$

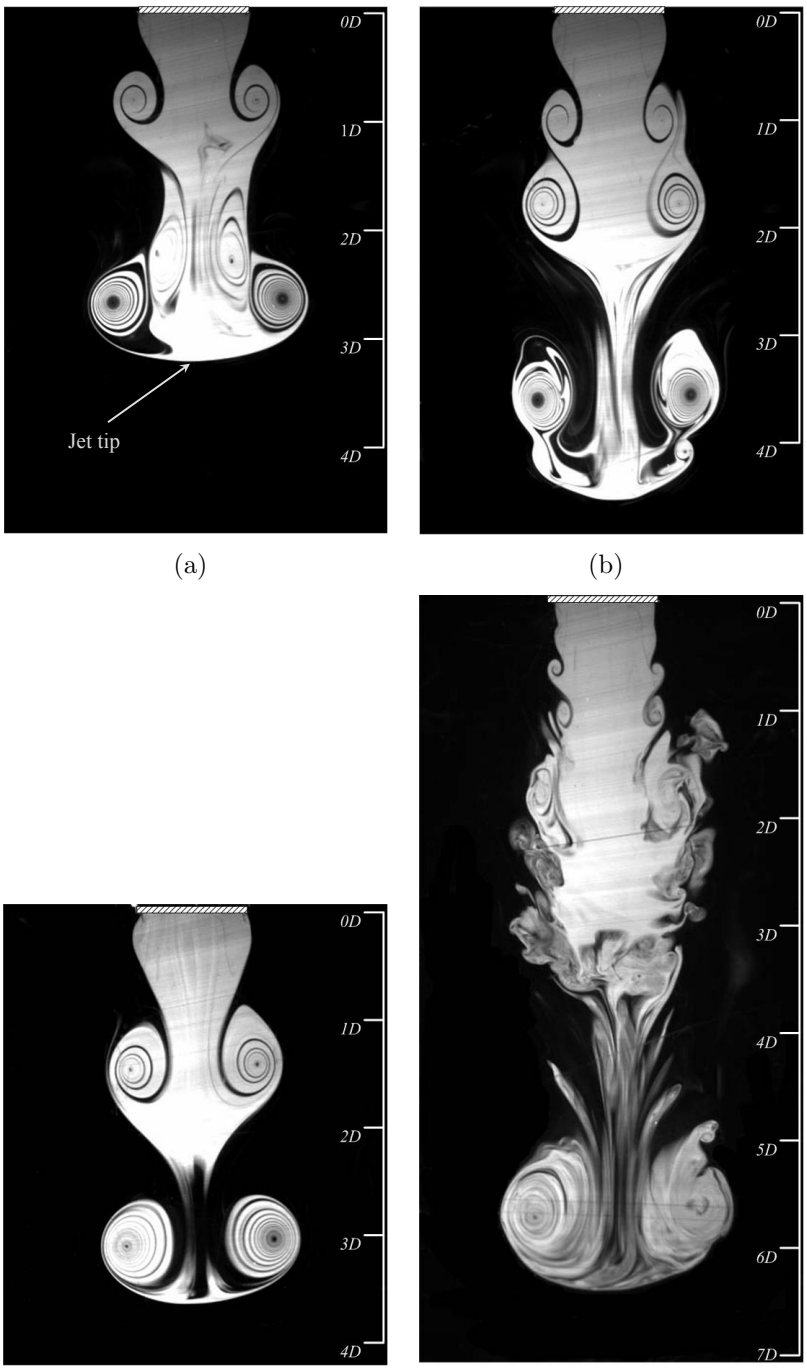

Figure 4.1: (a),(b) The leapfrogging of the first trailing vortex ring and the leading vortex ring for case 5 at $t^* = 4.80$ and $t^* = 6.55$. (c) The physical separation of the leading vortex ring for case 9 at $t^* = 5.66$. (d) The physical separation of the leading vortex ring for case 16 at $t^* = 10.18$.

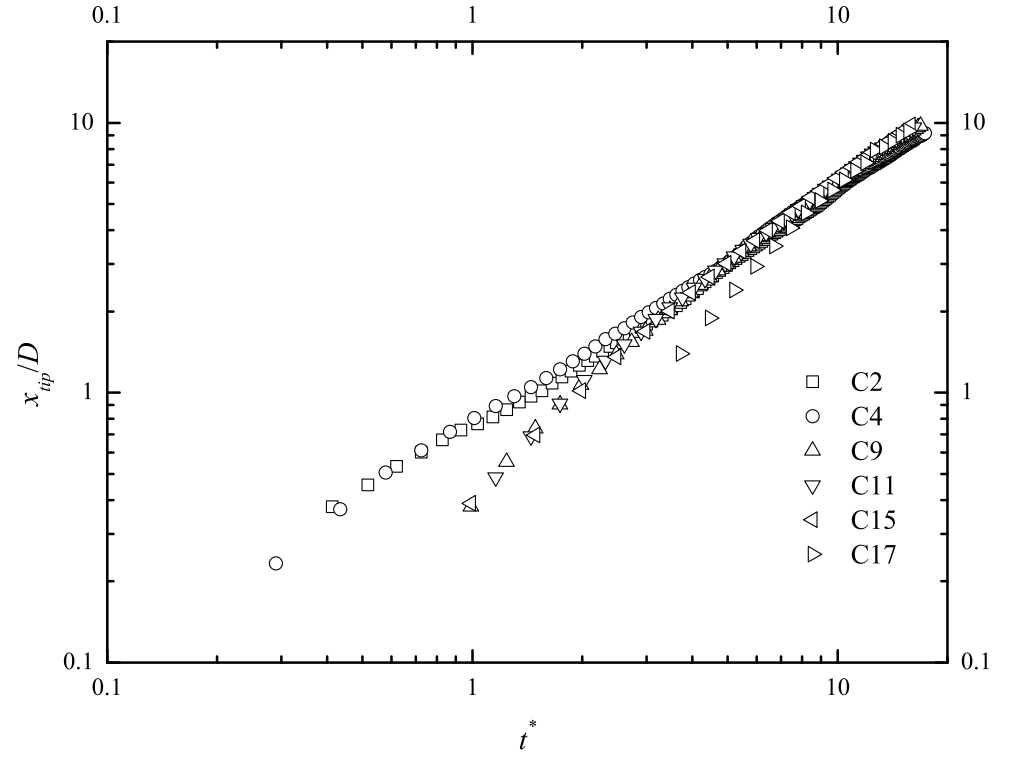

(a)

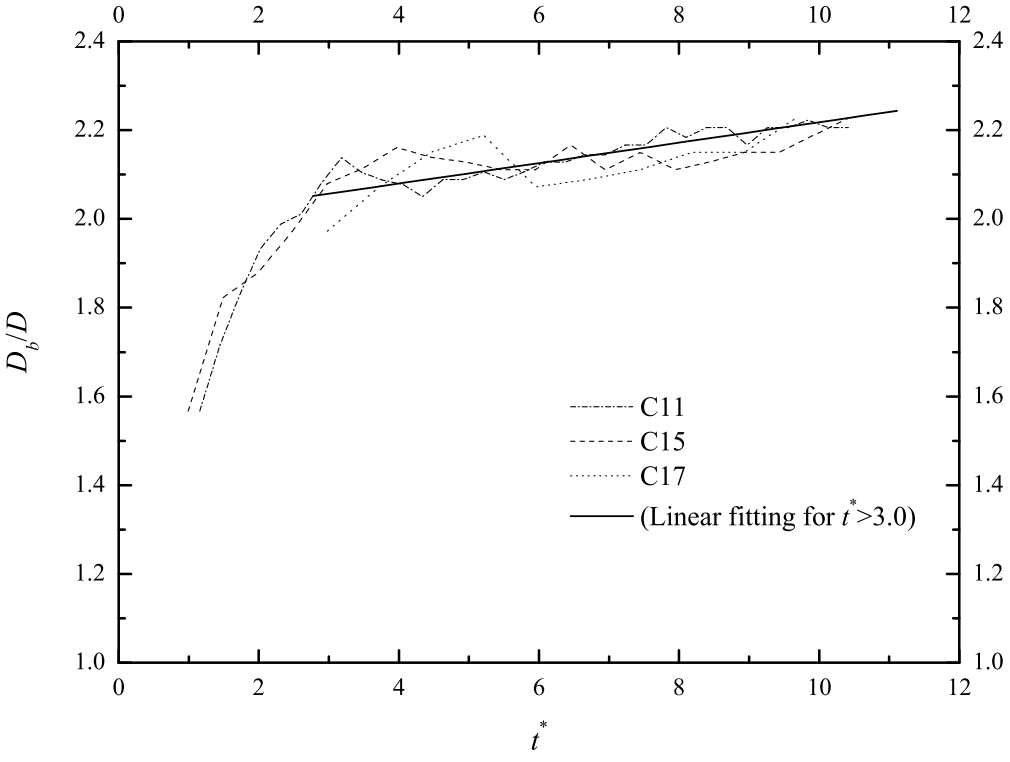

(b)

Figure 4.2: (a) Normalized penetration vs the formation time; (b) Growth of the diameter of the vortex ring bubble.

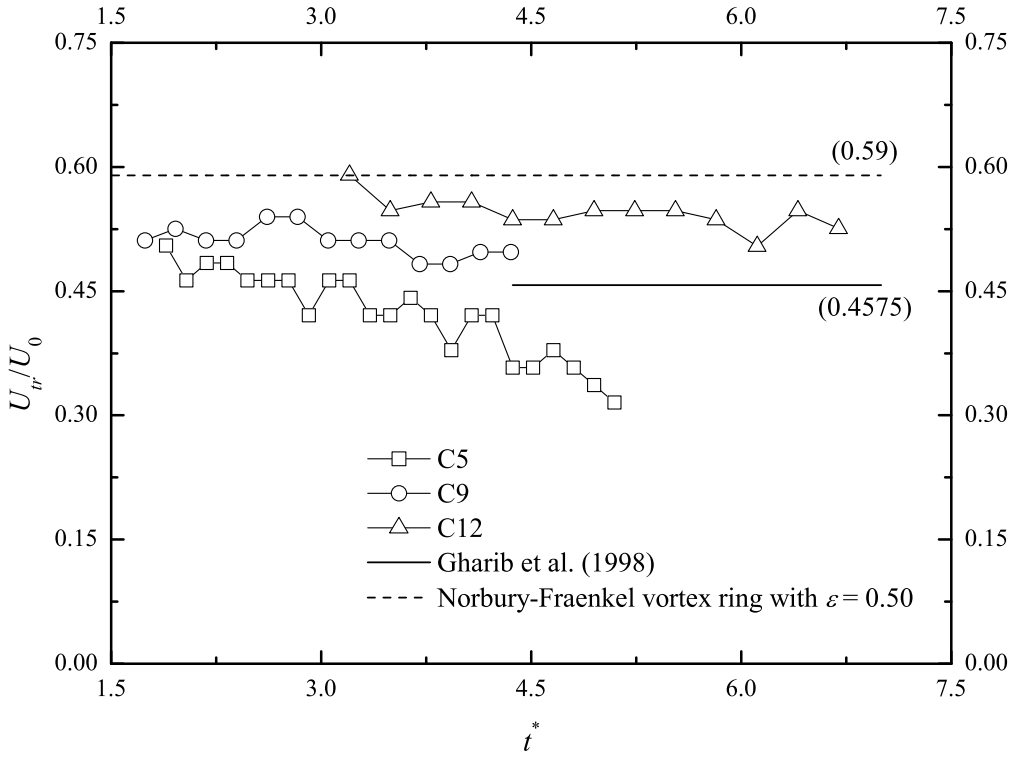

Figure 4.3: Translational velocity of the leading vortex ring.

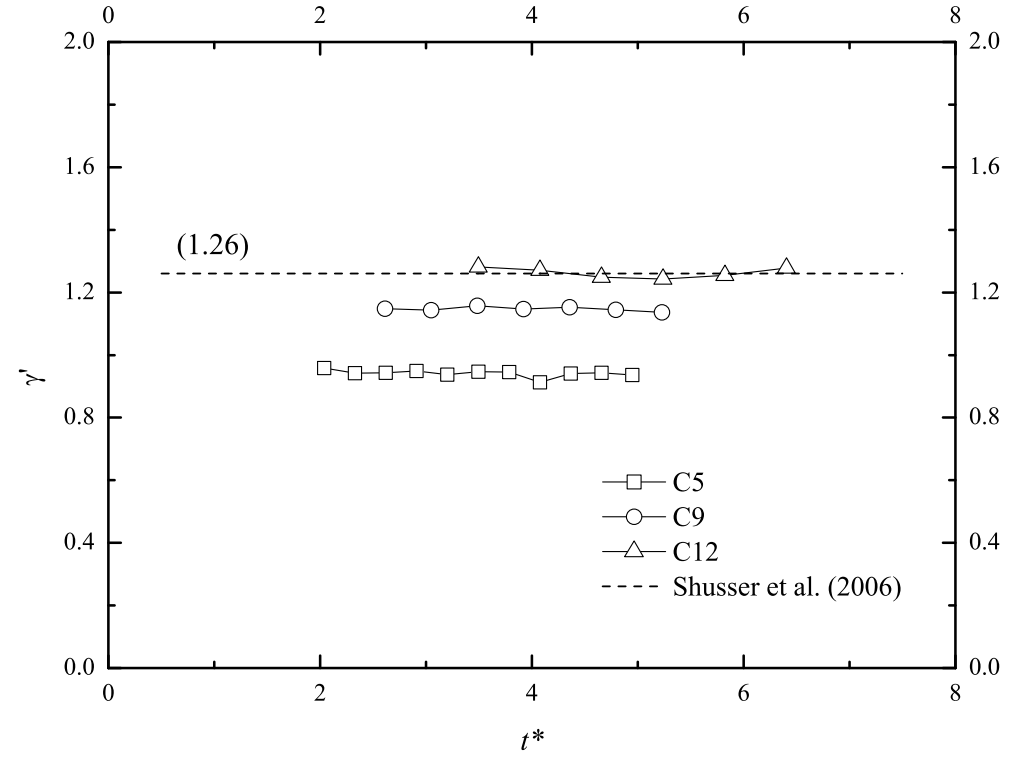

Figure 4.4: Comparison of the theoretical and experimental results of the vortex ring circulation (equation 4.9).

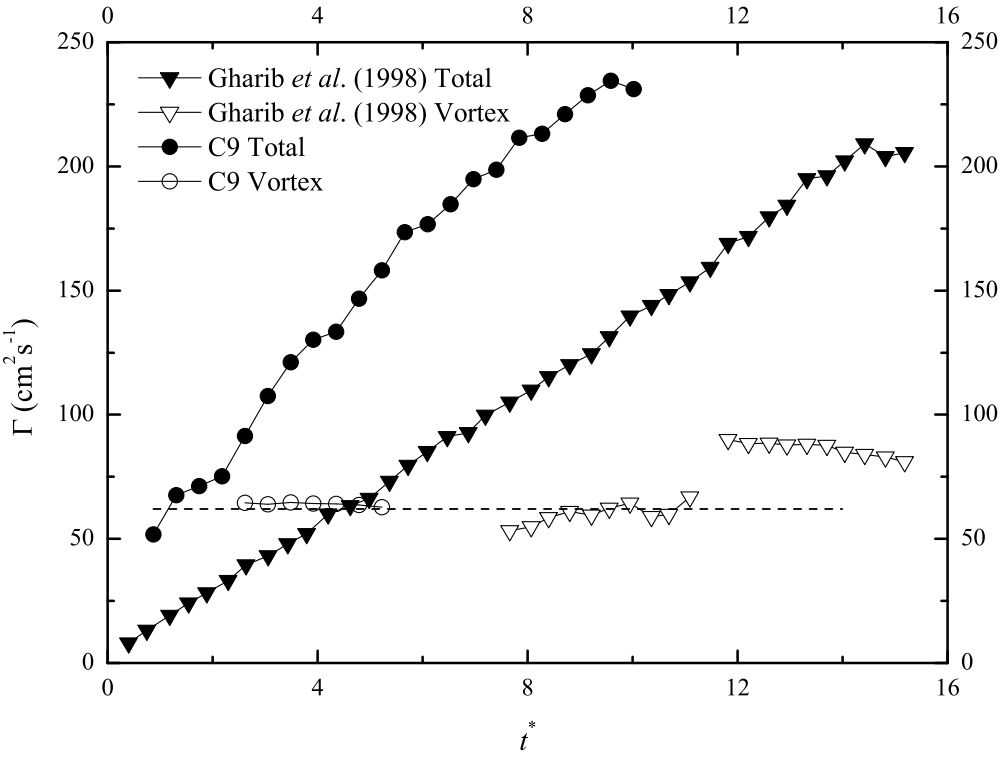

Figure 4.5: Circulation as a function of the formation time for case C9 and the experimental data of Gharib et al. (1998). Dash line indicates the circulation level of the pinched off vortex ring.

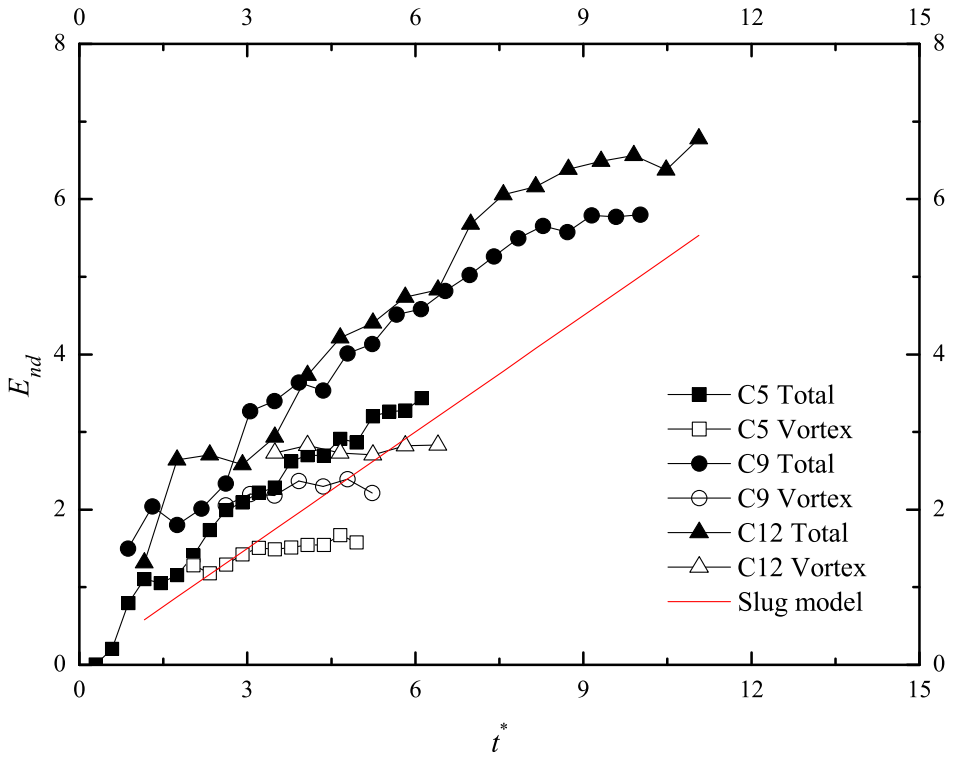

Figure 4.6: The dimensionless energy E_{nd} (equation 4.11) of the total fluid and the leading vortex ring as a function of the formation time.

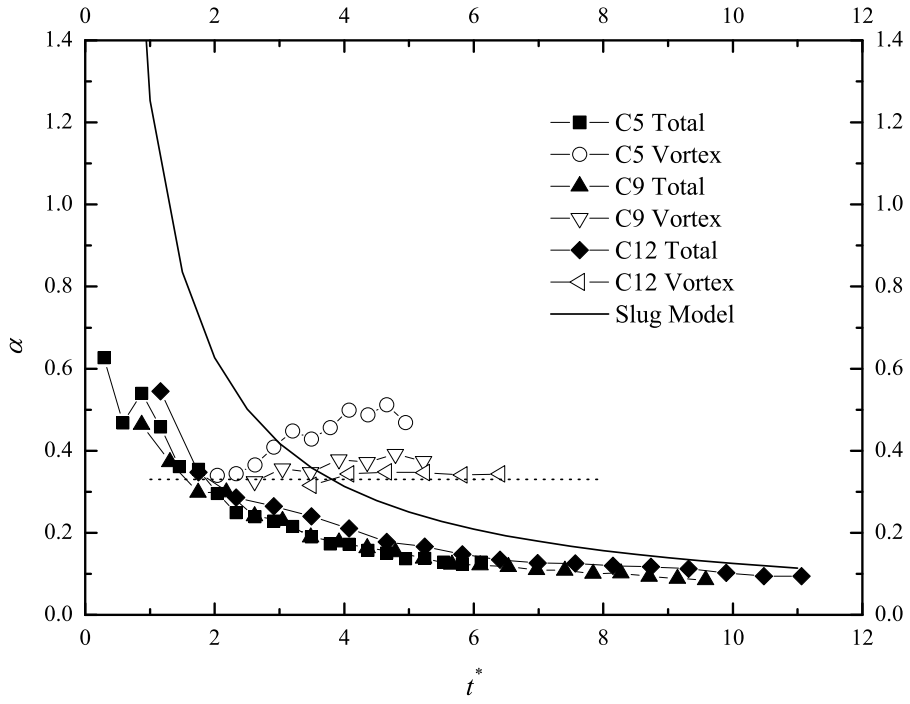

Figure 4.7: The dimensionless energy α of the total fluid and the leading vortex ring vary against the formation time t^* for different cases, and the corresponding limiting value of $\alpha_{\text{lim}} = 0.33$ (dot line).

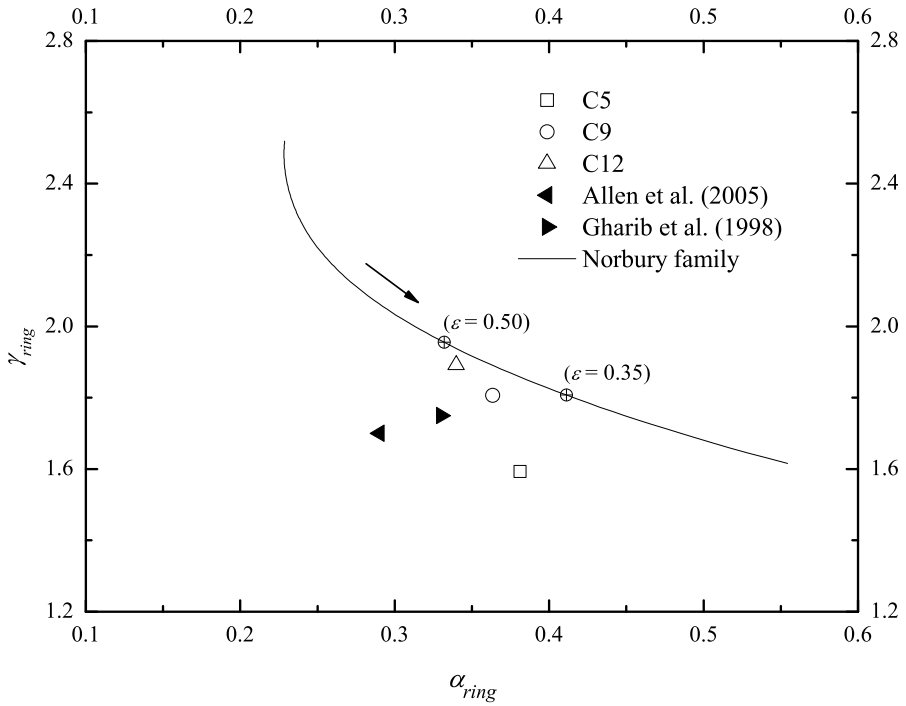

Figure 4.8: Comparison of α_{ring} and γ_{ring} with the theoretical values of Norbury-Fraenkel vortex rings; the arrow indicates the decreasing direction of the parameter ϵ.

Chapter 5

Development of Shear Layer in the Trailing Jet During Pinch-off

5.1 Introduction

According to the dynamic interpretation of the pinch-off process (Mohseni et al., 2001), the growth of the leading vortex ring is supported by the continuous influxes of mass as well as dynamic properties from its trailing jet until the complete separation of their vorticity fields. This physical mechanism was adopted in the model by Shusser and Gharib (2000a) for the pinch-off process, in which the trailing jet was approximated as a one-dimensional round jet of variable cross section. However, it has been observed in several experiments (Gharib et al., 1998; Schram and Riethmuller, 2001; Krueger et al., 2006) and numerical simulations (Rosenfeld et al., 1998; Mohseni et al., 2001; Wang et al., 2009) that the trailing jet would develop into a series of discrete vortices similar to those rolled up due to the Kelvin-Helmholtz instability. Zhao et al. (2000) investigated numerically the effects of trailing jet instability on vortex ring formation in the impulsively started jets with different flow parameters, like Reynolds number and shear layer thickness. Their results highlighted an important interaction

between the shear layer instability, which develops in the trailing jet at large formation times, and the dynamics of the leading vortex ring. Zhao et al. (2000) suggested that this interaction appears to accelerate the process of vortex ring pinch-off and has a significant effect on the vortex ring circulation.

This chapter is intended to investigate the interaction between the leading vortex ring and the trailing jet in a systematic way via experiments with particular attention on the trailing jet development. Focus would be on elaborating how the leading vortex ring would affect the instability characteristics of the trailing shear layer, as well as how the formation of trailing vortices would influence the pinch-off process. In addition, it had been observed in previous investigations (Gharib et al., 1998; Dabiri and Gharib, 2005; Wang et al., 2009) that the trailing vortices could be merged into the leading vortex ring as the jet develops, depending on flow conditions such as Reynolds number and velocity program. The merging of the trailing vortices usually leads to an abrupt addition of vorticity into the leading vortex ring. It also implies an important impact on the final disconnection of leading vortex ring from the trailing jet if the merging occurs during the pinch-off process. The combined effects of velocity program and Reynolds number on the vortex merging during the pinch-off process would be examined in detail.

The experimental setup for the results discussed in this chapter has already been described in Chapter 3. Starting jets are generated horizontally in a test tank using a piston-cylindrical arrangement. The diameter of the cylindrical nozzle D is 2.45 cm. The velocity of the piston is controlled by a solenoid valve and monitored by an ultrasonic flowmeter, which is connected to a PC via a data acquisition card. A total of 43 runs with different velocity program and Reynolds number have been conducted, but results from the three most representative piston velocity programs, as shown in figure 5.1, will be discussed here. The Reynolds number for these non-impulsively starting velocity programs

is defined as

$$\mathrm{Re}_D = \frac{U_{\max} D}{\nu}, \tag{5.1}$$

where $U_{\max}$ is the maximum $U_p(t)$ achieved during jet ejection. The flow conditions for the three cases are summarized in table 5.1. All the three cases have sufficient long duration so that the entire pinch-off process can be included.

Table 5.1: Summary of experimental parameters

Case	Maximum piston velocity $U_{\max}$ (m/s)	Reynolds number Re_D
C1	0.222	5600
C2	0.160	4100
C3	0.101	2600

5.2 Experimental results and discussion

5.2.1 Circulation of the leading vortex ring and the formation number

As established by Gharib et al. (1998), determination of the formation number requires the evaluation of the circulation of the steady vortex ring after its pinch-off and the total circulation supplied by the jet generator. Before proceeding to further discussion for the three cases, this important time scale is needed to be estimated first. The variation of the normalized total circulation and the vortex ring circulation, defined as

$$\Gamma_{nd} = \frac{\Gamma}{U_{\max} D}, \tag{5.2}$$

against the dimensionless formation time t^* are plotted in figure 5.2. The total circulation is obtained by integrating the vorticity contained within the lowest detectable contour level. This vorticity contour level is determined to be at 3.0 s^{-1}. Sensitivity analysis has been made by selecting different contour levels

at 4.0 s^{-1}, 3.0 s^{-1} and 2.0 s^{-1} as the boundary of the vortex ring. The circulation of the leading vortex ring is found to be sensitive to the choice of the cut-off level between 4.0 s^{-1} and 3.0 s^{-1}, especially at time after the leading vortex ring has pinched-off. At the limit of 2.0 s^{-1} level, noise signal would become unacceptable. As such, the vorticity contour level of 3.0 s^{-1} is chosen for the present experiment. As may have been expected, the total circulation increases almost linearly with time. Since the leading vortex ring continues to grow during its formation, a steady vortex ring can only be identified after $t^* > 7.0$. The dimensional circulation of the leading vortex ring in its final state are found to be at the level of approximately 84 cm^2s^{-1}, 77 cm^2s^{-1} and 61 cm^2s^{-1} for cases C1, C2 and C3, respectively. The corresponding formation numbers fall between 4.2 and 4.6 for each case, i.e., in good agreement with previous results of 3.6 to 4.5 for a broad range of flow conditions. It also verifies that the effect of non-impulsive velocity program tends to increase the formation number above $F = 4.0$ for impulsively staring jets (Gharib et al., 1998).

5.2.2 Qualitative observation of the trailing jet development

Besides the leading vortex ring, the large-scale coherent structures (CS), characterized by organized vorticity distribution, also exist in the shear layer of the trailing jet. The development of the coherent vortical structures in starting jets is to be examined in terms of the temporal evolution of the vorticity contours, as shown in figures 5.3, 5.4 and 5.5, for the three cases. In general, it can be seen that the vorticity field of the leading vortex ring remains connected to the trailing jet at the formation number, indicating that the leading vortex ring continues to absorb fluids and gain circulation from the generating jet during the pinch-off process. The physical separation between the leading vortex ring and the trailing jet happens at a later time, within a range of $t^* \approx 7 \sim 8$ for differ-

ent velocity programs. Thus the pinch-off process would take $3 \sim 4$ formation time units to complete. In a similar experiment by Krueger et al. (2006), the separation occurs at about $t^* \approx 9$ in terms of the vorticity contours (see figure 5 (d), (e) in their paper) for an impulsively starting jet with Reynolds number of $\mathrm{Re}_D = 1270$. One may speculate further that the physical separation might be delayed by lowering the Reynolds number.

By examining carefully the vorticity contour evolution, it can be observed that the earlier separation of vorticity fields at large Reynolds number cases (C1 and C2) may be associated with the formation of the trailing vortices and the merging of the first trailing vortex ring into the leading vortex ring. For C2, a small concentrated vorticity distribution, which will evolve to a secondary vortex, can be distinguished in the trailing jet near the nozzle exit at $t^* = 4.933$, as indicated by a arrow in the magnified vorticity contours (figure 5.4(f)). This initial CS in the trailing shear layer would grow in size and strength as the jet continues, and gradually develop into the first trailing vortex ring. Under the influence of the induced velocity by the leading vortex ring, the trailing vortex ring, with relatively weaker strength comparing to the leading one, would shrink in the radial extent and subsequently accelerate forward to the leading vortex ring (see figure 5.4(d)). This process in fact is very similar to the leapfrogging phenomenon for two coaxial vortex rings (Maxworthy, 1972; Riley and Stevens, 1993; Lim, 1997). In the present experiments, however, the first trailing vortex is entrained into the leading vortex ring instead of catching up with it and then emerging in front of it. This is mainly due to the fact that the trailing vortices are much weaker than the leading vortex ring. As a result of vortex merging, the circulation of the first trailing vortex ring is absorbed by the leading vortex ring, as indicated by the stepwise increase in vortex ring vorticity in figure 5.2. The vortex merging process would speed up the progress of the circulation acquirement of the leading vortex ring, which, otherwise, is performed by the

continuous vorticity flux from the trailing shear layer. Therefore, due to the entrainment of the first trailing vortex, complete separation of the new leading vortex ring with the trailing jet would be achieved earlier than cases without vortex merging.

Because of the limited temporal resolution of our DPIV system, the vorticity contours cannot show the continuous change of the CS. But the process of vortex merging can still be implied by the distorted structure of the vorticity contours of the leading vortex ring after the first trailing vortex ring is drawn into it, see figure 5.4(e). As the trailing vortex ring acts as a large disturbance to the leading one, the vorticity distribution within the core of the leading vortex ring will be rearranged towards its steady state (belonging to the Norbury-Fraenkel family of vortex rings). Similar temporal evolution of vortical structures in the trailing jet is also observed in C1. However, the vortex merging is not observed before the completion of the pinch-off process in C3. It seems that whether the vortex merging would occur during the pinch-off process is Reynolds number dependent.

As noted above, different behavior of the vortex merging process for the three cases may be associated with the evolution of trailing vortices at different Reynolds number. The trajectory of the first (V1) and second (V2) trailing vortices are plotted in figure 5.6. As shown, the first trailing vortex at different Reynolds numbers firstly rolls up at formation time $t^* \approx 4.8$ and at the axial position of $x/D \approx 0.35$. Since the trailing vortices are the direct result of the development of instability in the shear layer, figure 5.6 suggests that the growth of disturbance in the trailing shear layer is insignificant before the formation number. Trajectories of trailing vortices for the three cases also show that decreasing the Reynolds number of the starting jet would delay the formation of both the first and second trailing vortices slightly. Because the trailing vortices form later (in terms of the formation time) at smaller Reynolds number, the

distance between the leading vortex ring and the first trailing vortex would be greater, as shown in figure 5.7. Therefore, the interaction between them, which leads to the vortex merging process, is less likely to happen. Moreover, as shown in figure 5.6, the first trailing vortex in C1 and C2 disappears after $t^* \approx 6$ and 7 respectively because they are merged into the core of the leading vortex ring during the pinch-off process. In C1 (with the highest Reynolds number among the three cases), the second vortex merging between the new leading vortex ring (by engulfing the first trailing vortex) and the second trailing vortex is observed at about $t^* = 9$. For smaller Reynolds number case (C3), the first and second trailing vortices can develop fully into tight spirals and persist in the trailing jet even after the the end of the pinch-off process. Experimental results at larger formation time ($t^* > 8$) shows that the first merging in C3 occurs as late as $t^* \approx 11$. Based on the dynamics of the trailing vortices, it is believed that their formation and interaction with the leading vortex ring determine the characteristics of the pinch-off process, i.e. how the vorticity fields of the leading vortex ring and trailing jet separate. To explain further these effects of the tailing jet development, it is important to investigate the delivery of the dynamics properties by the trailing jet into the leading vortex ring.

5.2.3 Vorticity and momentum fluxes

For the following analysis, the focus will be on C2 ($Re = 4100$) where the formation number is about 4.6. We first examine the evolution of axial vorticity and momentum fluxes in the starting jet. The vorticity and momentum fluxes at each axial location in the ground coordinate system are defined as,

$$\frac{d\Gamma}{dt} = \int_0^\infty \omega(x,r)u(x,r)dr, \tag{5.3a}$$

and

$$\frac{dM}{dt} = \int_0^\infty 2\pi\rho u^2(x,r) r dr, \tag{5.3b}$$

respectively. The integration is conducted by a forth-order-accurate quadrature scheme at every axial position. Their axial variations are plotted in figure 5.8 at successive t^* during the initial formation stage and pinch-off process. As shown in figure 5.8(a), the momentum flux increases monotonically from the nozzle exit plane to the position of the vortex ring core before the formation number ($t^* = 3.067$). As the leading vortex ring travels further downstream, the trailing jet appears behind it (at $t^* = 3.964, 4.933$) and the momentum flux in the trailing jet seems almost constant, corresponding to the properties of a free jet stem. However, at $t^* \geqslant 5.957$, the momentum flux has a minimum value near the bottom of the leading vortex ring, indicating a drop of momentum added into the leading vortex ring. By $t^* = 8.096$, a secondary peak of momentum flux becomes obvious in the trailing jet, which, according to the vorticity contour evolution shown in figure 5.4, corresponds to the second trailing vortex ring. From figure 5.8(a), it can be concluded that conservation of momentum along the trailing jet can only be applied before the formation number in a starting jet, but it becomes not applicable owing to the formation of trailing vortices. Despite the variation of momentum flux in the trailing jet under the influence of the trailing vortices, its absolute value near the bottom of the leading vortex ring is not affected significantly.

Figure 5.8(b) presents the variation of axial vorticity flux in the starting jet. Before the formation number ($t^* = 3.067,\ 3.964$), the vorticity flux decreases slightly from the exit plane to a minimum just behind the leading vortex ring due to the viscous diffusion. When the leading vortex ring starts to pinch off from the trailing jet ($t^* = 4.933$), the decrease in vorticity flux at the rear of the leading vortex ring becomes more appreciable than that in the momentum flux, as the forming trailing vortices affect the vorticity distribution along the trailing

jet. At $t^* = 5.957$, a small peak of vorticity flux behind the leading vortex ring appears, corresponding the first trailing vortex. It is noted that the distortion of vorticity flux in core region of the leading vortex ring at $t^* = 7.022$ is the direct result of the vortex merging process (see figure 5.4(d)), which leads to a further drop in vorticity flux between the leading vortex ring and the trailing jet. By $t^* = 8.096$, a sharp secondary peak of vorticity flux at $x/D \approx 1.5$ suggests that the secondary trailing vortex is absorbing vorticity around itself, leading to the vanishment of the vorticity flux being fed into the leading vortex ring. Since no more vorticity will be added into the leading vortex ring, the pinch-off process should be completed by this time. The critical time of physical separation in case C2 should therefore be less than 8. Comparing it with figure 5.8(a), it can be seen that the momentum flux only has a slight drop while the vorticity flux has already disappeared. Thus, one may speculate that the growth of the leading vortex ring is supported mainly via the vorticity transportation, rather than the momentum or the kinetic energy flux. Due to the rapid decrease in vorticity flux, fluids in the trailing jet with mainly momentum and kinetic energy cannot be entrained into the core of the leading vortex ring any more, and cannot maintain its continuous growth. The fluids, instead, may serve to push the leading vortex ring forward as a solid body, i.e., only delivering momentum, until the translation velocity of the leading vortex ring U_{tr} exceed that of the generating jet.

A more direct way to show the effect of instability on the vortex ring pinch-off is to examine the flux quantities entering the leading vortex ring. By taking into account the translational velocity of the leading vortex ring U_{tr}, the relative vorticity and momentum flux feeding into the ring can be calculated, at the bottom of the leading vortex ring (the position of minimum vorticity flux behind

the ring) shown in figure 5.9, as,

$$\left.\frac{d\Gamma}{dt}\right|_r = \int_0^\infty \omega(x,r)[u(x,r) - U_{tr}]dr, \text{ and} \tag{5.4a}$$

and

$$\left.\frac{dM}{dt}\right|_r = \int_0^\infty 2\pi\rho u(x,r)[u(x,r) - U_{tr}]rdr, \tag{5.4b}$$

respectively, where U_{tr} is estimated by tracking the position of the maximum vorticity in the vortex ring core (referring to figure 5.10).

In figure 5.9, the vorticity and momentum fluxes relative to the leading vortex ring are plotted against the formation time t^*. Although the general trends for both vorticity and momentum fluxes before the formation number are similar, their quantitative behaviors are different. The initial acceleration of the piston has more appreciable effect on the momentum flux than the vorticity flux. After the formation number is reached, the vorticity flux starts to decrease gradually up to $t^* \approx 6$ under the influence of the first trailing vortex formation, while the momentum flux still continues to increase albeit with decreasing rate. The sudden jump in the vorticity flux at $t^* \approx 7$ should be attributed to the vortex merging process that takes place between the leading vortex ring and the first trailing vortex. The momentum flux is only slightly affected by the merging process, due to the fact that the first trailing vortex is not fully developed and has little influence on the irrotational flow around itself. When the vortex merging process completes, the vorticity flux drops sharply to almost zero at $t^* \approx 8$, corresponding to the end of the pinch-off process. Moreover, the second peak of both fluxes at $t^* \approx 10.3$ should correspond to the subsequent vortex merging between the pinched-off vortex ring and the second trailing vortex. The momentum flux into the leading vortex ring eventually vanishes at $t^* > 11$ when the formation of subsequent secondary vortices would become dominant in the trailing jet. The second vortex merging process is also observed in C1.

According to the discussion above, the trailing vortices start to affect the momentum and vorticity fluxes after the formation number that signifies the onset of the pinch-off process. The formation of the trailing vortices leads to the decrease in the vorticity and momentum fluxes fed into the leading vortex ring, especially in the vorticity flux. In terms of the relative vorticity flux, the pinch-off process completes at formation time $t^* \approx 8$. Multiple merging of the leading vortex ring with trailing vortices would possibly occur during the pinch-off process, depending on the Reynolds number. It is also noted that these fluxes, i.e., the rate at which the integrals of motion are 'delivered' to the leading vortex ring, would appear to vary when some manipulation techniques (such as variable exit size or imposing an external background flow) are used in the jet ejection process, resulting in different properties of the final vortex ring.

5.2.4 The instability of shear layer in the trailing jet

The preceding results show that the formation and growth of the trailing vortices can be attributed to the drop in vorticity and momentum fluxes during the pinch-off process and the subsequent separation of the leading vortex ring with the trailing jet. In this section, we intend to investigate the characteristics of the trailing jet instability as the starting jet develops, and to examine the factors that affect the trailing shear layer instability. According to the linearized stability theory, the in stability of axisymmetric parallel flows, like the shear layer in the starting jet, is determined by the velocity profile of the basic flow. Thus, the velocity profiles of the shear layer in the trailing jet during the vortex ring formation and pinch-off process will be examined below.

It is well known that the axisymmetric shear layer is inviscidly unstable to infinitesimal disturbances via the Kelvin-Helmholtz instability mechanism. For the trailing shear layer, it is reasonable to regard it as an axisymmetric unidirectional flow because of the negligible radial velocity component. Axial

velocity profiles of the trailing jet at several streamwise positions are plotted in figure 5.11 at two instances, i.e., before and immediately after the formation number. The difference between the velocity profiles at these two instances lies in the variation of its velocity profile along the axial direction. At $t^* = 3.067 < F$ (figure 5.11(a)), the axial velocity in the shear layer region at downstream location ($x/D = 0.409$) drops more smoothly, from U_0 at the jet centerline to zero at the outer boundary of the shear layer, than at upstream locations ($x/D = 0.032$ and 0.221). The radial expansion of the shear layer suggests that it becomes thicker near the leading vortex ring. In contrast, during the pinch-off process (figure 5.11(b)), the shear layer only expands slightly along the trailing jet, i.e., similar to the situation of a free shear layer. The trailing shear layer, just issued from the nozzle exit ($0 < x/D < 0.5$), is thinner during the pinch-off process than before this process (figure 5.11). According to the theory of instability for axisymmetric shear layer (Batchelor and Gill, 1962; Kambe, 1969), a velocity profile having a steep gradient will be more unstable than the flow with slowly varying profile. Therefore, the shear layer near the nozzle exit plane, where the possible disturbance could be initially introduced, would be more unstable during the pinch-off process than before. One then can speculate that the formation and growth of the trailing vortices would be the consequence of the more unstable trailing shear layer after the formation number of the starting jet is achieved. Due to the more unstable nature of the trailing shear layer when $t^* > F$, random disturbances would be amplified at greater rate when they are convected downstream. The deformed shear layer then gradually rolls up in a series of trailing vortices, which in turn change the vorticity and momentum fluxes fed into the leading vortex ring. So it is appropriate to state that the variation in the velocity profile near $t^* = F$ leads to the different characteristics of the trailing shear layer instability before and during the pinch-off process.

While the above results have related the instability of the trailing shear layer to its velocity profile, the reason for the change in the velocity profile is still unclear. By considering the translation of the leading vortex ring relative to the nozzle exit, it is found that the trailing shear layer is under the influence of the induced velocity field by the leading vortex ring. At the initiation of starting jet, the radial velocities near the nozzle exit mainly directs outward due to the initial over-pressure effect (Krueger, 2005). The separated shear layer would then roll up into a leading vortex ring near the nozzle exit. After its initial formation by absorbing circulation from ejected fluid, the leading vortex ring would translate downstream from the exit plane and a trailing jet appears connecting the source and the vortex ring. Consequently, the leading vortex ring would induce inward radical velocity components in the immediate vicinity upstream. As shown in figure 5.12(a), at $t^* = 3.067$ the trailing shear layer within the region $x/D = 0 \sim 0.5$ is subjected to the influence of this induced radial velocity. At $t^* = 4.933$ when the leading vortex ring core has moved downstream to $x/D \approx 1.4$, it is found in figure 5.12(b) that the induced radial velocity becomes almost negligible (less than 4% of the local axial velocity) in the region $x/D = 0 \sim 0.5$. It implies that at this time the shear layer in this region can be considered as a free shear layer without the influence of the leading vortex ring.

The influence of the induced radial velocity of the leading vortex ring can be interpreted in terms of its gradients along the radial direction. The temporal development of radial velocity distribution at $x/D = 0.409$ is plotted in figure 5.13. It shows that at $t^* = 3.067$ the trailing shear layer, whose extent can be found to be at about $0.3 < r/D < 0.7$ from figure 5.11(a), bears negative radial velocity gradient $\partial v/\partial r < 0$. The negative $\partial v/\partial r$ serves to enhance the momentum exchange between the ejected fluid in the trailing jet and the ambient fluid with relatively low velocity, via pushing the ambient fluid towards the

trailing jet. As a result, the velocity profiles in the shear layer would spread out radially. As the leading vortex ring translates downstream further, its induced radial velocities near the nozzle exit would die out gradually (as shown at $t^* =$ 3.964 and 4.933 in figure 5.13). The trailing shear layer could persist the velocity profile of a free shear layer after ejection. Since the induced velocity of the leading vortex ring diminishes as the distance to the ring core increases, the instability would be expected to develop first near the nozzle exit due to the less stabilizing effect from the leading vortex ring.

From the experimental results in the present study, the interaction between the leading vortex ring and the trailing jet and its influence on the vortex ring pinch-off have been illustrated. The leading vortex ring would exert a stabilizing effect on the trailing shear layer behind it by means of the negative gradient of the induced radial velocity $\partial v/\partial r$. As the leading vortex ring travels downstream away from the nozzle exit, its corresponding effect near the nozzle exit will become weaker than before the formation number, resulting in the more unstable shear layer near the nozzle exit and the subsequent roll-up of the trailing vortices. Further growth of the trailing vortices leads to the decrease in the vorticity and momentum fluxes fed into the leading vortex ring, which results in the separation of the leading vortex ring with the trailing jet. Therefore, we may conclude that in starting jets, it is the development of the instability of the trailing shear layer that has limited the growth of the leading vortex ring with greater circulation.

5.3 Pinch-off mechanism in terms of the trailing jet instability

As introduced in Chapter 2, the limiting process of the vortex ring formation in starting jet can be considered as the outcome of the Kelvin-Benjamin variational principle for steady axis-touching vortex rings. In the interpretations for

the pinch-off process (Gharib et al., 1998), the limiting value of the dimensionless energy α_{lim} for the final vortex ring may vary depending on generation mechanism or parameters of the starting jet. It was found that $\alpha_{\text{lim}} = 0.33 \pm 0.01$ for piston-cylinder mechanism. The determination of α_{lim} restricts the application of the theoretical explanation to different mechanisms of starting jets. With the understanding of the significant role of the trailing jet instability in the pinch-off process, we intend, in this section, to discuss a more general mechanism for the vortex ring pinch-off in starting flows in terms of the stabilizing effect of the leading vortex ring on the trailing shear layer. The pinch-off mechanism proposed in present study would offer an appropriate explanation on the widely observed variation in the formation number as well as the properties of the leading vortex ring, e.g. its dimensionless energy and circulation, in several different types of vortex ring generators.

5.3.1 Criterion for the initiation of the trailing jet instability

According to the experimental observation of coincidence the formation number and the roll-up of the trailing vortices, we assume that the vortex ring starts to pinch off when the initial disturbance corresponding to the first trailing vortex starts to develop in the trailing shear layer. And the instability characteristics of the trailing jet is found to be associated with the induced radial velocity of the leading vortex ring v_i, The greater radial velocity is induced, the less unstable the shear layer should be. This relation introduces the possibility that the magnitude of v_i at the nozzle exit can be used as a parameter to identify the initial development of the first trailing vortex in the trailing shear layer, i.e. the onset of the vortex ring pinch-off.

Theoretically, for incompressible flow, the velocity field $\mathbf{u}(\mathbf{x})$ induced by a

specific vorticity distribution $\omega(\mathbf{x})$ can be expressed as

$$\mathbf{u}(\mathbf{x}) = \frac{1}{4\pi} \int \frac{\omega(\mathbf{x}') \times \mathbf{r}}{r^3} d\mathbf{x}', \tag{5.5}$$

where $\mathbf{r} = \mathbf{x} - \mathbf{x}'$ and $r = |\mathbf{r}|$ (Saffman, 1995). Equation 5.5 suggests that the magnitude of v_i depends on the distance to the core region of the leading vortex ring, and the magnitude and distribution of vorticity in the ring. In starting jet, however, it is difficult to determine analytically the vorticity distribution of a unsteady vortex ring during its formation stage. With appropriate simplification, the details of the vorticity in the leading vortex ring could be accounted by its integration, i.e. circulation. Then v_i near the nozzle exit (at about $x/D \approx 0$) could be determined by two parameters, namely the axial location of the vortex ring core x_{core} and the circulation of the leading vortex ring Γ_{ring}. In addition, it is known that the instability of the axisymmetric shear layer is dependent on the strength of the shear layer, i.e., the velocity difference ΔU between the stream and ambient flow.

Based on the above discussion on the relation of induced radial velocity with the dynamics of the leading vortex ring, a dimensional analysis is conducted to determine the dimensionless parameters related to the instability characteristics of the trailing shear layer. The variables associated with v_i near the nozzle exit include the circulation of the leading vortex ring Γ_{ring}, the axial trajectory of its core x_{core}, the strength of the shear layer ΔU (equal to U_0 when the jet is issued in a quiescent ambient fluid). Therefore, we can write the expression for the radial velocity v_i in the trailing shear layer as

$$v_i = f(\Gamma_{ring}, x_{core}, \Delta U). \tag{5.6}$$

Using dimensional analysis, the value of dimensionless radial velocity $v_i/\Delta U$ is

found only to depend on the dimensionless parameter A, defined as follows:

$$\frac{v_i}{\Delta U} = f(\frac{\Gamma_{ring}}{x_{core}\Delta U}) = f(A). \tag{5.7}$$

This functional relation suggests that the magnitude of v_i is determined only by the value of dimensionless parameter A. It is then reasonable to conjecture that the first trailing vortex would start to develop at a critical value of A, which will be examined by the present experimental results.

The value of A against the formation time for the three cases at different Reynolds number is plotted in figure 5.14. In the calculation of A, the trajectory and the integration region for circulation are obtained from a continuous sequence of vorticity counters for the starting jets. Within the accuracy of the experimental data, it seems that the curves of A for the three cases are almost identical, implying a universal characteristic of the starting jet. As the starting jet proceeds, A decreases monotonically. The physical implication of A is that it represents the capability of the leading vortex ring to suppress the exponential amplification of the perturbations in the trailing shear layer to approach the nonlinear development regime. The greater the value of A is, the less unstable the trailing shear layer would be. Since the formation of trailing vortex ring appears only after the formation number, we assume that the formation number should actually coincide with the time of the disturbance that could later evolve into the first trailing vortex is about to be issued from the jet exit. This assumption leads to a straightforward method to determine the critical value of A (A_c) corresponding to the critical time, by the formation number found in the present experiments. It is shown in figure 5.14 that A is approximately equal to 1.1 ± 0.1 for three cases at their respective formation number $F = 4.2 \sim 4.6$. Thus, one can conclude that, based on a simple dimensional analysis and experimental results, the critical value of the dimensionless parameter A below which

the disturbances in the shear layer would magnify and subsequently develop into trailing vortices, is found to be in a narrow range of 1.1 ± 0.1. Note that the preliminary result of the critical value of A could be refined if it can be derived analytically by means of the hydrodynamic stability analysis and the solution for the induced velocity of the leading vortex ring. It is an interesting topic for further study.

This quantitative result about the trailing jet instability may suggest a criterion for determining the formation number in the starting jet, which states that the leading vortex ring starts to pinch off when the parameter A of the starting jet decrease to a critical value $A_c \approx 1.1$. Although the universality of A_c still needs to be verified in different types of starting flows, it could be hinted to some extent by the fact that the instability of the trailing jet is independent of the final state of the pinched-off leading vortex ring, which may vary among different vortex generation mechanisms. Therefore, the criterion based on the instability parameter A should be more robust and general in predicting the formation number (i.e. the onset of pinch-off process).

5.3.2 Dynamic mechanism of the pinch-off process

By the slug model, the dimensionless energy of the total ejected fluid α_{total} decreases inexorably as the formation time. On the other hand, α_{ring} diminishes as the core of the leading vortex ring thickens. By straightforward reasoning, vortex ring formation process should be restricted by the thickest vortex ring, i.e. Hill's spherical vortex, with $\alpha_{ring} = 0.16$ (Linden and Turner, 2001). However, Gharib et al. (1998) and many followings obtained $\alpha_{\text{lim}} = 0.33 \pm 0.01 > 0.16$ for pinched-off vortex ring in starting jets. They suggested that the limiting dimensionless energy α_{lim} is an unknown parameter that depends on the peakiness of the vorticity profile which in turn depends on velocity program and Reynolds number. Therefore, the reason why the leading vortex ring cannot

evolve into a thicker one in starting jets with piston-cylinder arrangement until $\alpha_{ring} = 0.16$ is still not resolved yet. The failure to produce the thickest vortex ring also suggest that there might be other underlying mechanisms, rather than the Kelvin-Benjamin variational principle, restricting the vortex ring formation process. From the above experimental results and discussion, it is reasonable to speculate that the vortex ring pinch-off should be the consequence of the decrease in vorticity fed into the leading vortex ring due to the formation of trailing vortex rings.

It has been established that the trailing jet instability plays a determinant role in the formation of the leading vortex ring in starting jets. Its influence on the pinch-off process is achieved through the growth of trailing vortices which decreases the vorticity supply into the leading vortex ring. The fundamental mechanism for the vortex ring pinch-off would be that the trailing jet can no longer supply sufficient circulation (or vorticity) relative to its impulse and kinetic energy that could maintain the rotating motion of the leading vortex ring. In previous theories, the pinch-off process was considered as a relaxation process of the leading ring to an equilibrium state (Gharib et al., 1998; Mohseni and Gharib, 1998), or the separation was regarded to be completed when the translational velocity of the leading vortex ring equals the maximum axial velocity of the trailing shear layer (Shusser and Gharib, 2000a; Mohseni et al., 2001). By taking into account the effect of instability on reducing the vorticity flux, the previous theories in terms of the Kelvin-Benjamin variation principle or vortex ring's translational velocity could be developed into a more fundamental and general model for the pinch-off process, in which the characteristics of the leading vortex ring and total starting jet, such as α_{ring}, γ_{ring}, can be predicted.

In a starting jet, a vortex ring with small core size is generated shortly after the onset of jet ejection. As the vortex ring grows in size by absorbing the jet fluid, it translates downstream due to self-induction. During this process,

A would decrease as shown in figure 5.14. When A decreases to the critical value A_c, the initial perturbation that would evolve into the first trailing vortex later is issued from the jet exit. It determines the formation number F. As the perturbation is convected downstream, it could be amplified sufficiently to roll-up into a trailing vortex, whose growth would then affect the vorticity to the leading vortex ring. Due to the drop in vorticity flux, the trailing jet fluid near the rear of the leading vortex ring, with lower circulation relative to its impulse and kinetic energy, cannot roll into the core of the leading vortex ring to support its growth. As a result, the vorticity field of the leading vortex ring gradually separates from that of the trailing jet during the pinch-off process. The fluids ejected after the formation number are left in the trailing jet to form a series of trailing vortices. Therefore, the final properties of the leading vortex ring can be regarded as only the outcome of the specific rate of delivery of circulation, impulse and kinetic energy, which are restricted by the trailing jet instability or other mechanisms (such as the starting jet with background co-flow discussed in section 5.3.3). After the completion of the pinch-off process, the leading vortex ring would approach its equilibrium state as stated in the relaxation explanation (Gharib et al., 1998; Mohseni and Gharib, 1998).

In the previous investigations on vortex ring formation in starting flows, there are actually appreciable variations of the formation number as well as the dimensionless energy α_{ring} and circulation γ_{ring}, as shown in table 2.1. Based on the present investigation, the physical mechanism for pinch-off process in terms of trailing jet instability may offer an alternative explanation for the observed variation in the formation number and properties of the leading vortex ring for different vortex ring generators. To verify the instability criterion, two cases with different generator conditions are to be discussed below.

5.3.3 Starting jets with uniform background co-flow or counter-flow

In many practical applications, jets are issued in ambient fluid that is not quiescent and background flow must be considered. It inspired researchers to investigate the formation of vortex rings generated by the starting jet with uniform background co-flow or counter-flow. Under the influence of a bulk counter-flow, Dabiri and Gharib (2004) suggested that vortex ring pinch-off is delayed sufficiently that a leading vortex ring with greater circulation can be generated. In contrast, Krueger et al. (2003) and Krueger et al. (2006) found a reduction in the jet vorticity flux with increased co-flow, resulting in a reduction in the strength of the leading vortex ring. As the ratio of the co-flow velocity to the jet velocity $R_v = U_{co}/U_0$ increased from 0.5 to 0.75, the formation number drops from about 3 to below 1 and the leading vortex ring virtually disappeared. It is noted that the definition of the dimensionless formation time has also been modified by taking into account the effect of the background flow.

Because the presence of a background flow will change the jet shear layer characteristics and affect the vortex ring roll-up and the pinch-off process, the above results in starting jets with uniform background co-/counter-flows will be examined by using the instability approach proposed in this study. First, when the background counter-flow U_{ct} is imposed, it is observed that if counter-flow is initiated prior to the formation number (see cases CF05-2 and CFE in Dabiri and Gharib (2004)), vortex ring pinch-off will be completely suppressed until fluid ejection has terminated or the thickest vortex in Norbury-Fraenkel family of vortex ring, i.e. Hill's spherical vortex, is achieved. Under those conditions, the leading vortex ring is able to accommodate all the circulation delivered by the vortex generator. The interesting effect of counter-flow appears as a manifestation of the instability criterion, as discussed below.

By establishing bulk counter-flow, the translational velocity of the leading

vortex ring U_{tr} will decrease by the speed of counter-flow U_{ct} in the reference frame fixed on the ground. Therefore, the leading vortex ring would stay near the nozzle exit for a longer period of time, resulting in a relatively small value of x_{core}. On the other hand, the circulation Γ_{ring} and the strength of the shear layer $\Delta U = U_0$ are not significantly altered due to the 'blocking' effect of the leading vortex ring, which to some extent keeps the trailing jet from the influence of the counter-flow. Therefore, the value of the parameter A will be larger than the usual case without any background flows. According to the instability criterion, the parameter A will take longer time to decrease to the critical value A_c for small U_{ct}. For sufficiently strong background counter-flow, the axial translation of the leading vortex ring would be greatly inhibited, resulting in $A > A_c$ until the starting jet stops. Thus, the disturbance in the shear layer cannot be amplified sufficiently to start rolling up into a trailing vortex. The leading vortex ring could be kept near the nozzle exit and continuously gain circulation from the trailing shear layer, as observed by Dabiri and Gharib (2004). Although they did not present the quantitative information about the variables related to the parameter A, qualitative analysis appears to suggest that the present instability criterion for pinch-off is essentially in agreement with their experimental results. In summary, the decay of the pinch-off process in the presence of uniform counter-flow result from the effect of the counter-flow to freeze the leading vortex ring near the nozzle exit.

The effect of uniform background co-flow on the dynamics of vortex ring formation can be considered theoretically in two aspects. Because of background flow in the jet direction, it could diminish the strength of the separated shear layer to

$$\Delta U\big|_{co\_flow} = U_0 - U_{co}. \tag{5.8}$$

Due to the weak vorticity flux, the circulation of the leading vortex ring is accordingly decreased. Krueger et al. (2006) found that if the background co-

flow with velocity ratio $R_v = U_{co}/U_0 = 0.36$ was initiated simultaneously with the jet, the resulting vortex ring would have less circulation than in the cases without co-flow. Moreover, the translational velocity of the leading vortex ring U_{tr} could be increased by the co-flow, but its increment should be less than U_{co} during vortex ring formation because of the interference of the nozzle and the trailing jet. Because the background co-flow results in the lower Γ_{ring} and larger x_{core}, the value of A would decrease faster than in the cases without co-flow even though the decrease in trailing shear layer strength might counteract to this trend slightly. According to the instability criterion, the pinch-off process would therefore occur much earlier. The pinched-off vortex ring is smaller and has less circulation than that generated in quiescent ambient fluid.

Another distinct feature discovered by Krueger et al. (2003) and Krueger et al. (2006) is that at large velocity ratio R_v, the leading vortex ring pinches off from the generating jet almost immediately after flow initiation, resulting in a very weak leading vortex ring. As R_v increases beyond 0.55, the formation number decreases sharply from approximately 3.5 to nearly 1.0 over a range in R_v that is centered around a critical velocity ratio of $R_{crit} \approx 0.60 \pm 0.05$. The instabilities in the trailing shear layer have much smaller amplitude and are difficult to distinguish. Thus, the sudden drop in the formation number at large R_v suggests that the strong background co-flow introduces another mechanism for the rapid decrease of vorticity flux after jet initiation, rather than the mechanism in terms of the trailing jet instability for smaller R_v cases. By examining the change in flow dynamics caused by the strong background co-flow, it is found that the fast pinch-off may be attributed to the noticeably less intense trailing shear layer ($\Delta U = U_0 - U_{co}$). The weak trailing shear layer is no longer able to support the further growth of the leading vortex ring if the vorticity in the trailing jet is too low relative to the kinetic energy and impulse. This explanation is in agreement with the relative large dimensionless energy

of the final vortex ring $\alpha_{ring} = 0.47 \sim 0.63$ at high velocity ratio comparing to $\alpha_{ring} = 0.33$ for cases with quiescent ambient fluid. The above analysis indicates that other factors besides the trailing jet instability, such as the great background co-flow in the study of Krueger et al. (2006), could also lead to the decrease of vorticity flux in the trailing jet and affect the onset of the pinch-off process.

5.3.4 Starting jets with temporal-varying nozzle diameter

When studying the starting flow through the jet exit with temporally variable diameter, special attention should be paid to the apparatus used to achieve the temporal variation of the exit diameter. Previous experimental studies on starting jets with temporal-varying exit diameter mainly used either elastic nozzle type exit (Dabiri and Gharib, 2005) or iris orifice type exit (Allen and Naitoh, 2005). In addition, it should be noted that the temporal variation of jet exit diameter is usually coupled with the change of the jet velocity due to the constant volume flux of the ejected fluid.

Although Mohseni et al. (2001) implied the possibility of generating vortex ring with low dimensionless energy by increasing the nozzle or orifice exit diameter during jet ejection, Dabiri and Gharib (2005) found that a temporally increasing exit diameter provides no obvious effect on the circulation the leading vortex ring can finally gain. They suggested that the results may be attributed in part to the thickness of the shear layer at the relatively low Reynolds number. Given the mechanism used to achieve temporal variation of the nozzle diameter, the experimental results should also be associated with the concomitant variation in jet velocity. Because the volume flux of the jet was kept constant, the increase in nozzle diameter would result in decrease in the jet velocity U_0. In their experiments, U_0 was decreased by half through the temporal increase of

the exit diameter. Thus the vorticity flux in the trailing jet drops quickly due to the weaker shear layer (with smaller ΔU). The decreasing U_0 may also account for the slight drop in vortex ring circulation as the opening process becomes faster (figure 7 in Dabiri and Gharib (2005)).

On the other hand, when a temporally-decreasing nozzle exit diameter is introduced, the circulation of the leading vortex ring would be increased by up to 35% over the static nozzle case. The increase in vortex ring circulation should be attributed to the acceleration of the jet flow by closing the nozzle exit, which leads to stronger trailing shear layer and larger vorticity flux. The gradual increase in the jet velocity could result in relatively slower translation of the leading vortex ring, and keep x_{core} at a low value, as suggested by figure 13 in Dabiri and Gharib (2005). Therefore, it is reasonable to speculate that both increase in vortex ring circulation and relative slow vortex ring translation maintain the parameter A greater than the critical value, inhibiting the roll-up of trailing vortices and enabling the continuous vorticity supply into the leading vortex ring. In addition, the experimental results of the present study also demonstrated that gradually increased velocity programs (see figure 5.1) are capable of obtaining thicker vortex ring than the constant velocity cases.

Based on the above discussion, the effect of temporally variable exit diameter should be considered via the concomitant result of variable jet velocity U_0. By comparing the cases of decreasing and increasing nozzle diameter, it can be concluded that the acceleration velocity program is more effective to affect the dynamics of vortex ring formation and pinch-off than deceleration velocity program.

5.4 Concluding remarks

Experiments using digital particle image velocimetry (DPIV) were performed to investigate the effect of development of the trailing jet instability on the pinch-off process. It was found that a series of trailing vortices starts to roll up only after the formation number, $F = 4.2 \sim 4.6$, is achieved. Subsequently, the growth of trailing vortices leads to the rapid decrease in the vorticity flux being fed into the leading vortex ring. When the vorticity flux vanishes, the leading vortex ring separates completely from the trailing jet, indicating the end of the pinch-off process. Results also suggest that the roll-up and subsequent development of the trailing vortices constrain the growth of leading vortex ring with larger circulation. The formation of trailing vortices due to the Kelvin-Helmholtz instability was found to be associated with the induced velocity field of the leading vortex ring. According to the linearized stability analysis for axisymmetric shear layer, the thick shear layer, which results from the negative radial velocity gradient $\partial v/\partial r < 0$ induced by the leading vortex ring, is less unstable than the thin shear layer without the influence of the leading ring when it translates downstream. A dimensionless parameter 'A', defined as $A = \Gamma_{ring}/x_{core}\Delta U$, has been proposed to characterize the stabilizing effect of the leading vortex ring on the trailing shear layer near the nozzle exit. Experimental results reveals that A decreases as formation time progresses. The instability of the trailing jet starts to develop when a critical value $A_c = 1.1 \pm 0.1$ is reached, and it also corresponds to the onset of the pinch-off process.

Based on the effect of the trailing jet instability on the pinch-off process, a theoretical criterion for the formation number was established in terms of the dimensionless parameter A. In combination with the Kelvin-Benjamin variational principle, the instability criterion for the the formation number could offer a more general and fundamental explanation for the physical mechanism of the pinch-off process. According to this explanation, the pinch-off process essen-

tially results from the drop of vorticity flux the trailing shear layer feeds into the leading vortex ring. The development of the trailing jet instability and the growth of the trailing vortices, which can be characterized by the parameter A, is considered as a significant factor for the drop of the vorticity flux being fed into the leading vortex ring. By applying the instability criterion to the starting jets with uniform background flows or with temporally-varying exit diameter, it offers an appropriate explanation on the variation of the formation number and properties of the leading vortex ring.

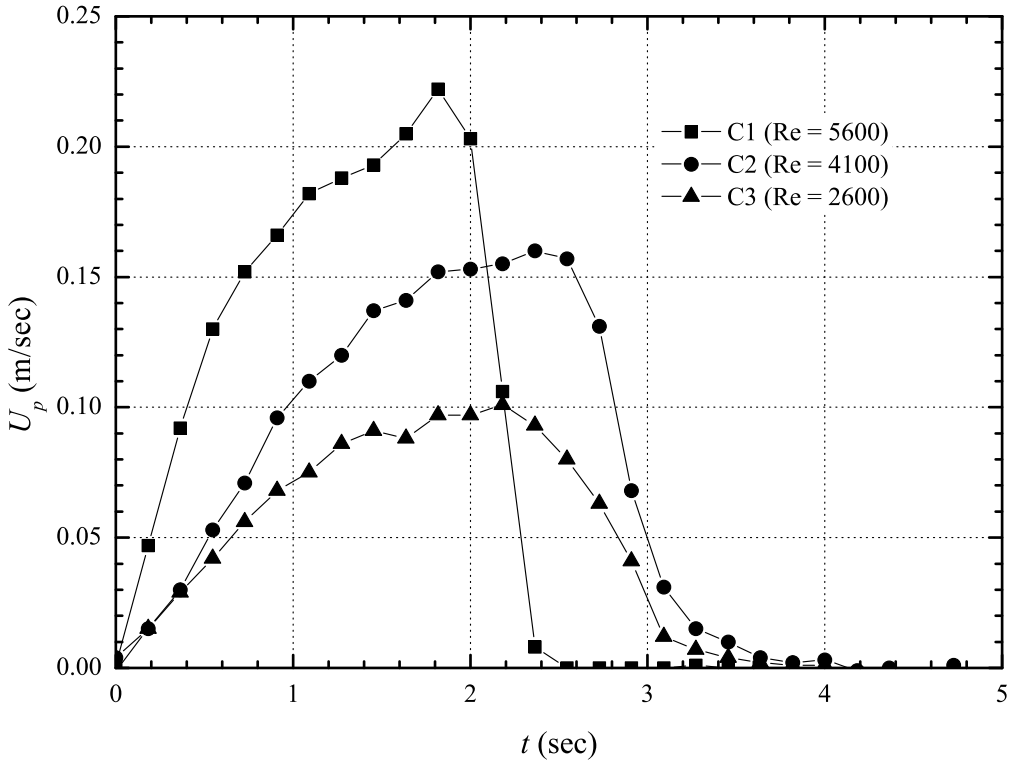

Figure 5.1: Piston velocity programs for the three cases with different Reynolds number

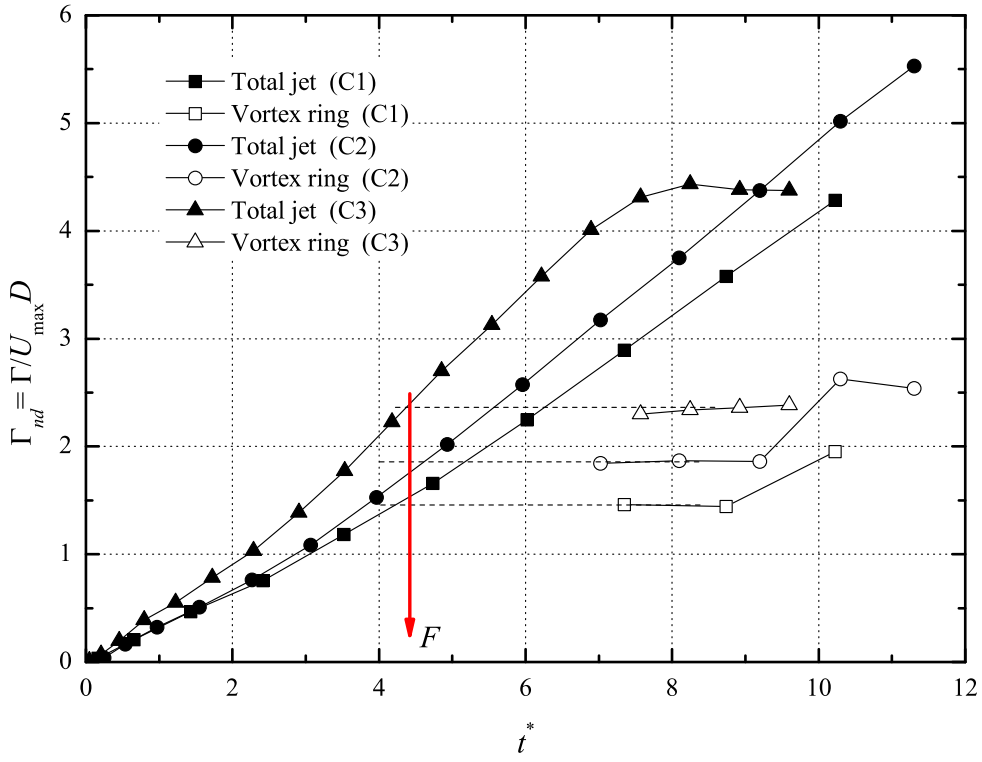

Figure 5.2: Normalized circulation of the total jet and the leading vortex ring as a function of formation time for the three cases

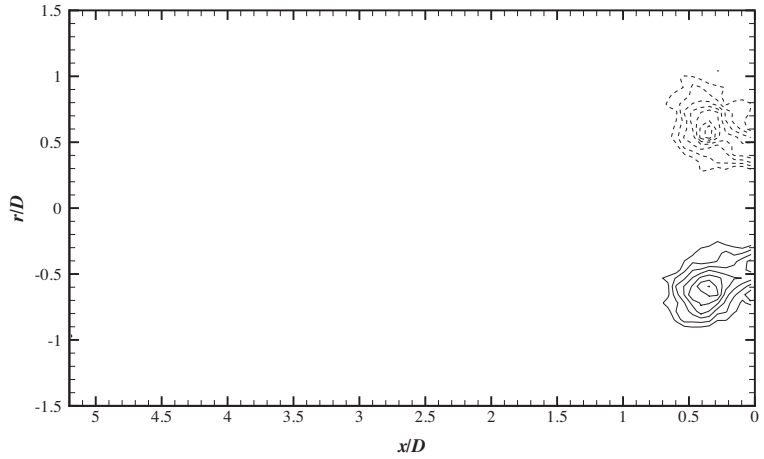

(a) $t^* = 1.431$

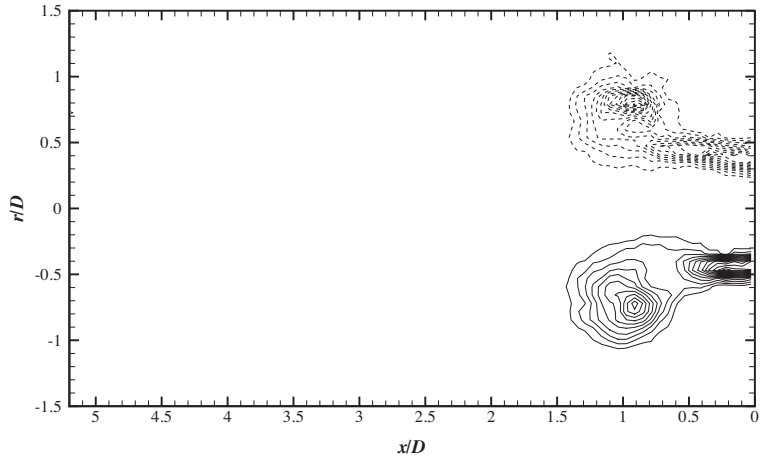

(b) $t^* = 3.521$

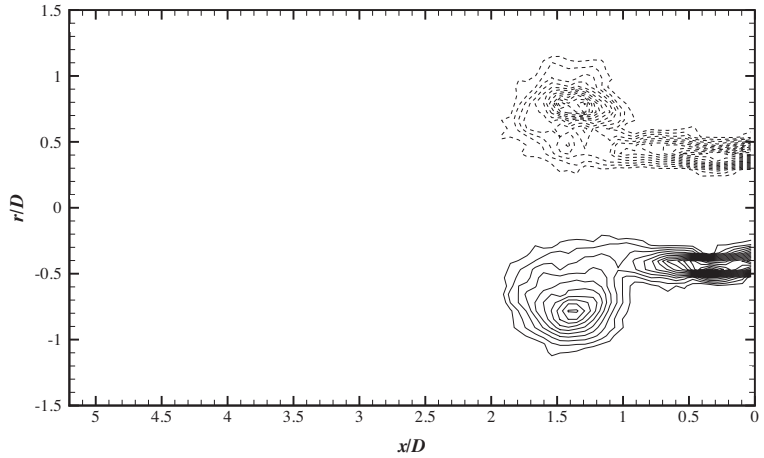

(c) $t^* = 4.733$

Figure 5.3: Temporal evolution of the vorticity field for C1

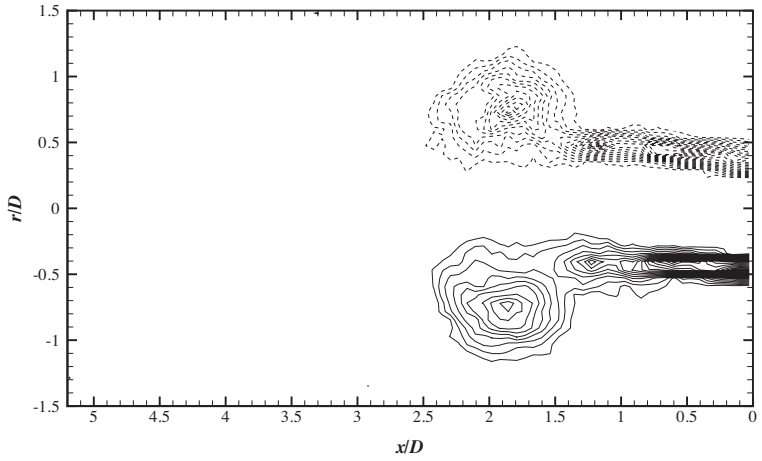

(d) $t^* = 6.022$

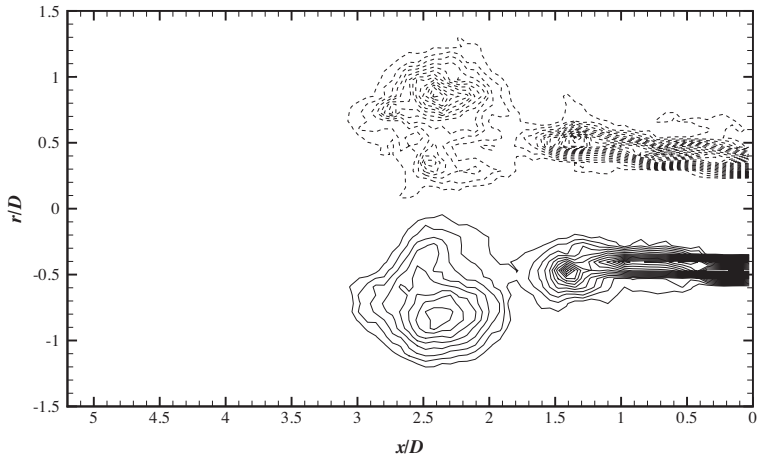

(e) $t^* = 7.350$

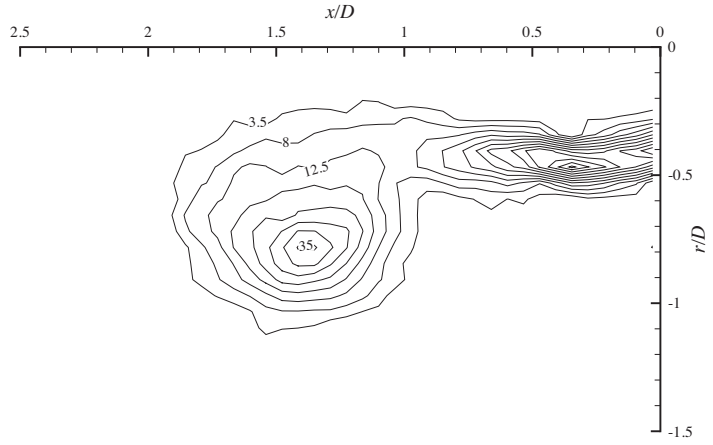

(f) $t^* = 4.733$

Figure 5.3: Temporal evolution of the vorticity field for C1 (cont.)

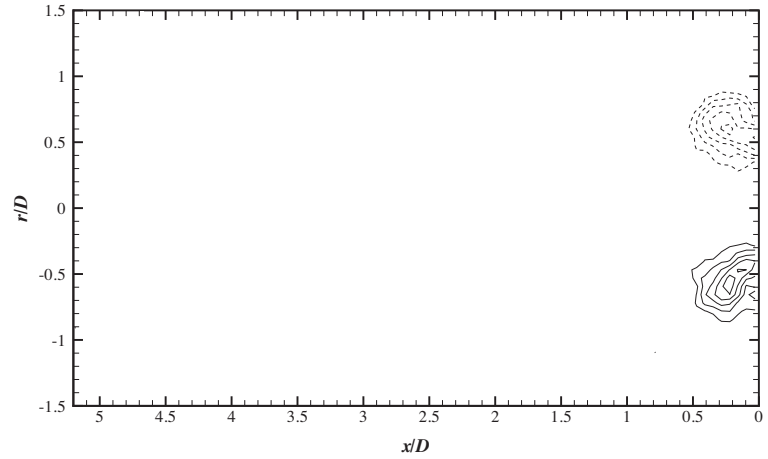

(a) $t^* = 0.969$

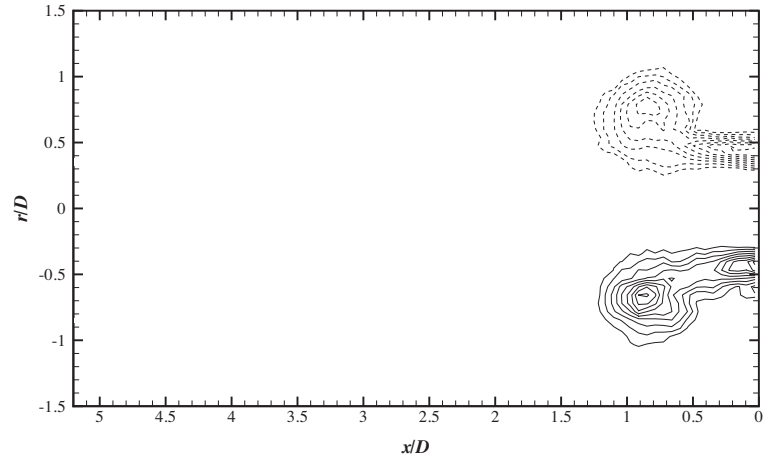

(b) $t^* = 3.067$

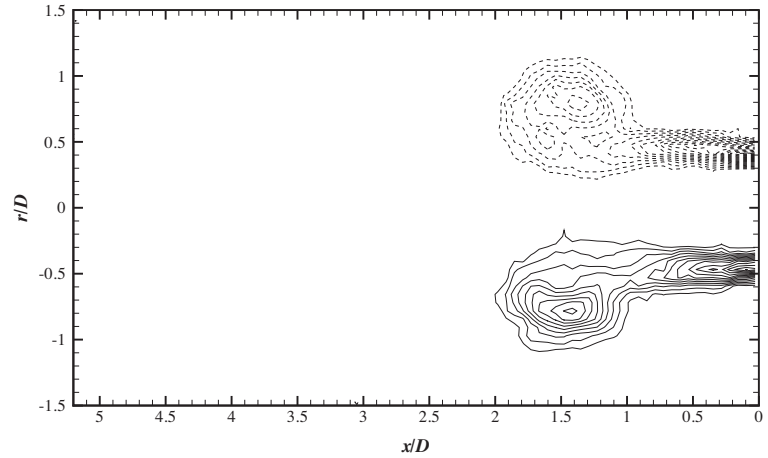

(c) $t^* = 4.933$

Figure 5.4: Temporal evolution of vorticity field for C2.

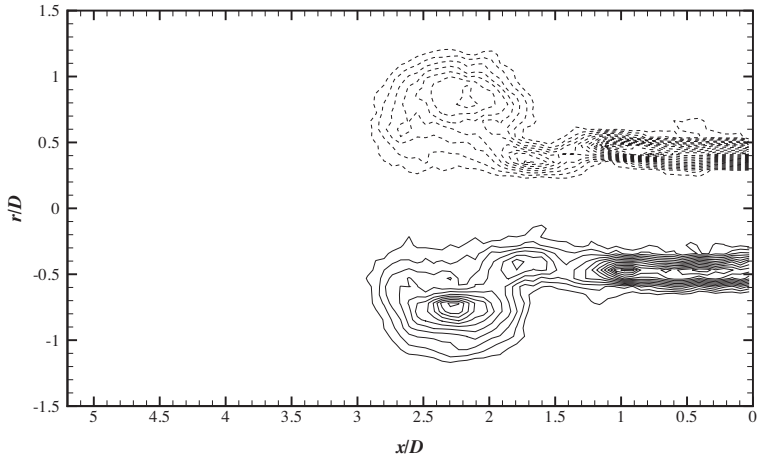

(d) $t^* = 7.022$

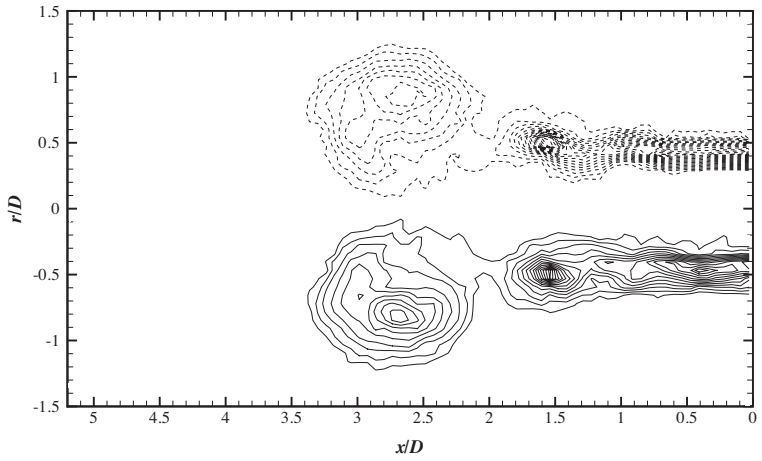

(e) $t^* = 8.096$

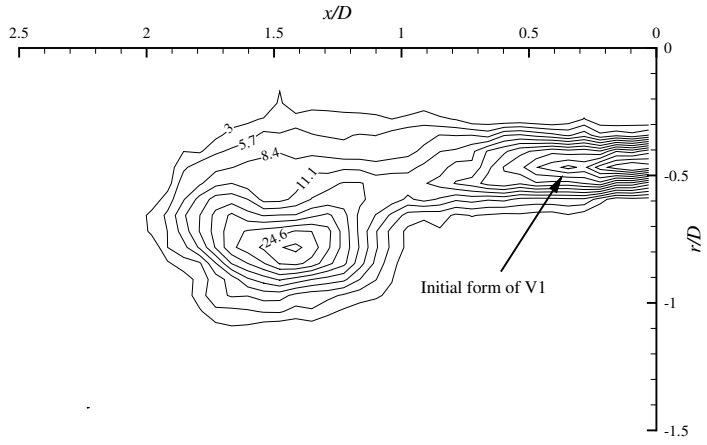

(f) $t^* = 4.933$

Figure 5.4: Temporal evolution of vorticity field for C2 (cont.)

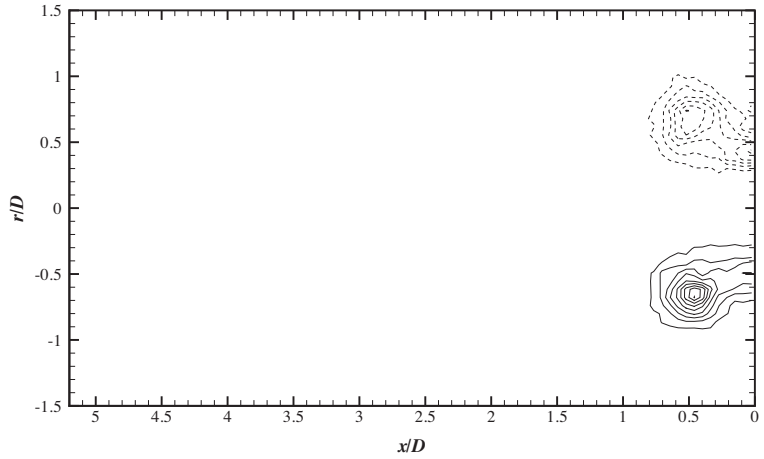

(a) $t^* = 1.725$

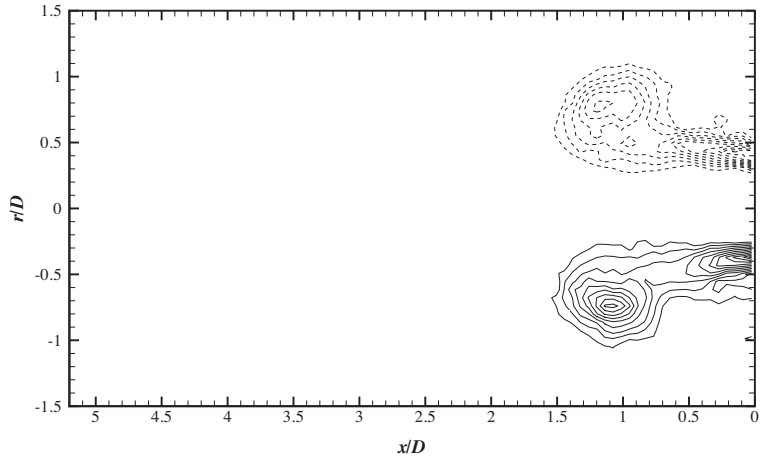

(b) $t^* = 3.530$

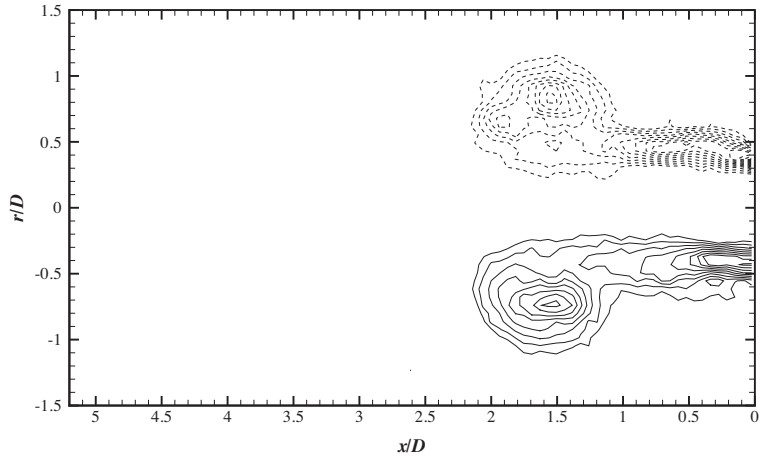

(c) $t^* = 4.852$

Figure 5.5: Temporal evolution of vorticity field for C3.

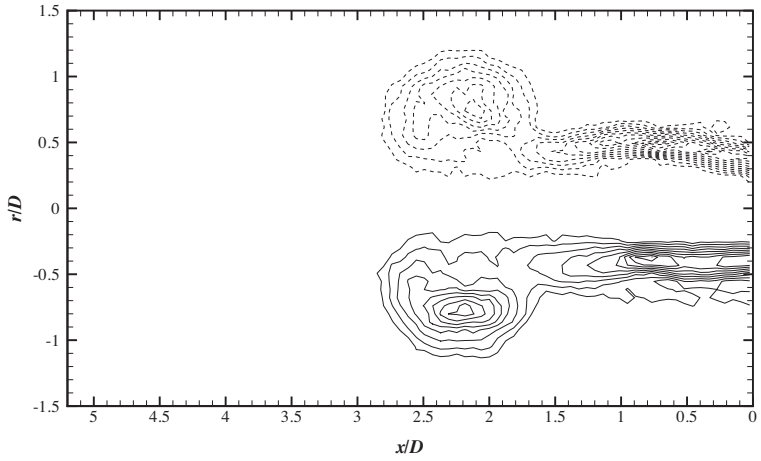

(d) $t^* = 6.129$

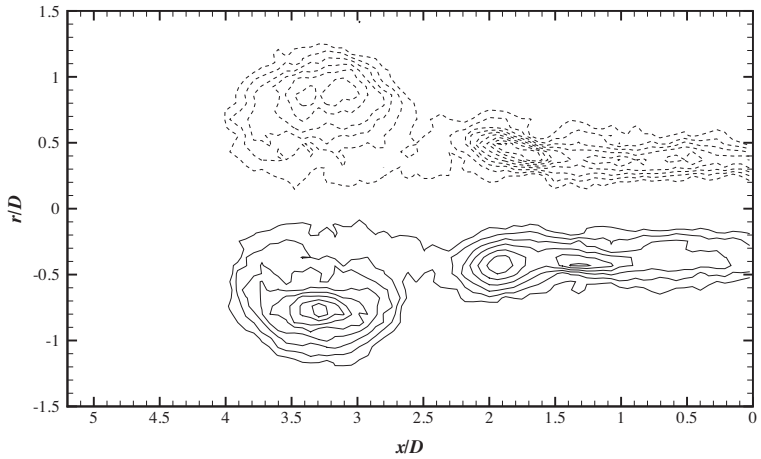

(e) $t^* = 8.247$

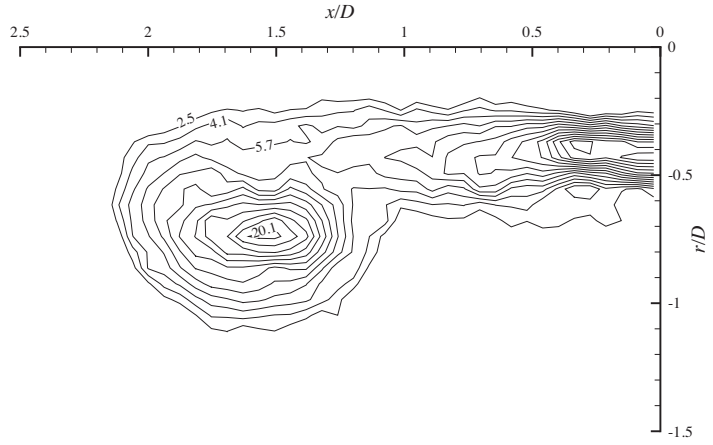

(f) $t^* = 4.852$

Figure 5.5: Temporal evolution of vorticity field for C3 (cont.)

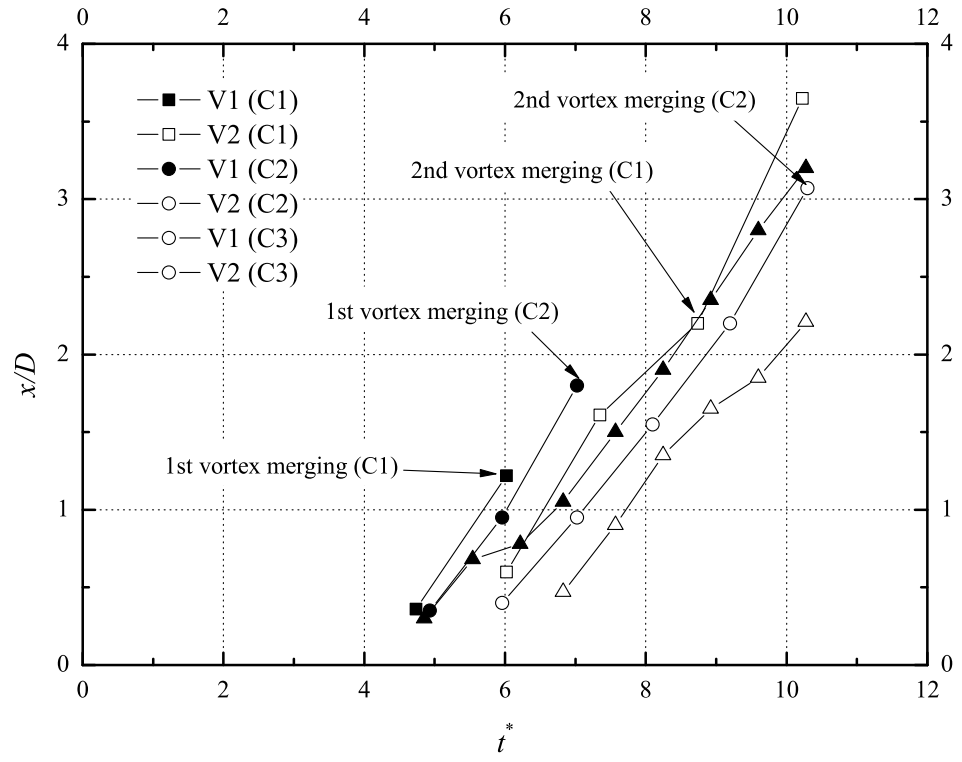

Figure 5.6: The axial trajectory of the first (V1) and second (V2) trailing vortex rings

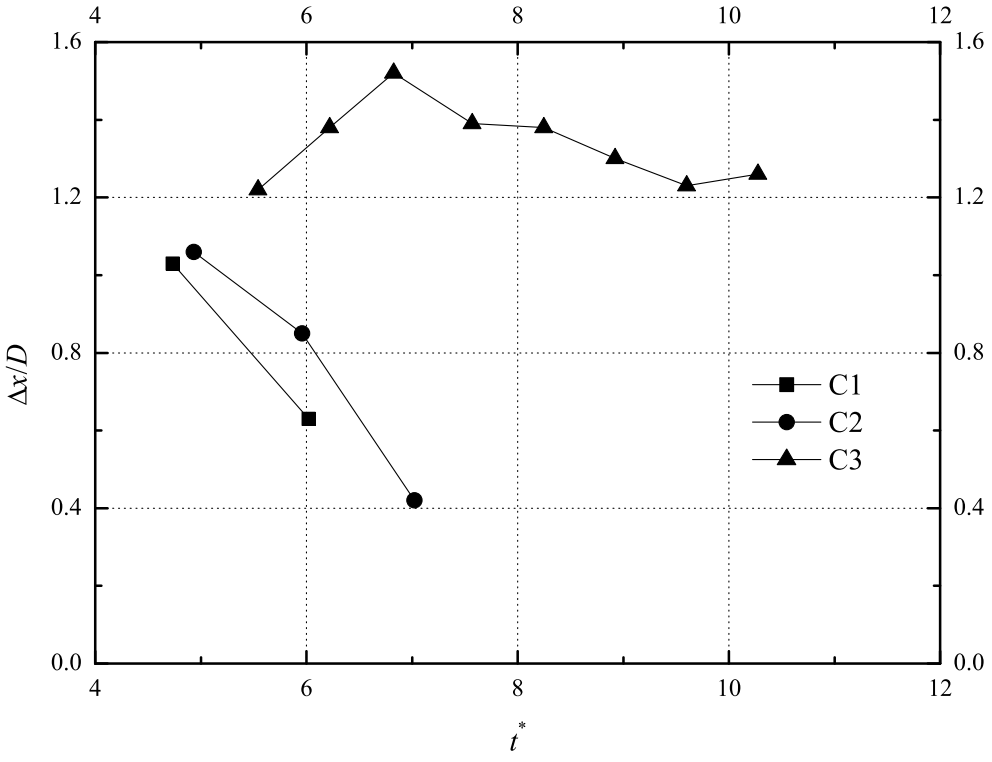

Figure 5.7: The variation of axial distance between the leading vortex ring and the first trailing vortex ring (V1) against the formation time

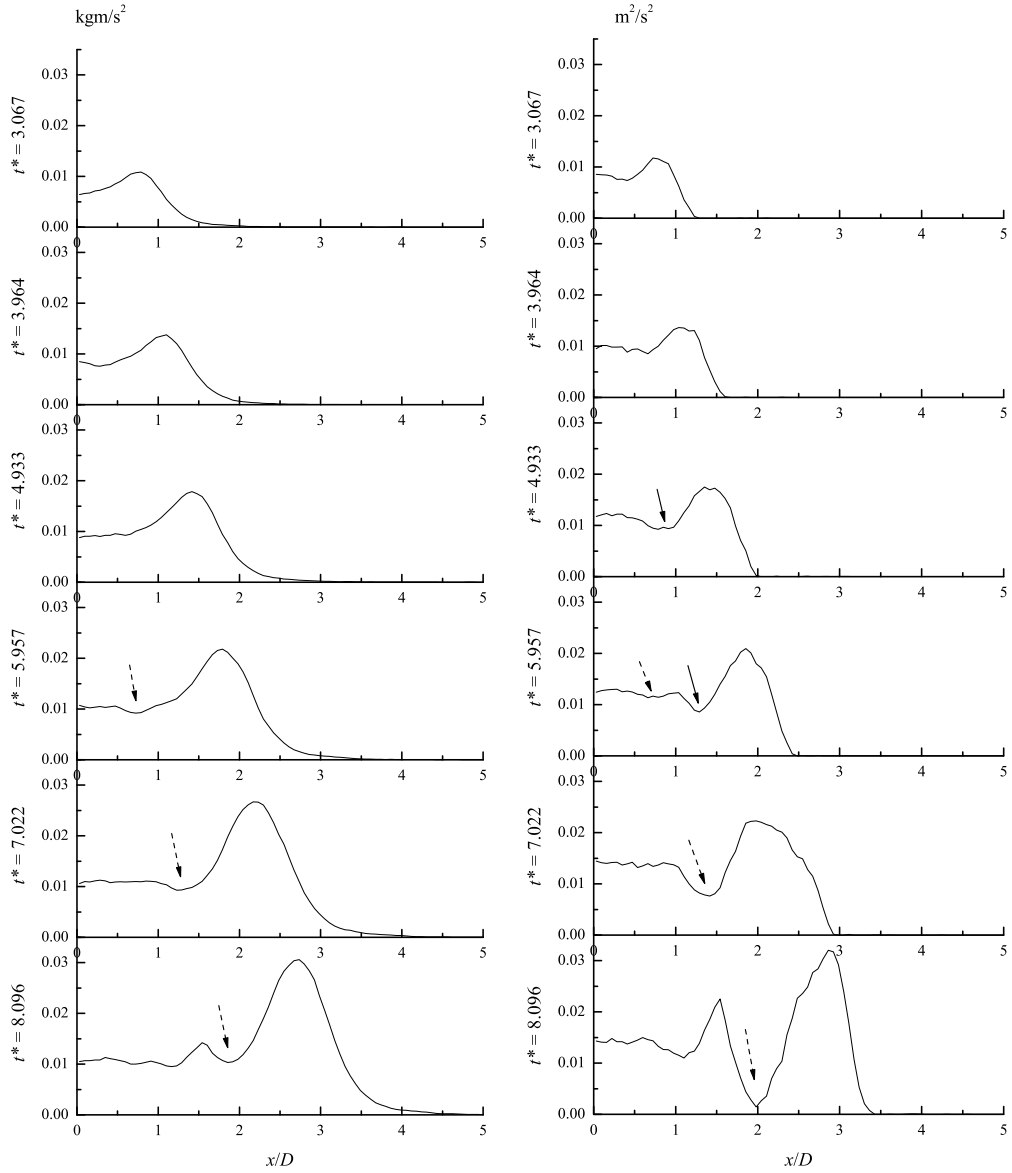

(a) Momentum flux (b) Vorticity flux

Figure 5.8: Axial variation of the momentum and vorticity fluxes during the pinch off process for C2. Arrows with solid line indicates the boundary between V1 and the leading vortex ring, and arrows with dash line indicate the boundary between V1 and V2.

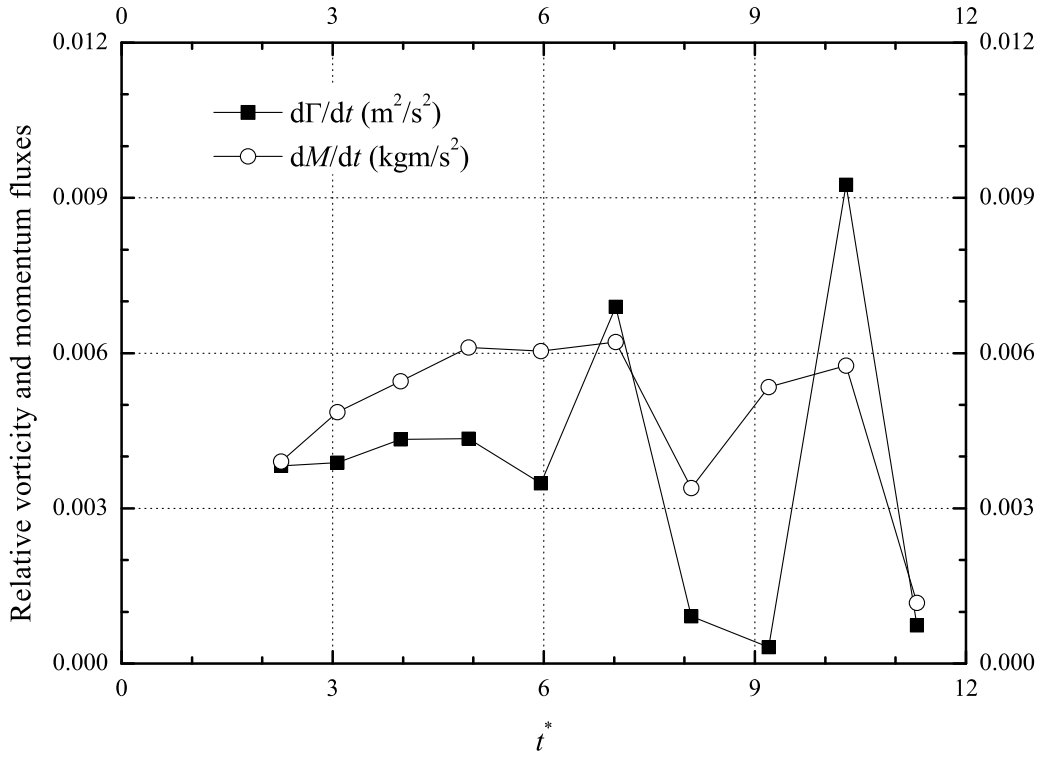

Figure 5.9: Fluxes of momentum and vorticity being fed into the leading vortex ring during its formation and pinch-off process for C2.

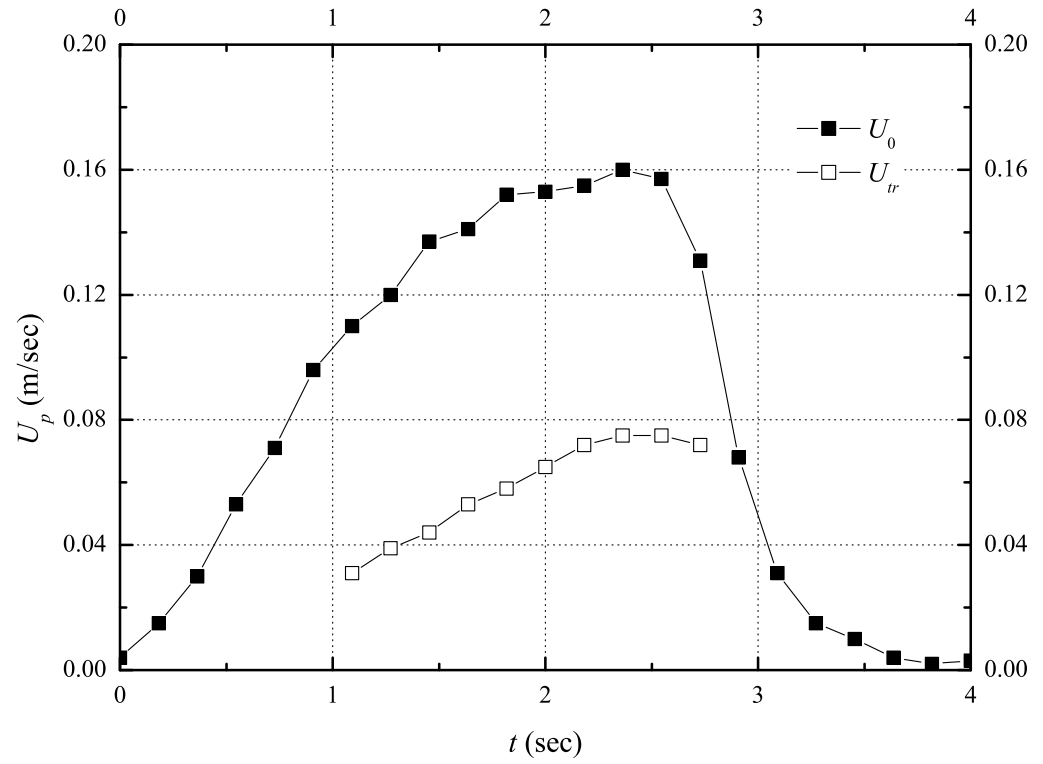

Figure 5.10: Piston velocity programs of the starting jet and the translational velocity of the leading vortex ring for C2.

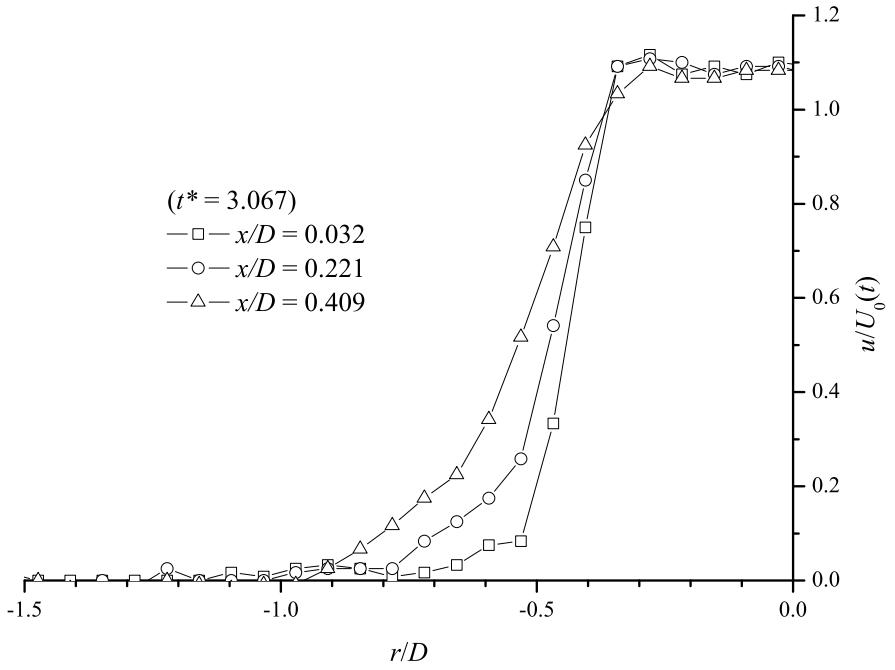

(a) Velocity profile before the pinch-off

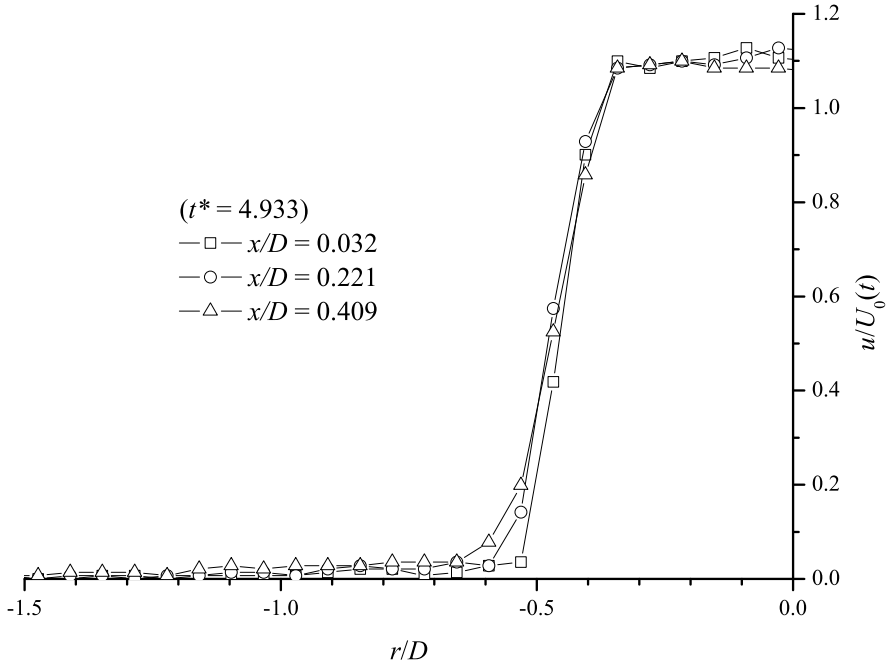

(b) Velocity profile dring the pinch-off

Figure 5.11: Axial velocity profiles near the nozzle exit before and during the pinch-off process for C2.

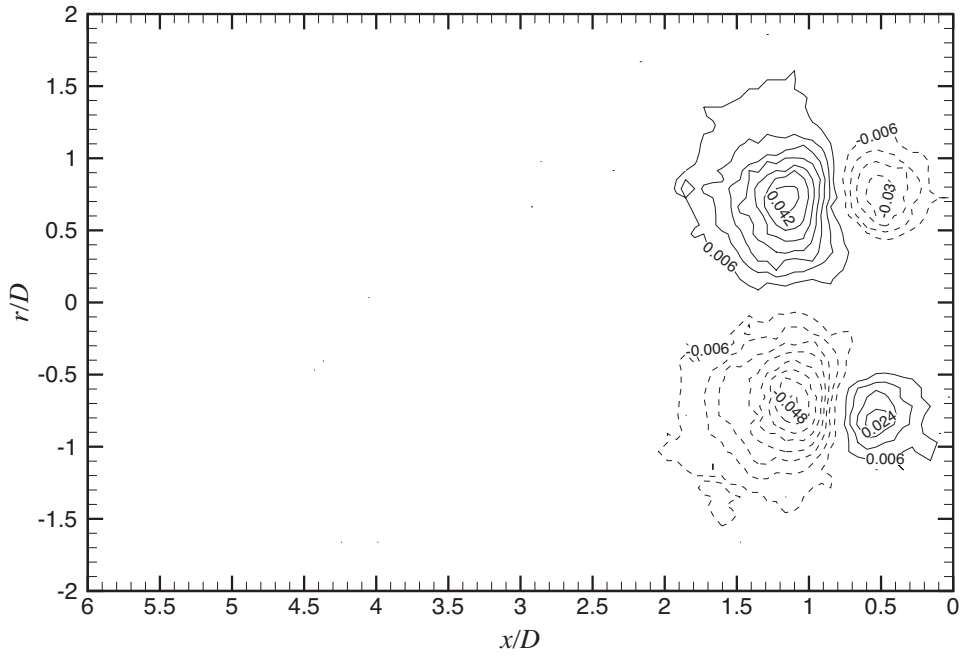

(a) Radial velocity contours before pinch-off ($t^* = 3.067$)

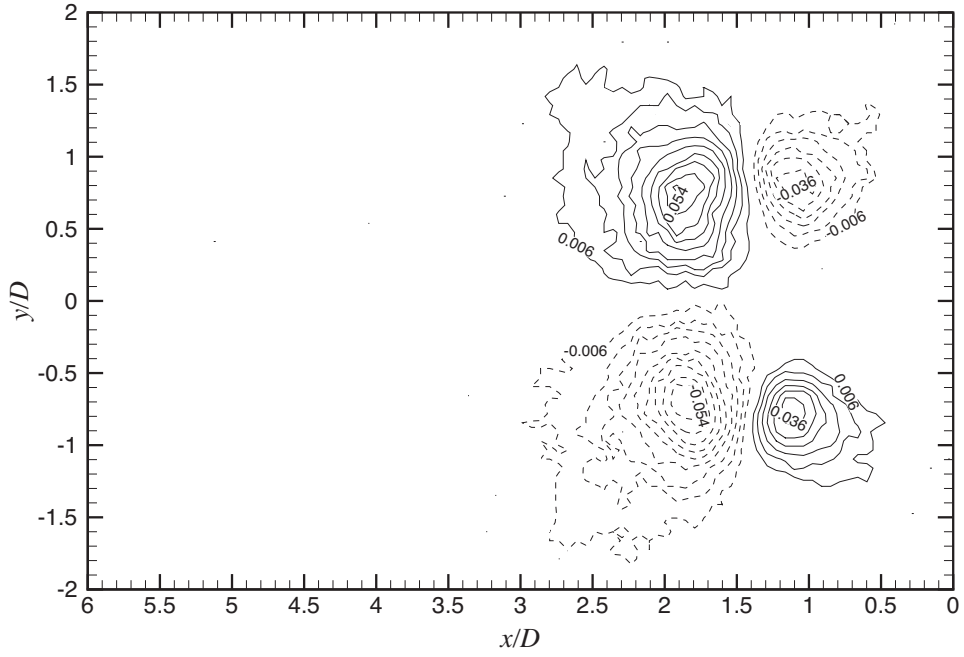

(b) Radial velocity contours during pinch-off($t^* = 4.933$)

Figure 5.12: Contours of the radial velocity before and during the pinch-off process for C2.

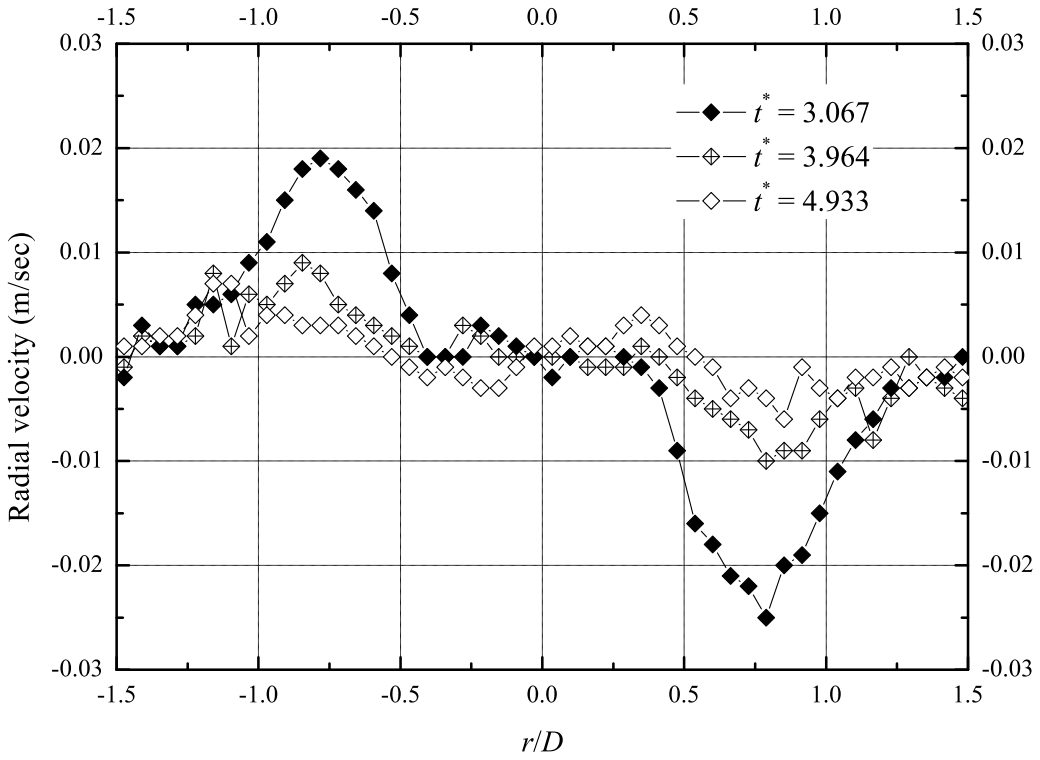

Figure 5.13: Temporal evolution of the radial velocity profiles at axial location $x/D = 0.409$ for C2

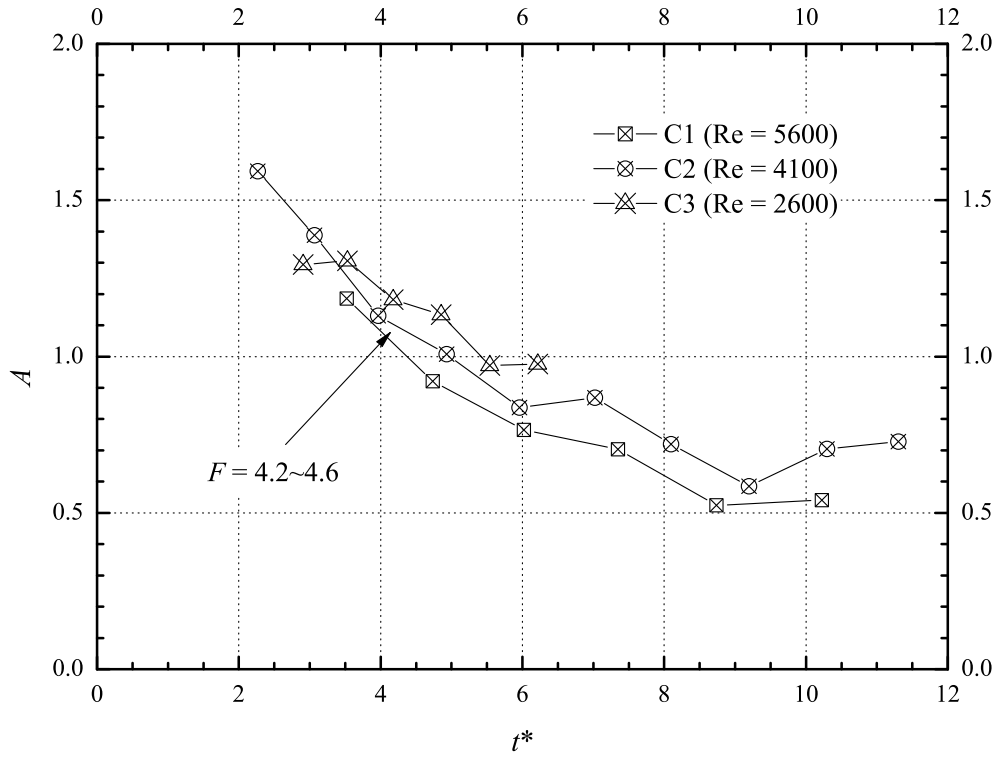

Figure 5.14: The variation of the parameter A against the formation time for the three cases

Chapter 6

A Model for the Pinch-off Process in Starting Jets

6.1 Introduction

The detachment (or pinch-off) of the leading vortex ring from the trailing jet is of fundamental interest to many researchers. Gharib et al. (1998) discovered that the leading vortex ring would start to pinch off from the trailing jet when the piston had discharged the column of fluid at stroke length $L(t)$ equal to four jet exit diameters ($4.0D$). If the piston stops before $L/D = 4.0$, all the discharged fluid would be absorbed into the leading vortex ring. This critical formation time is commonly referred to as the formation number. Existence of the universal formation number in the range of 3.6 to 4.5 for starting jets with various exit geometry, velocity program, and Reynolds number was demonstrated to be the outcome of the Kelvin-Benjamin variational principle, which states that for a steady vortex ring, the kinetic energy of impulse-preserving rearrangements of the vorticity field by an arbitrary solenoidal velocity field is maximum. As such, Gharib et al. (1998) suggested that the formation number could be identified as the time when the starting jet is no longer able to supply energy at the rate

compatible with this energy requirement.

The physical implication of the formation number should be that for the starting jet with maximum stroke ratio ($L_{\max}/D$), which is the total stroke length piston travels before it stops normalized by the nozzle diameter, greater than the formation number, its flow field would consist of a leading vortex ring followed by a trailing jet. The maximum circulation the leading vortex ring can obtain should be equal to that emanated from the nozzle exit plane up to the formation number. However, it should be noted that the leading vortex ring might not be physically detached from its trailing jet at the formation number. The fluid in the trailing jet discharged before the formation number would continue to be absorbed by the growing vortex ring, and gradually separate from that discharged after the formation number at later time. While the fluid discharged after the formation number would be left behind the leading vortex ring and form the trailing jet. The whole pinch-off process is illustrated schematically in figure 6.1. Similarly, Gharib et al. (1998) also suggested that the pinch-off process was not a sudden process and its completion might take up to 2 formation time units. The understanding of pinch-off process is important to evaluate the analytical models proposed so far for the vortex ring formation.

Theoretically, pinch-off could be considered as a relaxation process of the leading vortex ring to an equilibrium state. A model developed by Mohseni and Gharib (1998) determined the formation number by the intersection of two curves obtained from matching bulk hydrodynamic quantities (circulation, impulse, and kinetic energy) with those quantities for Norbury-Fraenkel family of vortex ring. Two equations then were obtained by equating these quantities for the slug model with corresponding quantities in the Norbury-Fraenkel vortices. The value of formation number was found to be between 3 and 4.5, consistent with results obtained from experiments (Gharib et al. (1998), Pawlak et al. (2007)) and simulations (Rosenfeld et al. (1998), Zhao et al. (2000)) for

the starting jet with straight nozzle configuration. According to the description of the pinch-off process, the formation number predicted by their model should correspond to the beginning of the pinch-off process (figure 6.1(a)) since they mainly focused on the characteristics of the resulting vortex ring and not of the generation process.

Shusser and Gharib (2000a) also modeled the vortex ring formation by using a kinematic hypothesis that the vortex ring completes its formation and pinches off from its trailing jet when the translational velocity of the vortex ring becomes equal to the jet flow velocity near the ring. The translational velocity of the leading vortex ring was estimated by the properties of Norbury-Fraenkel vortices, and the local trailing jet velocity was related to the piston velocity via conservation of mass. The dynamic properties of the vortex ring were also approximated by those of the total jet using the slug model. By comparing the vortex ring velocity with the trailing jet velocity near the ring, they derived the limiting value of the dimensionless energy $\alpha_{\text{lim}} = 0.31$, which matches well the experimental value $\alpha_{\text{lim}} = 0.33$. Thus, they suggested that the dynamical (based on Kelvin-Benjamin variational principle) and kinematic approaches (based on comparison of the velocities) are equivalent.

Although the basic perspectives of above models were different, both bore an assumption that before the onset of the pinch-off process, all the fluid discharged from nozzle exit is transferred to the leading vortex ring so that the properties of the leading vortex ring could be estimated by the slug model. In other words, both models do not distinguish the leading vortex ring and the trailing jet before the pinch-off. Hence, the approaches of Mohseni and Gharib (1998) and Shusser and Gharib (2000a) may only be capable of predicting the time at which the dynamic properties provided by the generator become equal to the maxima that the leading vortex ring could attain, rather than the time at which the leading vortex ring actually acquires its maximum circulation and separates from the

trailing jet.

It is important to realize that the universal formation number around 4.0 may be only applicable for starting jets which can be characterized by sufficiently large stroke ratio, sufficiently high Reynolds number and sufficiently thin shear layers produced by the ejection, such as those produced by piston-cylinder arrangement with straight nozzle Mohseni et al. (2001). The formation number, however, might vary within the range from 1.0 to 5.0 with different generator configurations. For example, the formation number could be reduced to around 2.0 in experiment for the starting jet with converging nozzle, which contracted smoothly and gradually with cross section area contraction ratio of 52:1, to avoid the formation of Gortler vortices (Yu et al., 2007). With very thick shear layers produced by parabolic velocity profile at the nozzle exit plane, the formation number could even be reduced to around 1.0 (Rosenfeld et al. (1998) and Zhao et al. (2000)). In this chapter, effort has been made to elucidate the difference on formation number between starting jets with commonly used straight nozzle and converging nozzle that has small convergence angle, in terms of the dynamic quantities fed by the trailing jet into the leading vortex ring.

Similar flow structure was found in a starting buoyant plume (Turner, 1962), which consists of a 'cap', analogous to the leading vortex ring, and a 'stem', which is the same as the trailing jet in the starting jet. Based on the structure of the starting buoyant plume, a two-stage model was proposed by Shusser and Gharib (2000b) to investigate the formation of vortex ring in the cap of the plume. The first stage of the process is the initial formation of the ring-like structure in the plume cap. The flow field consists of only a forming vortex ring. During the second stage, continuing action of the heat source creates a rising flow of the lighter fluid (the stem of the plume) following the ring (the cap of the plume). The flux from the stem into the ring continues until the latter has grown large enough to pinch off. It is noted that the evolutions of the 'cap' and

the 'stem' of the starting plume are considered separately in the second stage. Due to the similarity between jet and buoyant plume, this approach is adopted for the starting jet in the present investigation.

In this chapter, we focus on elucidating the physical process of pinch-off in starting jets by a two-stage model, which takes into account the difference between the leading vortex ring and its trailing jet. The next section will explain the physical situation and the formulation in the model for both straight nozzle type and converging nozzle type vortex ring generators. It is followed by discussion on the properties of the leading vortex ring calculated by the model, and comparison with experimental results obtained by various researchers.

6.2 Process of the leading vortex ring formation and pinch-off

In the present model, the initial leading vortex ring generated by rolling up of the separated cylindrical shear layer would absorb all the fluid issued from the nozzle exit. The leading vortex ring growth is dominated by its radial expansion but it does not leave the nozzle exit plane until an optimum size of the vortex ring is reached. Then a transition from vortex ring's radial expansion to axial translation distinguishes the development in Stage II from that in Stage I. During Stage II, as the leading vortex ring travels downstream, a trailing jet begins to appear and continuously feeds the vortex ring with vorticity, momentum and kinetic energy until pinch-off occurs. The detailed formation and pinch-off process is schematically shown in figure 6.2.

6.2.1 Stage I: Initial generation of the leading vortex ring

First, we assume that the piston reaches a constant velocity U_0 immediately after the jet was initiated from a nozzle with exit diameter of D. The first stage

is the formation of vortex ring by fluid discharged with an initial momentum. The vortex ring grows rapidly in size by absorbing all of the fluid ejected from the nozzle, but it does not translate appreciably. It has been observed in experiments of Didden (1979) and Weigand and Gharib (1997) that no motion in axial direction was noticeable until it reaches $D_{ring} = 1.08D$. Therefore, we specify $D_{ring} = 1.08D$ as the condition for the end of Stage I. Due to the slow translation of the vortex ring, it is reasonable to make an assumption that no trailing jet appears. Moreover, recent flow visualization by Olcay and Krueger (2008) had shown that during the onset of jet ejection, the volume of entrained ambient fluid would be much less than the volume of the ejected fluid from the nozzle. Entrainment effect is therefore not considered in modeling at Stage I.

As illustrated in figure 6.2(a), the fluid discharged through the nozzle exit consists of a forming vortex ring (in light grey) and a central part (i.e., the irrotational fluid in the vortex ring bubble). The volume of the vortex ring V_r and the volume of the central part V_c, can be calculated by integration as:

$$V_r = 2\pi^2 R_r R_{core}^2, \tag{6.1a}$$

$$V_c = 2\pi R_r^2 R_{core} - \pi^2 R_r R_{core}^2 + \frac{4}{3}\pi R_{core}^3. \tag{6.1b}$$

The total volume V_t discharged from nozzle exit can be regarded as a column of fluid with the height of stroke length and the base area of the nozzle exit, namely

$$V_{total} = \frac{1}{4}\pi D^2 L. \tag{6.1c}$$

Since entrainment effect is negligible during Stage I, the ejected volume should be conserved, which results in

$$\frac{1}{4}\pi D^2 L = \pi^2 R_r R_{core}^2 + 2\pi R_r^2 R_{core} + \frac{4}{3}\pi R_{core}^3. \tag{6.2}$$

Here, R_r is the radius of the leading vortex ring, and R_{core} is the radius of the vortex ring core. At this stage, the sufficient small size of the vortex ring core, in which the vorticity is confined, makes it reasonable to approximate the dimensionless mean core radius of the Norbury-Fraenkel family of vortex ring as $\epsilon \approx R_{core}/R_r$. The exact definition and implication of the mean core radius ϵ will be discussed in Stage II.

As the vortex ring grows, both R_r and R_{core} would increase with time. Since the vortex ring at initial stage is having smaller core size as compared to the nozzle diameter, the roll-up of vortex sheet at the nozzle edge can be approximated as self-similar inviscid process in two dimensions. Based on the similarity law for axisymmetric jet discussed by Saffman (1978), growth of the radius of the vortex ring R_r can be expressed as

$$R_r/D = 0.5 + C_R t^{*2/3}, \tag{6.3}$$

where coefficient C_R is equal to 0.17 from the experimental result of Didden (1979). Therefore, the end of Stage I can be found to be at $t^* = 0.12$ from the criterion that $D_{ring} = 1.08D$ at end of Stage I. It shows that Stage I is indeed a very transient period.

In summary, equations 6.2 and 6.3 describe the initial development of the starting jet in Stage I ($0 < t^* < 0.12$). The properties of the leading vortex ring and the total jet, such as ring size, total volume and dynamic properties, at the end of Stage I would be used as the initial conditions for the calculation in Stage II. Note that difference in generator configuration is not considered in Stage I since its effect in this short period would not influence the further development of the starting jet significantly.

6.2.2 Stage II: Growth of the leading vortex ring before the pinch-off

After the initial formation of the leading vortex ring, development of the starting jet is characterized by the appearance of a trailing jet behind the translating leading vortex ring. The growth of the vortex ring is supported by the flux from the trailing jet until it pinches off. Thus, the total kinetic energy, impulse and circulation delivered by the jet cannot be regarded as those only for the leading vortex ring due to the existence of the trailing jet. Those quantities of the leading vortex ring, however, may be estimated by the flux from the trailing jet into the ring.

The local trailing jet velocity U_{tj} near the ring can be related to the average velocity at the jet exit U_0 based on following assumptions. First, we assume that the trailing jet can be approximated as a one-dimensional axisymmetric flow and entrainment of ambient fluid in the trailing jet is negligible. Second, for two configurations of the jet generator, the difference in the growth of the trailing jet must be considered. For the starting jet with straight nozzle configuration (in the left of figure 6.2(c)), mass and momentum along the trailing jet should be constant based on the approximation of one-dimensional flow without entrainment. Therefore, it can be obtained that the trailing jet velocity U_{tj} and its radius R_{tj} would not change along the trailing jet, resulting in

$$U_{tj}|_{sn} = U_0, \quad R_{tj}|_{sn} = \frac{D}{2}. \tag{6.4a}$$

Henceforth, subscript 'sn' denotes quantities only for the straight nozzle configuration, and 'cn' denotes the quantities only for the converging nozzle configuration. It is consistent with the flow visualization results of Olcay and Krueger (2008). They showed that the radius of the trailing jet is almost constant before the appearance of the secondary vortices in the trailing jet. On the other

hand, for the starting jet with converging nozzle setup, the trailing jet tends to shrink due to the converging streamlines. It should be noted that the concept of converging nozzle in the model should be restricted to nozzles with small convergence angle. To take the shrinking trend into account, the radius of the trailing jet near the ring is approximated as the difference between ring radius and core radius ($R_r - R_{core}$), as shown in the right of figure 6.2(c). In fact, the size of the core R_{core} would normally grow faster than the size of the ring R_r (see Hettel et al. (2007), figure 19). Then, by applying conservation of mass in the trailing jet, we obtain

$$U_{tj}|_{cn} = \frac{D^2}{4R_r^2(1-\epsilon)^2}U_{0,} \quad R_{tj}|_{cn} = R_r - R_{core}. \tag{6.4b}$$

where ϵ is the dimensionless mean core radius of the Norbury-Fraenkel family of the vortex ring (see figure 1 in Norbury (1973)), defined as the ratio of mean radius of the vortex ring core to the radius of the vortex ring.

In order to predict the variation of dynamic properties (circulation, impulse, and kinetic energy) of the leading vortex ring at Stage II, their fluxes from the trailing jet into the leading vortex ring need to be estimated. Heeg and Riley (1997) showed that the total circulation rate $d\Gamma_{total}/dt$ is actually slightly above the slug model value $d\Gamma_{total}/dt = 0.5U_0^2$ at large time owing to boundary-layer growth inside the nozzle. Didden (1979) found that the best approximation of the vorticity flux through the nozzle exit was

$$\frac{d\Gamma_{total}}{dt} = 0.57U_0^2 \quad \text{for } t^* > 0.6. \tag{6.5}$$

Equation 6.5 can be regarded as the rate of the total circulation provided by the starting jet. With regard to the leading vortex ring, its circulation is derived from the vorticity flux into the ring. Similar to the slug model at the nozzle exit plane, one can derive the vorticity flux near the rear of the leading vortex ring

as,

$$\frac{d\Gamma}{dt} = \int_0^\infty (U_{tj} - U_{tr})\omega dr \approx \frac{1}{2}U_{tj}^2 - U_{tj}U_{tr}, \tag{6.6}$$

where U_{tr} is the translational velocity of the leading vortex ring, and would increase as the ring grows. For impulse and kinetic energy, their flux from the trailing jet are given by

$$\frac{dI}{dt} = \pi(R_r - R_{core})^2 \rho U_{tj}(U_{tj} - U_{tr}), \tag{6.7}$$

$$\frac{dE}{dt} = \frac{1}{2}\pi(R_r - R_{core})^2 \rho U_{tj}^2(U_{tj} - U_{tr}). \tag{6.8}$$

For the flux of dynamic properties, no subscript is used in equation 6.6 – 6.8 because they are valid for both straight nozzle and converging nozzle configurations.

Finally, as confirmed by many investigations (Mohseni et al., 2001; Linden and Turner, 2001), the leading vortex ring can be approximated as a member of Norburys family of vortex rings, which is characterized by the dimensionless mean core radius ϵ. Accordingly, the translational velocity of the leading vortex ring u is given by Fraenkels second order formulas (Fraenkel, 1972) as

$$U_{tr} = B\sqrt{\frac{\rho\Gamma^3}{\pi I}} \quad \text{with} B = \frac{1}{4}\sqrt{1 + \frac{3}{4}\epsilon^2}\left[\ln\frac{8}{\epsilon} - \frac{1}{4} + \frac{3\epsilon^2}{8}\left(\frac{5}{4} - \ln\frac{8}{\epsilon}\right)\right] \tag{6.9}$$

For the vortex rings with small cross section ($\epsilon < 0.5$), the accuracy of Fraenkels approximation has been estimated to be very good, with the error less than 2% (Shusser et al., 2006). Impulse and kinetic energy of the leading vortex ring can be expressed in terms of its circulation and size, i.e.,

$$I = \rho\pi\Gamma R_r^2\left(1 + \frac{3}{4}\epsilon^2\right), \tag{6.10}$$

$$E = \frac{1}{2}\rho R_r\Gamma\left(\ln\frac{8}{\epsilon} - \frac{7}{4} + \frac{3}{8}\epsilon^2\ln\frac{8}{\epsilon}\right), \tag{6.11}$$

As the growth of the leading vortex ring, the value of the dimensionless core radius ϵ would increase during Stage II.

Based on equations 6.4(a,b) and 6.6 – 6.11, the flow development during the second stage can be determined. Dimensionless variables are introduced as

$$\left.\begin{array}{l} t^* = \frac{tU_0}{D}, \hat{R}_r = \frac{R_r}{D}, \hat{R}_{core} = \frac{R_{core}}{D}, \hat{R}_{tj} = \frac{R_{tj}}{D}, \epsilon = \frac{R_{core}}{R_r}, \hat{U}_{tj} = \frac{U_{tj}}{U_0}, \\ \hat{U}_{tr} = \frac{U_{tr}}{U_0}, \hat{I} = \frac{I}{\rho\pi D^3 U_0}, \hat{E} = \frac{E}{1/2(\rho\pi D^3 U_0^2)}, \hat{\Gamma} = \frac{\Gamma}{U_0 D}. \end{array}\right\} \tag{6.12}$$

Substituting 6.9 into 6.6 – 6.8, and applying normalization 6.12 to the resultant equations 6.6 – 6.8, 6.10, and 6.11, we obtained a system of differential-algebraic equations:

$$\frac{d\hat{I}}{dt^*} = \hat{R}_{tj}\hat{U}_{tj}\left(\hat{U}_{tj} - B\sqrt{\frac{\hat{\Gamma}^3}{\pi^2\hat{I}}}\right), \tag{6.13}$$

$$\frac{d\hat{E}}{dt^*} = \hat{R}_{tj}\hat{U}_{tj}^2\left(\hat{U}_{tj} - B\sqrt{\frac{\hat{\Gamma}^3}{\pi^2\hat{I}}}\right), \tag{6.14}$$

$$\frac{d\hat{\Gamma}}{dt^*} = \frac{1}{2}\hat{U}_{tj}\left(\hat{U}_{tj} - B\sqrt{\frac{\hat{\Gamma}^3}{\pi^2\hat{I}}}\right), \tag{6.15}$$

$$\hat{I} = \hat{\Gamma}\hat{R}_r^2\left(1 + \frac{3}{4}\epsilon^2\right), \tag{6.16}$$

$$\hat{E} = \frac{\hat{R}_r\Gamma^2}{\pi}\left(\ln\frac{8}{\epsilon} - \frac{7}{4} + \frac{3}{8}\epsilon^2\ln\frac{8}{\epsilon}\right). \tag{6.17}$$

By substituting normalized equation 6.4a or 6.4b into equations 6.13 – 6.17 for starting jets with straight nozzle and converging nozzle respectively, the properties of the leading vortex ring were solved by using the conditions obtained at the end of Stage I.

6.3 Modelling results and discussion

6.3.1 Initial formation of the leading vortex ring

By solving the equations 6.2 and 6.3, the radius of the leading vortex ring core R_{core} can be obtained as functions of formation time t^*, as shown in figure 6.3. At the end of Stage I, the radius of ring core R_{core} was calculated to be $0.0451D$ and the dimensionless mean core radius ϵ is calculated to be 0.0833. The leading vortex ring is of very small core size during the initial stage of the jet development. The experiment by Didden (1979) reported that the trajectory of the vortex core varied according to the similarity law (defined in equation 6.3) up to the formation time $t^* = 0.6$, which is larger than the end of Stage I defined here $t^* = 0.12$. Therefore, one may expect that the vortex ring is self-similar even when it starts translating.

Figure 6.3 also shows the normalized radius of the vortex core versus formation time from similarity law (Saffman, 1978) that has been confirmed by numerous experimental studies. Hettel et al. (2007) confirmed the similarity law that the dependence of the radius of the vortex spiral R_{core}/D on formation time t^* was approximately equal to $0.125t^{*2/3}$, while the prediction in present model shows a slightly greater growth rate. The deviation from the simulation is probably due to the simplified geometry of the vortex ring in this model, which tends to underestimate the volume of the center part V_c and results in greater volume of the vortex ring V_r and bigger ring core size.

Because the first stage is identified as a very transient period, it is appropriate to involve the over-pressure effect on the properties of the leading vortex ring during this period. It has been reported that the slug model consistently underestimates the total circulation and energy by a nearly constant amount for the impulsively starting jet (Didden, 1979; Krueger, 2005; Yu et al., 2007). The error in slug model arises primarily from neglecting the over-pressure at the

nozzle exit plane, which developed as a result of the unsteady flow initiation and distorted the velocity profile at the nozzle exit. For the nozzle configuration, Krueger (2005) proposed an over-pressure correction Γ_{op} to the circulation prediction by slug model for small formation time as $\Gamma_{op}/(U_0 D) \approx 1/\pi$. In order to obtain the circulation of vortex ring at the end of Stage I, the over-pressure correction is included as,

$$\hat{\Gamma}|_{end\_I} = \hat{\Gamma}_{slug}|_{end\_I} + \hat{\Gamma}_{op} \approx \left(\frac{1}{2}t^*\right)_{t^*=0.12} + \frac{1}{\pi} = 0.3783. \tag{6.18}$$

Moreover, we assume the initial vortex ring at the end of Stage I can be approximated as a Norbury-Fraenkel vortex ring, so as to enable the smooth transition of the properties of the ring form Stage I to Stage II. Therefore, the kinetic energy and impulse of the leading vortex ring at the end of Stage I are calculated from equations 6.16 and 6.17 by substituting in the value of circulation $\hat{\Gamma} = 0.3783$, mean core radius $\epsilon = 0.0833$ and vortex ring radius $\hat{R}_r = 0.5414$. In summary, the initial conditions for Stage II are:

$$\left.\begin{aligned} &\hat{I}|_{end\_I} = 0.1114, \quad \hat{E}|_{end\_I} = 0.0697 \\ &\hat{\Gamma}|_{end\_I} = 0.3783, \quad \hat{R}_r|_{end\_I} = 0.5414, \epsilon|_{end\_I} = 0.0833. \end{aligned}\right\} \tag{6.19}$$

It should also be noted that except for calculating the end state we do not include any dynamical aspect of the vortex sheet roll-up in this stage. Instead, the model relies on conservation of the ejected volume in combination with the theoretical similarity law with the empirical fitted coefficient.

6.3.2 Formation number and separation time

By solving the system of equations 6.13 – 6.17 with corresponding initial conditions from equation 6.19, we can predict the trajectory, size, and dynamic properties of the leading vortex ring in Stage II until it pinches off from the

trailing jet. First, the onset and end of the pinch-off process should be identified before discussing the evolution of the leading vortex ring. Since the end of Stage II is determined by the separation time when the leading vortex ring physically detaches from the trailing jet, the model fails after Stage II when the flux into the leading vortex ring from the trailing jet does not exist any longer. Mohseni et al. (2001) pointed out that the formation process is governed by two dimensionless parameters that are formed from the three integrals of motion (circulation, impulse, and kinetic energy) and the translational velocity of the leading vortex ring, i.e., the dimensionless energy and circulation. The dimensionless energy α defined as

$$\alpha = \frac{E}{\sqrt{\rho I \Gamma^3}} = \frac{\hat{E}}{2}\sqrt{\frac{\pi}{\hat{I}\hat{\Gamma}^3}}. \tag{6.20}$$

Therefore, the pinch-off process of the leading vortex ring can be quantified in terms of the variation of the dimensionless energy, as discussed as follows.

Based on the Kelvin-Benjamin variational principle, Gharib et al. (1998) suggested that the onset of the pinch-off process, by definition coinciding with the formation number, can be determined by the time when the total dimensionless energy α_{total} provided by the jet generator decreases beyond a certain limiting value $\alpha_{\lim}$. It has been observed experimentally by Gharib et al. (1998), Allen and Naitoh (2005) that for the vortex rings in the jet with constant velocity program, $\alpha_{\lim} = 0.33 \pm 0.05$ without a clear trend for different generation mechanisms. But at the formation number, the dimensionless energy of the leading vortex ring α_{ring} should be still higher than $\alpha_{\lim}$ since it has not obtained its maximum circulation. During the pinch-off process, as the vortex ring core thickens, α_{ring} is expected to diminish to the limiting value $\alpha_{\lim}$. Therefore, the criterion for determining the separation time is that the leading vortex ring completes its formation and separates form the trailing jet once the dimensionless energy of

the leading vortex ring α_{ring} becomes less than the limiting value α_{lim}.

The variations of dimensionless energy α_{ring} of the leading vortex ring against formation time t^* for converging nozzle and straight nozzle configurations are presented in figure 6.4. For converging nozzle case, the dynamic properties of total jet flow are estimated by the slug model with a correction on the circulation given in equation 6.5 as

$$\hat{I}_{total} = \hat{I}|_{end\_I} + \frac{1}{4}(t^* - 0.12), \tag{6.21a}$$

$$\hat{E}_{total} = \hat{E}|_{end\_I} + \frac{1}{4}(t^* - 0.12), \tag{6.21b}$$

$$\hat{\Gamma}_{total} = \hat{\Gamma}|_{end\_I} + 0.57(t^* - 0.12). \tag{6.21c}$$

Then α_{total} is calculated from equations 6.21(a)–(c), and also plotted in figure 6.4(a). The formation number is predicted roughly at around 2.2. Both the total jet energy α_{total} and formation number are consistent with the experiment of starting jets using converging nozzle by Yu et al. (2007) in which the formation number was found to be at about 2.2. The physical separation of the leading vortex ring occurred later on. To predict the separation time for converging nozzle configuration, the dimensionless energy of the leading vortex ring α_{ring} is also plotted in figure 6.4(a). At small formation time, α_{ring} is close to the total energy of the jet α_{total}. But for $t^* > 1.0$, the difference between α_{ring} and α_{total} increases because some energy provided by the jet should be left behind in the trailing jet. When approaching the end of Stage II, the rate of change of α_{ring} seems to slow down, indicating the invariant properties of the ring after it was completely formed. According to the criterion stated above, we compare the variation of α_{ring} with this limiting value α_{lim}, and estimate the value of the separation time by the intersection of ring energy curve and the limiting value. As shown in figure 6.4(a), it suggests that the separation time of the leading vortex ring is approximately at $t^* = 5.0$.

The result of formation number and separation time for converging nozzle suggested that at $t^* \approx 2.2$, the jet with converging nozzle provides the fluid with energy consistent with those for the steady translating vortex ring, namely $\alpha_{total} = \alpha_{lim}$. However, at the formation, the leading vortex ring has not obtained its maximum circulation. The leading vortex ring would continue absorbing fluid from the trailing jet after the formation number and approach its maximum-circulation state at about $t^* \approx 6.0$ when $\alpha_{ring} = \alpha_{lim}$. This critical time corresponds to the physical separation of the leading vortex ring and the trailing jet at, and is termed as the separation time. This is the whole process of vortex ring pinch-off in starting jet with converging nozzle.

For straight nozzle configuration, Gharib et al. (1998) showed that the slug model could predict the evolution of total energy α_{total} with reasonable accuracy. The solution of the model with constant trailing jet approximation gives the variation of the dimensionless energy of the vortex ring α_{ring}. As shown in figure 6.4(b), the predicted formation number is at about 3.9, which matches well with prior results (Gharib et al., 1998; Rosenfeld et al., 1998; Zhao et al., 2000). And the separation time for straight nozzle is found to be a bit greater than 7.0. Similar phenomenon was observed by Sau and Mahesh (2007) that for cylindrical nozzle even though the formation number is found to be approximately 3.6, the leading vortex ring clearly pinches off from the trailing jet at around $t^* \approx 11$. By comparing figure 6.4(a) and 6.4(b) for converging nozzle and straight nozzle configurations, the difference in the evolution of dimensionless energy and the formation number exhibits the effect of nozzle geometry on the trailing jet development as specified in last section. It indicates that by modifying the conditions corresponding to the generation mechanism, the current model is capable of predicting the pinch-off process in both straight nozzle and converging nozzle configurations.

As for the Kelvin-Benjamin variational principle, it should be noted that

the total dimensionless energy is usually estimated by the slug model. The dimensionless energy of the steady leading vortex ring after pinch-off usually makes use of the experimental results by Gharib et al. (1998). The limiting value $\alpha_{\text{lim}} = 0.33 \pm 0.05$ has been theoretically predicted by Mohseni and Gharib (1998), but their estimate of the translational velocity as $U_{tr} = U_p/2$ limits its generality for different discharging processes of the fluid from the nozzle. The properties of the leading vortex rings are functions of different rates of generation of primary and secondary vorticity. The universal value of dimensionless energy $\alpha_{ring} = 0.33$ only exist in some particular starting jets, like those with impulsive start, constant velocity program, and moderate Reynolds number. By using time-varying diameter of the jet exit, Mohseni et al. (2001) and Allen and Naitoh (2005) had successfully produced thick vortex rings with non-dimensional energy as low as 0.22 and 0.17, respectively (see table 2.1). The experimental results in Chapter 4 has verified that the steady vortex ring after pinch-off can be considered as a member of the theoretical Norbury-Fraenkel family of vortex ring. However, the mean core radius ϵ of the vortex ring for a specific generation mechanism still cannot be derived analytically. The discussion in Chapter 5 may suggest an approach to determining the value of the mean core radius ϵ by means of development of the trailing jet instability during the vortex ring formation. It is a very interesting issue worth further work.

6.3.3 Interaction between the leading vortex ring and the trailing jet

For converging nozzle configuration, the initial converging streamlines would lead to the decrease of the trailing jet radius and a corresponding increase in the velocity of the trailing jet. This trend is examined by the prediction of the translational velocity of the leading vortex ring and the local velocity of the jet at the rear of the vortex ring, as shown in figure 6.5(a). The translational velocity

of the ring U_{tr} increases with a slightly reducing slope until the separation time $t^* \approx 5.0$. The increasing translational velocity U_{tr} suggests that even after the formation number $t^* = 2.2$, the vortex ring does not reach its steady state, but it is still in the formation phase by gaining momentum from the trailing jet until their physical separation. It shows in figure 6.5(a) that the variation of U_{tr} only agrees well with the experimental result in figure 4.3 at around the formation number $t^* = 2.2$, but overestimates it near the end of Stage II ($t^* \approx 5.0$). As may have been expected, the trailing jet velocity U_{tj} in this model increases rapidly against time and becomes equal to about $2.1U_0$ at the end of Stage II ($t^* \approx 5.0$). On the other hand, in figure 6.5(b), the value of u for straight nozzle configuration agrees well with those found by Gharib et al. (1998) and Schram and Riethmuller (2001), especially near the formation number $t^* = 4.0$.

The discrepancy in translational velocity between prediction and experimental result may be attributed to the fact that the model is not capable of taking into account the influence of the Kelvin-Helmholtz-type vortex rings forming in the trailing jet. As illustrated in a sequence of PLIF images in figure (3) of Yu et al. (2007), a noticeable feature during the vortex ring pinch-off is the formation of vortex rings in the trailing jet. Once the first trailing vortex ring is formed, it would absorb the vorticity from upstream and downstream, causing the flux of dynamic properties into the leading vortex ring to reduce. Without considering this effect, the model tends to overestimate the translational velocity of the leading vortex ring. This effect suggests that the interaction between the leading vortex ring and the trailing vortices is a crucial factor for determining the properties of the leading vortex during the pinch-off process. We would like to note that further analytical work on this instability of the trailing jet is worth studying so as to provide a more accurate description of the pinch-off process.

The prediction of the variation of the radius of the leading vortex ring and its core is presented in figure 6.6. The result for converging nozzle case (figure

6.6(a)) shows that the radius of the ring core indeed grows faster than that of the ring. Comparison with the experimental results of Ai (2006) implies that the model generally underestimates the growth of the vortex ring radius at small formation time, but matches well with the experimental results near the end of Stage II. In figure 6.6(b), the present model for straight nozzle configuration shows good agreement with the growth of the size of the vortex ring, especially at the early period of the formation process. For initial development of the starting jet ($t^* < 0.6$), Didden (1979) found the growth of the vortex ring diameter given by equation 6.3. For further development, Liess (1978) have reported a power-law dependence of the change of ring diameter on the formation time, i.e.,

$$D_{ring}/D = 1.18(t^*)^{1/5} \quad \text{for } 1.0 \leqslant t^* \leqslant 3.3. \tag{6.22}$$

The characteristic mean core radius in straight nozzle jet increases rapidly during the second stage of development. Its value is found to be at about 0.45 when the leading vortex ring completes its formation at about $t^* \approx 7.0$. This value is in consistence with the experimental result of the properties of the vortex ring with dimensionless energy α of 0.33. Likewise, in figure 6.6(a) for the converging nozzle case, the mean core radius ϵ also approaches the value of 0.45 at the end of pinch-off process. It implies that the model can obtain the invariance of the properties of the leading vortex ring towards its steady state for different generator configurations.

6.3.4 Penetration of jet tip

Another interesting feature in starting jet is the penetration of the jet tip. The axial position of the vortex ring core x_{core} can be predicted by integration of the translational velocity of the vortex ring. Based on the simplified geometry of vortex ring in this model (see figure 6.2), the axial position of jet front (or

jet tip) can also be derived by the core position plus added by ring core radius R_{core}. The predicted jet penetration for both straight nozzle and the converging nozzle configurations is presented in figure 6.7. Due to the faster translational velocity of the leading vortex ring in the converging nozzle case, its penetration is estimated to be stronger than that in the straight nozzle case. Their curves also exhibit varying slope during the period from the onset of pinch-off process (when t^* equals formation number) to the end of pinch-off process (when t^* equals separation time), approaching to a steady state of the leading vortex ring. The jet penetration compares well with the experimental results (see figure 4.2(a)) for the starting jet with converging nozzle for different Reynolds number.

6.4 Concluding remarks

An analytical model was proposed based on some modifications to the model of Shusser and Gharib (2000b) for starting plume, so as to study the dynamic process of vortex ring formation and pinch-off in starting jets with different generator configurations. By altering the approximation on the growth of trailing jet, the model was capable of predicting the vortex ring pinch-off process in both starting jets generated by converging nozzle and straight nozzle. The development of starting jet was modeled into two stages before the leading vortex ring actually pinches off from the trailing jet. By considering the existence of trailing jet during the vortex formation, the detailed vortex ring formation and pinch-off process can be elucidated by the properties of the leading vortex ring, such as the size, trajectory, velocity and dynamic properties. At Stage II, the pinch-off process can be characterized by two time scales, i.e., formation number and separation time. By applying the Kelvin-Benjamin variational principle, the values of formation number and the separation time for converging nozzle case were found to be about 2.2 and 5 respectively, in good agreement

with corresponding experimental results of Ai (2006). And for straight nozzle configuration, the separation time of a bit greater than 7.0, in combination with the formation number of 4.0 predicted by the slug model (Gharib et al., 1998), identifies the whole pinch-off process in starting jet with straight nozzle. In addition, comparison with previous experimental results suggests that the prediction on separation time could be improved by considering the formation of the first trailing vortex ring in the trailing jet.

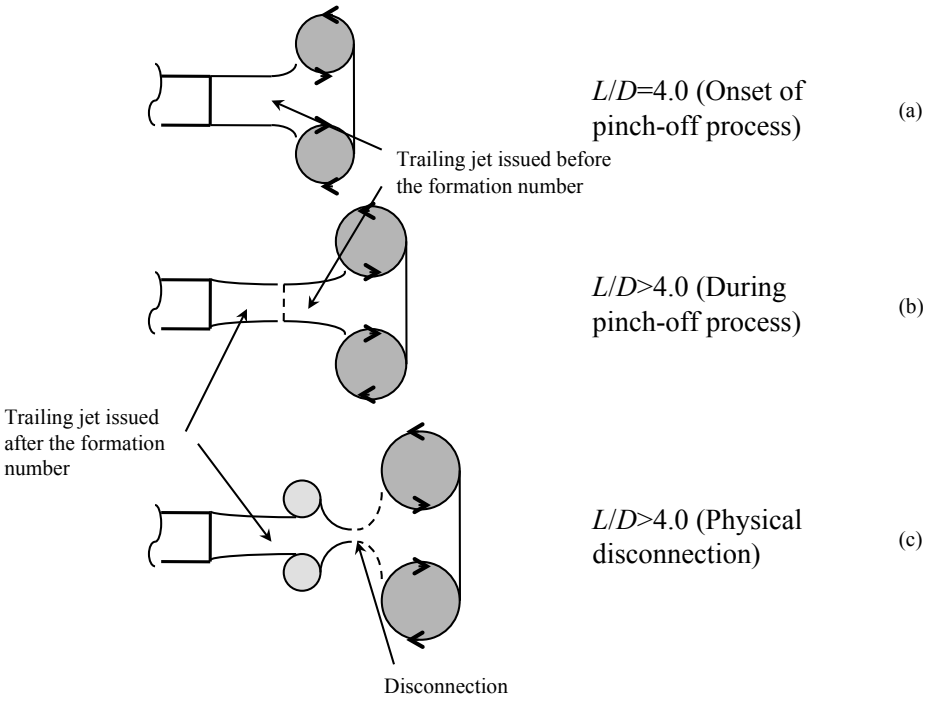

Figure 6.1: Illustration of pinch-off process in a starting jet with $L_{\max}/D > 4$. In real flow, the trailing jet is continuous. The dash line and disconnection is only used to distinguish fluids issued before and after the formation number.

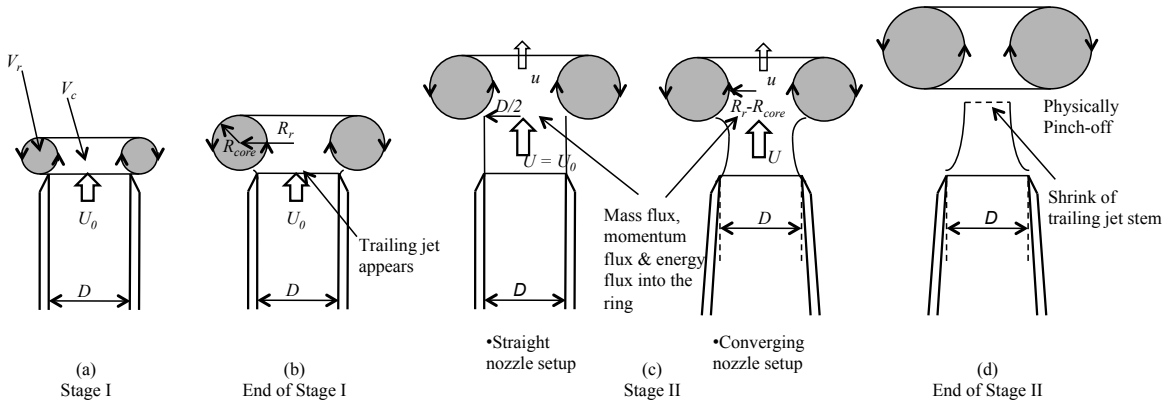

Figure 6.2: Sketch for the vortex ring evolution in the starting jet.

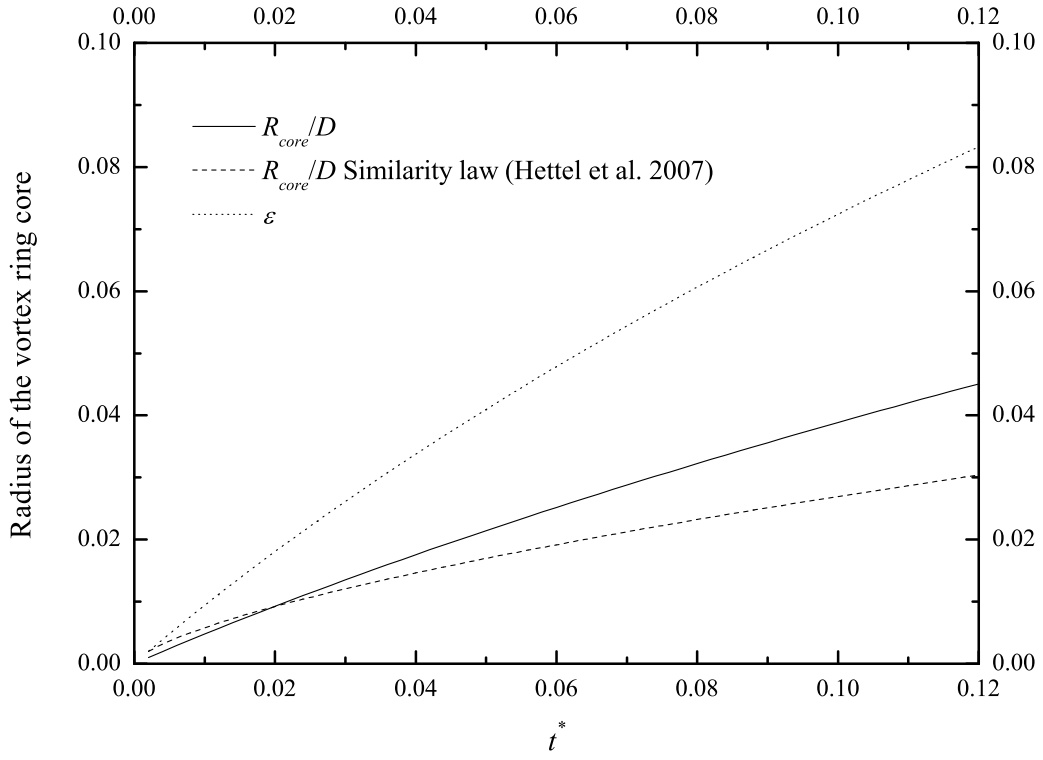

Figure 6.3: Growth of the radius of the leading vortex ring core during Stage I, and comparison with the similarity law (equation 6.3).

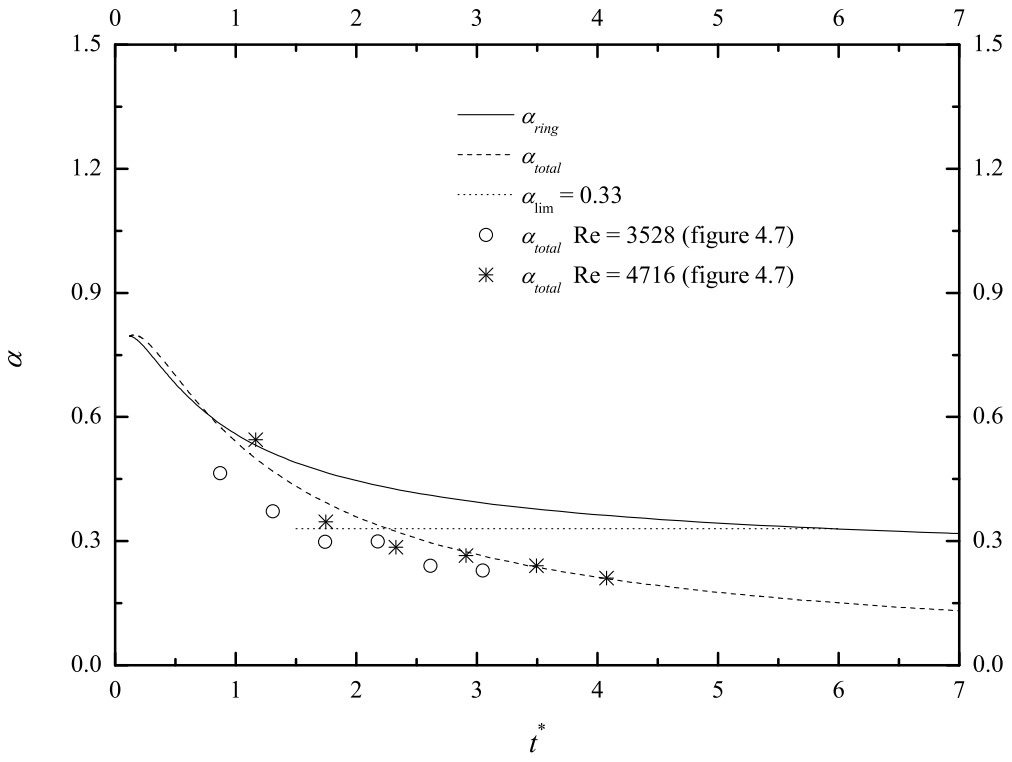

(a)

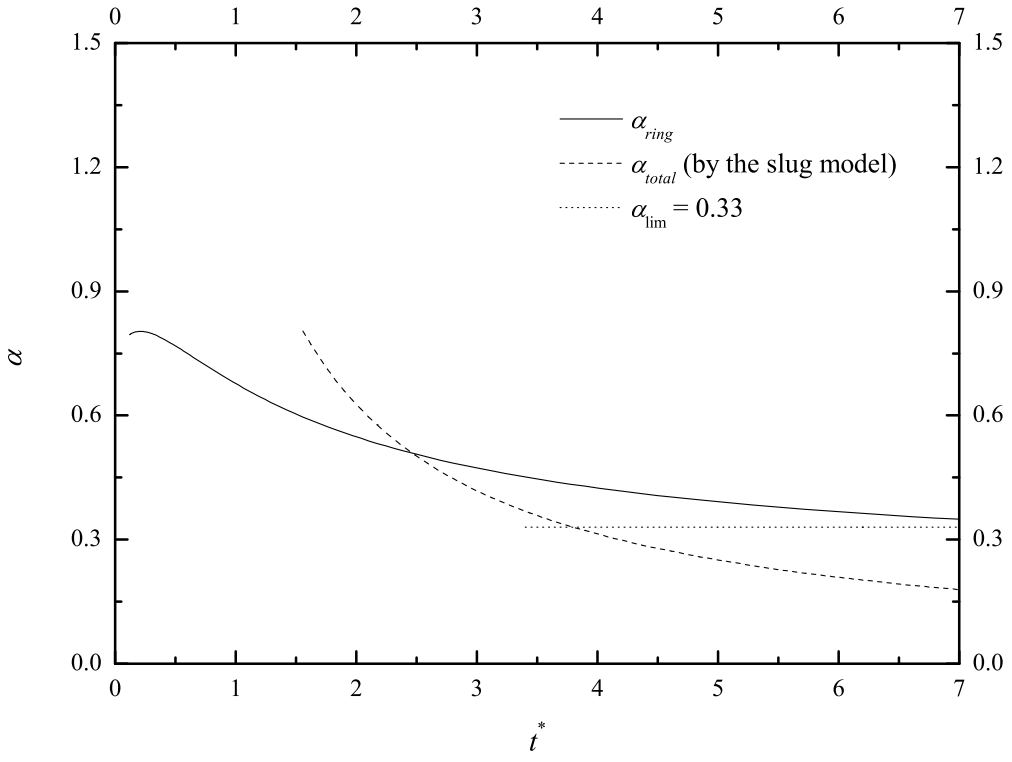

(b)

Figure 6.4: Variation of the dimensionless energy of the leading vortex ring and the total jet during Stage II for (a) the starting jet with converging nozzle and (b) the starting jet with straight nozzle

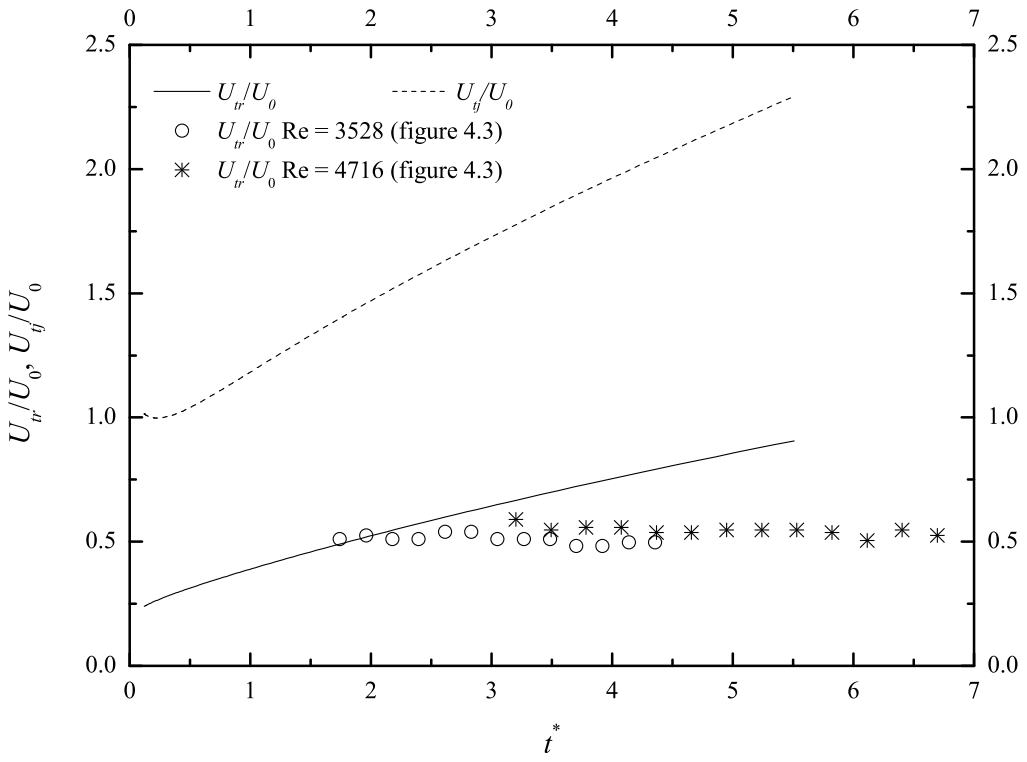

(a)

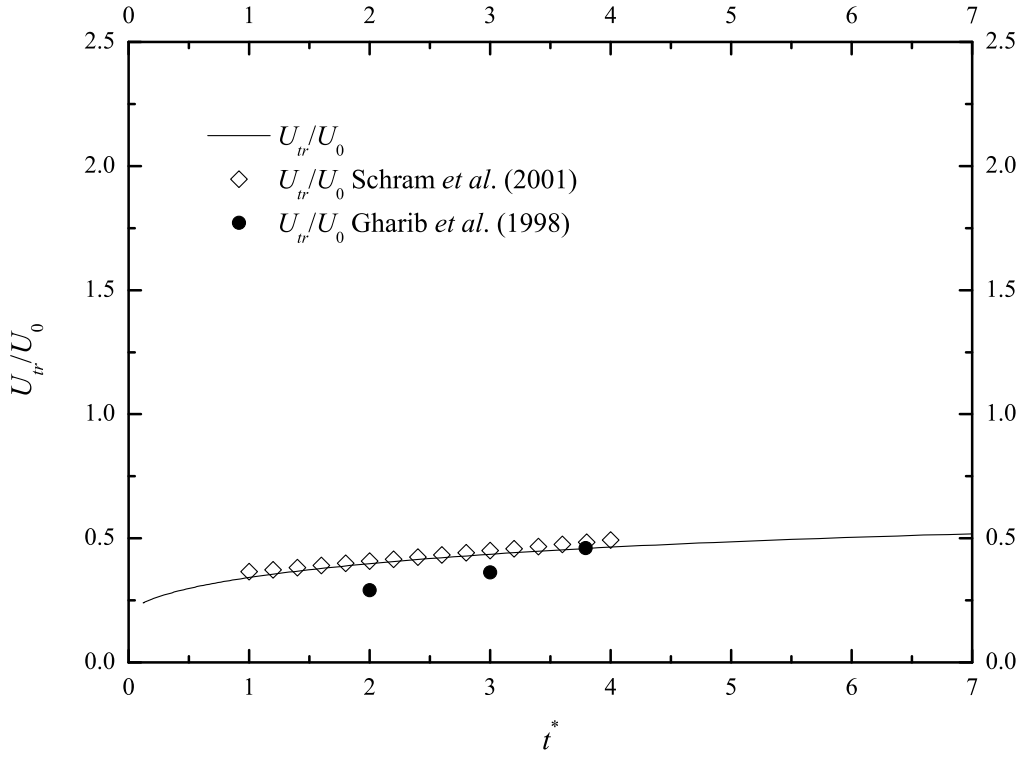

(b)

Figure 6.5: Evolution of the velocity of the trailing jet U_{tj} and the leading vortex ring U_{tr} for (a) the starting jet with converging nozzle and (b) the starting jet with straight nozzle, and the comparison with experimental results.

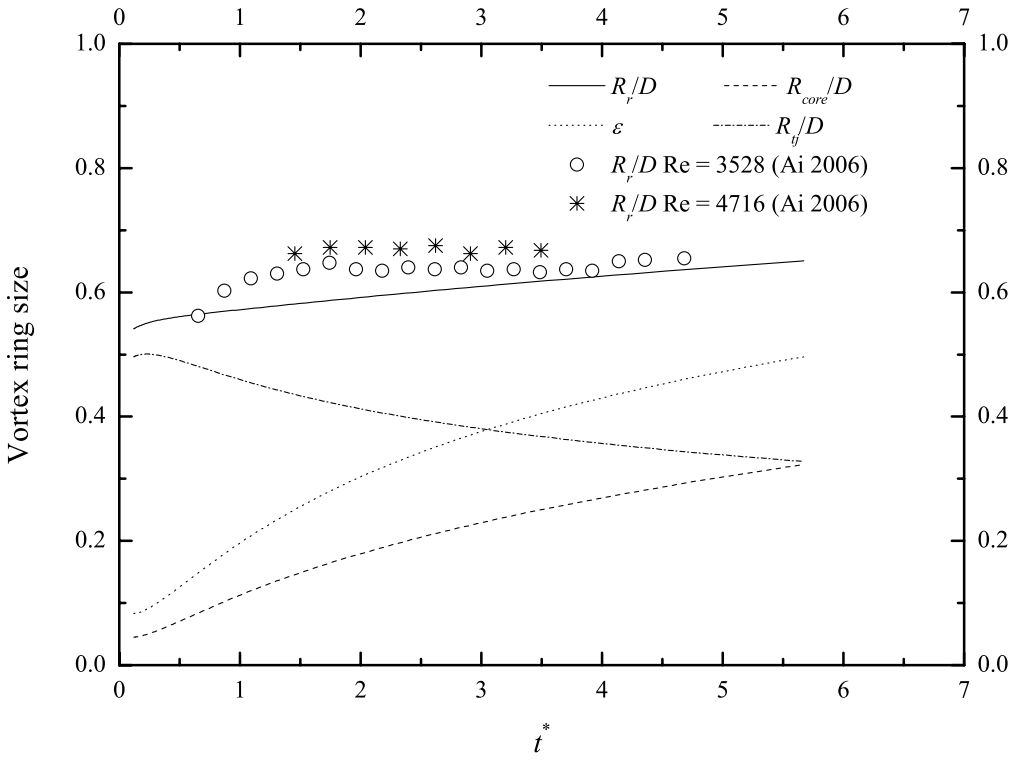

(a)

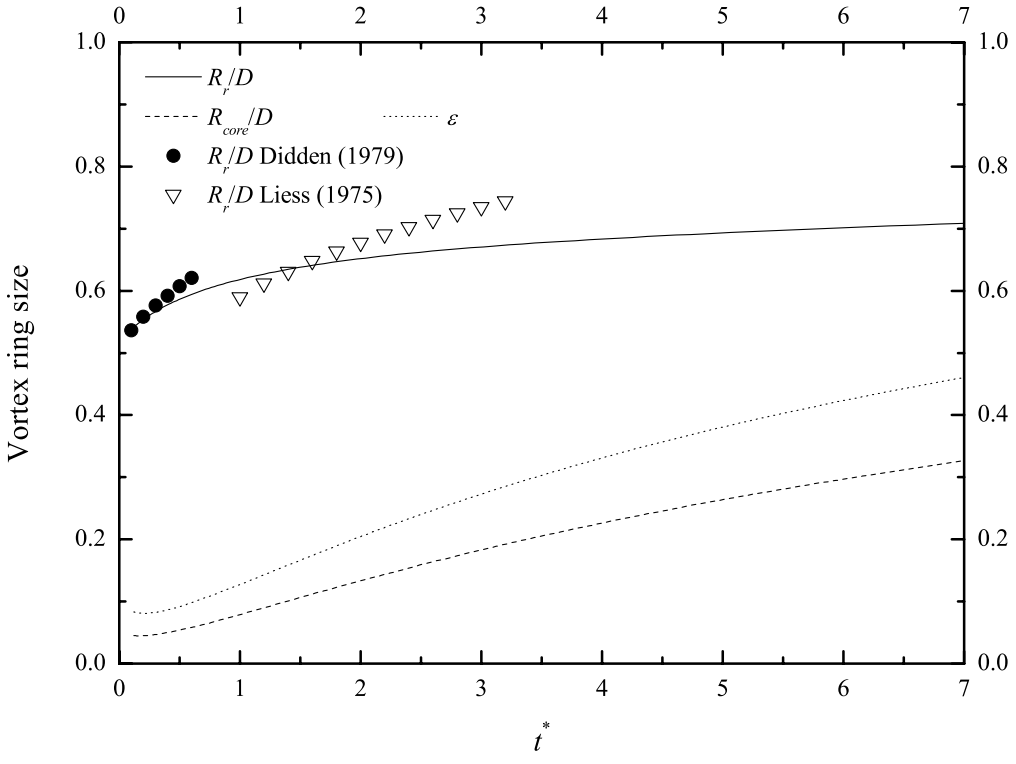

(b)

Figure 6.6: Evolution of radius of the leading vortex ring R_r, of the ring core R_{core} and the value of dimensionless mean core radius ϵ for (a) the starting jet with converging nozzle and (b) the starting jet with straight nozzle.

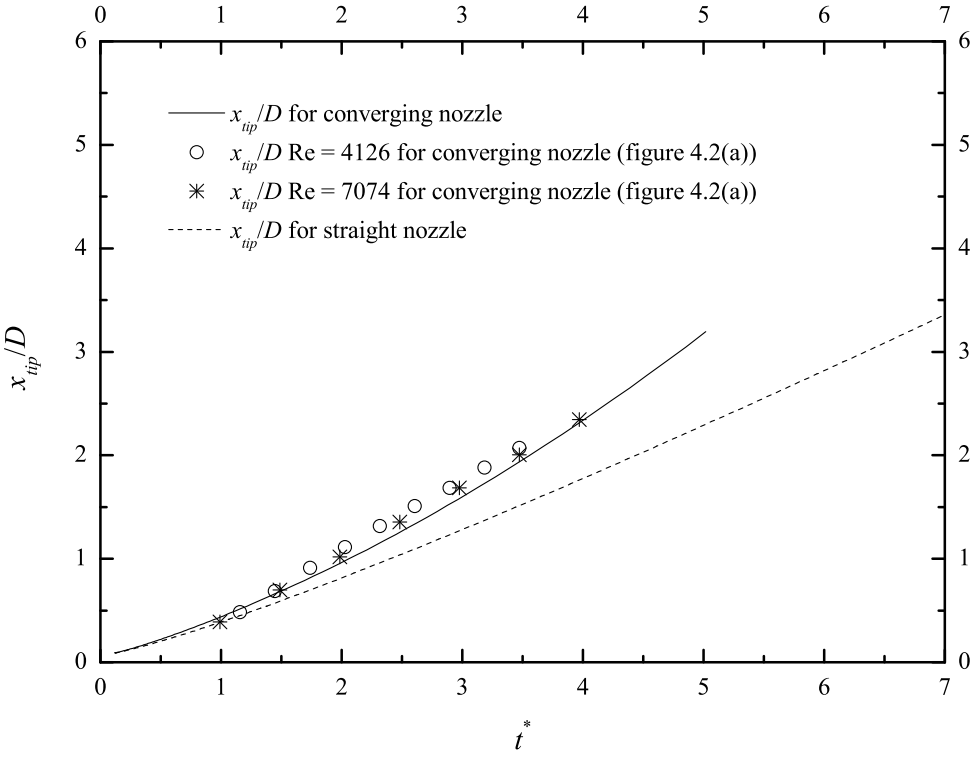

Figure 6.7: Normalized penetration of jet tip x_{tip}/D for both converging nozzle and straight nozzle configurations, compared with experimental results.

Chapter 7

Conclusions and Recommdation

7.1 Conclusions

The present experimental and theoretical study mainly focused on elucidating the dynamics of the pinch-off process in starting jets and determining the properties of the leading vortex ring. First, the previous experimental results of Ai (2006) on the gravity-driven starting jet were discussed to demonstrate the consistence of the leading vortex ring in various generation mechanisms to the Norbury-Fraenkel family of vortex rings. Secondly, the shear layer instability in the trailing jet was studied experimentally in order to examine its development as well as its effect on the pinch-off process. According to the experimental results, the physical mechanism of the pinch-off process was explained in terms of the effect of the trailing jet instability on the vorticity flux being fed into the leading vortex ring. Finally, based on the dynamic fluxes between the leading vortex ring and the tailing jet, an analytical model was proposed to predict the characteristics of the entire pinch-off process in a starting jet, as well as the evolution of the properties of the leading vortex ring. The major conclusions of the present study will be summarized as follows.

Before developing the model for the entire pinch-off process, the invariant

properties of the leading vortex ring, which were found in starting jets generated by piston-cylinder mechanism, were verified in the gravity-driven starting jet with converging nozzle. From the experimental results of Ai (2006), it was proven that the properties of the pinched-off vortex ring, i.e., the dimensionless energy α and circulation γ, were invariants for various generation mechanisms of the starting jet. The dimensionless energy α and circulation γ were found to be 0.33 and 1.85 ($\gamma' \approx 1.26$) respectively, consistent with the Norbury-Fraenkel family of vortex rings. The results suggest that the leading vortex ring in starting circular jet with gravity-driven mechanism could still be approximated by the theoretical Norbury-Fraenkel family of vortex rings. The properties of the Norbury-Fraenkel vortex rings then can be utilized to estimate the properties of the leading vortex ring in different vortex generation mechanisms.

In the investigation of the development of the trailing jet instability, starting jets with non-impulsive velocity program and different Reynolds numbers ($Re_D = 2600, 4100, 5600$) were produced by using the piston-cylinder mechanism. As shown by the evolution of vorticity contours, the trailing vortices start to develop in the trailing jet only after the formation number ($F = 4.2 \sim 4.6$ for the three tested cases) is achieved. Subsequently, the growth of trailing vortices leads to the rapid decrease in the vorticity flux being fed into the leading vortex ring. When the vorticity flux vanishes, the leading vortex ring separates completely from the trailing jet, indicating the end of the pinch-off process. Therefore, it was concluded that that the roll-up and further development of trailing vortices constrain the growth of leading vortex ring with larger circulation. The instability of trailing shear layer was found to be associated with the induced velocity field of the leading vortex ring. According to the hydrodynamic instability theories for axisymmetric shear flow, the thick shear layer, which results form the negative radial velocity gradient $\partial v/\partial r$ induced by the leading vortex ring, is less unstable than the thin one without external influence. In ad-

dition, the interaction between the leading vortex ring and the trailing vortices could lead to the vortex merging process between them. In cases with higher Reynolds numbers ($Re_D = 4100, 5600$), the merging of the leading vortex ring and the first trailing vortex was observed during the pinch-off process, which serves to prompt the completion of the separation of the leading vortex ring from the trailing jet.

By applying dimensional analysis, A dimensionless parameter 'A', defined as $\Gamma_{ring}/(x_{core}\Delta U)$, has been proposed to characterize the stabilizing effect of the leading vortex ring on the instability shear layer. Experimental results from the three cases revealed that 'A' would decrease as formation time progresses and a critical value $A_c = 1.1 \pm 0.1$ indicates the initial development of the trailing vortices and determines the onset of pinch-off process. Based on the dynamics of the pinch-off process, it is suggested that the critical value of the parameter A could be regarded as a theoretical criterion for determining the onset of the pinch-off process, i.e., the formation number. In addition, the instability criterion for the the formation number was used to propose a more general and fundamental explanation for the pinch-off process of the leading vortex ring in a variety of generation conditions. According to this explanation, the pinch-off process essentially results from the drop in vorticity flux being fed into the leading vortex ring. The shear layer instability developing in the trailing jet is a significant factor responsible for the drop in vorticity flux in many generation mechanisms of the starting jet. By applying this pinch-off mechanism to the starting jets with uniform background flows or with temporally varying exit diameter, an appropriate explanation can be provided for the observed variation of the formation number and properties of the leading vortex ring.

Finally, a model for predicting the details of the dynamics of the leading vortex ring in terms of the dynamic properties (circulation, impulse and kinetic energy) from the trailing jet during the pinch-off process was proposed. In the

model, a two-stage process has been identified before the complete separation of the leading vortex ring from its trailing jet. The first stage involves the growth of the leading vortex ring by absorbing all the ejected fluid from the nozzle until certain optimum size is achieved. This stage is identified as a very short period after the jet ejection ($t^* < 0.12$). The second stage is characterized by the appreciable translational velocity of the leading vortex ring followed by a trailing jet. During Stage II, the leading vortex ring is approximated as a member of the Norbury-Fraenkel family of vortex rings with growing characteristic core radius ϵ such that dimensionless energy α, as well as its translational velocity and penetration depth can be estimated. The pinch-off process is signified by two time scales, i.e. the formation number F, which indicates the onset of the pinch-off process, and the separation time, which corresponds to the time when the leading vortex ring becomes physically separated from the trailing jet and is therefore referred to as the end of pinch-off process. The prediction of the formation number and the characteristics of the vortex ring are found to be in good agreement with previous experimental results on the starting jets. However, it is noted that the effect of the trailing jet instability is not taken into account in the present model due to the difficulty in obtaining quantitative results about the nonlinear dynamics of the shear layer.

7.2 Recommendations for further work

Since the important role of the trailing jet instability in the pinch-off process of the leading vortex ring has been demonstrated experimentally in the present study, it is worthwhile to pursue a detailed investigation of the development of the shear layer instability in order to obtain quantitative results about the parameter A, as well as the drop in vorticity flux due to the growth of the trailing vortices. The instability of the axisymmetric shear layer in the starting

jets, which is characterized by the specific velocity profile (such as the hyperbolic tangent function) and the thickness δ, could be analyzed by using the linearized stability theory. Due to the nature of the parallel flows, the convective instability would first be developed in the shear layer under certain conditions of the shear layer thickness δ and the Reynolds number Re. As to the parameter 'A', we remain open to the possibility that other variables of the flow conditions may also be involved in the dimensional analysis of the instability initiation when a different vortex shedding configurations is considered, such as the wake of a circular cylinder.

Although the dimensional analysis is useful to provide a dimensionless parameter characterizing the induced radical velocity near the nozzle exit, the functional relation between the magnitude of the induce velocity and the properties of the leading vortex ring will be needed to derive for a quantitative description of the influence of the leading vortex ring on the trailing jet. Moreover, by modelling the behavior of the trailing shear layer under the influence of external velocity field, the relation between the induced radial velocity v_i and the thickness of the shear layer δ should also be quantified. In combination with the results of instability analysis, the critical value of the dimensionless parameter A_c can be derived analytically. The theoretical result of A_c might offer a physical implication of the parameter A about the instability development in the trailing jet.

Finally, the prediction of the present model in terms of the dynamical fluxes between the leading vortex ring and the trailing jet could be substantially improved if the drop in these fluxes can be derived as a function of the formation time t^* during the pinch-off process. This can be obtained from either the theoretical study on the nonlinear development of the trailing vortices, or the experimental study of trailing jet dynamics with higher temporal resolution.

Author's Publications

- Yu, S. C. M., Ai, J. J., Gao, L. & Law, A. W. K. 2008 Vortex Formation Process of a Starting Square Jet. AIAA journal **46**, 223–231
- Gao, L., Yu, S. C. M., Ai, J. J. & Law, A. W. K. 2008 Circulation and energy of the leading vortex ring in a gravity-driven starting jet. Phys. Fluids **20**, 093604
- Gao, L. & Yu, S. C. M. 2010 A model for the pinch-off process of the leading vortex ring in a starting jet. J. Fluid Mech. **656**, 205–222

Bibliography

Afanasyev, Y. (2006), "Formation of vortex dipoles", Physics of fluids, Vol. 18, p. 037103.

Ai, J. J. (2006), "On starting square jets and forced plumes", Ph.D. thesis, Nanyang Technological University.

Allen, J. and Naitoh, T. (2005), "Experimental study of the production of vortex rings using a variable diameter orifice", Physics of Fluids, Vol. 17, p. 061701.

Auerbach, D. (1987), "Experiments on the trajectory and circulation of the starting vortex", Journal of Fluid Mechanics, Vol. 183, pp. 185–198.

Batchelor, G. and Gill, A. (1962), "Analysis of the stability of axisymmetric jets", Journal of Fluid Mechanics, Vol. 14, No. 04, pp. 529–551.

Benjamin, T. (1976), "The alliance of practical and analytical insights into the nonlinear problems of fluid mechanics", Applications of methods of functional analysis to problems in mechanics, Vol. 503, pp. 8–29.

Cossali, G., Coghe, A. and Araneo, L. (2001), "Near-field entrainment in an impulsively started turbulent gas jet", AIAA journal, Vol. 39, No. 6, pp. 1113–1122.

Dabiri, J. (2009), "Optimal vortex formation as a unifying principle in biological propulsion", Annu. Rev. Fluid Mech., Vol. 41, pp. 17–33.

Dabiri, J. and Gharib, M. (2004), "Delay of vortex ring pinchoff by an imposed bulk counterflow", Physics of Fluids, Vol. 16, p. L28.

Dabiri, J. and Gharib, M. (2005), "Starting flow through nozzles with temporally variable exit diameter", Journal of Fluid Mechanics, Vol. 538, pp. 111–136.

Didden, N. (1979), "On the formation of vortex rings: rolling-up and production of circulation", Zeitschrift f"ur Angewandte Mathematik und Physik (ZAMP), Vol. 30, No. 1, pp. 101–116.

Fraenkel, L. (1972), "Examples of steady vortex rings of small cross-section in an ideal fluid", Journal of Fluid Mechanics, Vol. 51, No. 01, pp. 119–135.

Gharib, M., Rambod, E., Kheradvar, A., Sahn, D. and Dabiri, J. (2006), "Optimal vortex formation as an index of cardiac health", National Acad Sciences.

Gharib, M., Rambod, E. and Shariff, K. (1998), "A universal time scale for vortex ring formation", Journal of Fluid Mechanics, Vol. 360, pp. 121–140.

Glezer, A. (1988), "The formation of vortex rings", Physics of Fluids, Vol. 31, p. 3532.

Glezer, A. and Coles, D. (1990), "An experimental study of a turbulent vortex ring", Journal of Fluid Mechanics, Vol. 211, pp. 243–283.

Heeg, R. and Riley, N. (1997), "Simulations of the formation of an axisymmetric vortex ring", Journal of Fluid Mechanics, Vol. 339, pp. 199–211.

Hettel, M., Wetzel, F., Habisreuther, P. and Bockhorn, H. (2007), "Numerical verification of the similarity laws for the formation of laminar vortex rings", Journal of Fluid Mechanics, Vol. 590, pp. 35–60.

Huang, H., Dabiri, D. and Gharib, M. (1997), "On errors of digital particle image velocimetry", Measurement Science and Technology, Vol. 8, p. 1427.

James, S. and Madnia, C. (1996), "Direct numerical simulation of a laminar vortex ring", Physics of Fluids, Vol. 8, p. 2400.

Johari, H., Zhang, Q., Rose, M. and Bourque, S. (1997), "Impulsively started turbulent jets", AIAA journal, Vol. 35, No. 4, pp. 657–662.

Kambe, T. (1969), "The stability of an axisymmetric jet with parabolic profile", J. Phys. Soc. Japan, Vol. 26, pp. 566–575.

Kaplanski, F. and Rudi, Y. (2005), "A model for the formation of optimal vortex rings taking into account viscosity", Physics of Fluids, Vol. 17, p. 087101.

Keane, R. and Adrian, R. (1992), "Theory of cross-correlation analysis of PIV images", Applied scientific research, Vol. 49, No. 3, pp. 191–215.

Kelvin, L. (1880), "Vortex statics", Phil. Mag., Vol. 10, pp. 97–109.

Kouros, H., Medina, R. and Johari, H. (1993), "Spreading rate of an unsteady turbulent jet", AIAA journal, Vol. 31, pp. 1524–1526.

Krueger, P. (2005), "An over-pressure correction to the slug model for vortex ring circulation", Journal of Fluid Mechanics, Vol. 545, pp. 427–443.

Krueger, P., Dabiri, J. and Gharib, M. (2003), "Vortex ring pinchoff in the presence of simultaneously initiated uniform background co-flow", Physics of fluids, Vol. 15, p. L49.

Krueger, P., Dabiri, J. and Gharib, M. (2006), "The formation number of vortex rings formed in uniform background co-flow", Journal of Fluid Mechanics, Vol. 556, pp. 147–166.

Krueger, P. and Gharib, M. (2003), "The significance of vortex ring formation to the impulse and thrust of a starting jet", Physics of fluids, Vol. 15, p. 1271.

Lahbabi, F., Boree, J., Nuglisch, H. and Charnay, G. (1993), "Analysis of starting and steady turbulent jets by image processing techniques", in Experimental and numerical flow visualization, 1993: presented at the 1993 ASME Winter Annual Meeting, New Orleans, Louisiana, November 28-December 3, 1993, American Society of Mechanical Engineers, p. 315.

Lessen, M. and Singh, P. (1973), "The stability of axisymmetric free shear layers", Journal of Fluid Mechanics, Vol. 60, No. 03, pp. 433–457.

Liess, C. (1978), "Experimentelle Untersuchung des Lebenslaufes von Ringwirbeln", Tech. rep., Max-Planck-Institut f. Strornungsforschung Bericht.

Lim, T. (1997), "A note on the leapfrogging between two coaxial vortex rings at low Reynolds numbers", Physics of Fluids, Vol. 9, p. 239.

Lim, T. and Nickels, T. (1995), Vortex rings, Kluwer.

Linden, P. and Turner, J. (2001), "The formation of optimalvortex rings, and the efficiency of propulsion devices", Journal of Fluid Mechanics, Vol. 427, pp. 61–72.

Marugan-Cruz, C., Vera, M., Martinez-Bazan, C. and Pawlak, G. (2008), "Influence of Trailing Jet Instability on the Dynamics of Starting Jets", Progress in Industrial Mathematics at ECMI 2006, pp. 758–762.

Maxworthy, T. (1972), "The structure and stability of vortex rings", Journal of Fluid Mechanics, Vol. 51, No. 01, pp. 15–32.

Maxworthy, T. (1977), "Some experimental studies of vortex rings", Journal of Fluid Mechanics, Vol. 81, No. 03, pp. 465–495.

McKenna, S. and McGillis, W. (2002), "Performance of digital image velocimetry processing techniques", Experiments in fluids, Vol. 32, No. 1, pp. 106–115.

Michalke, A. and Hermann, G. (1982), "On the inviscid instability of a circular jet with external flow", Journal of Fluid Mechanics, Vol. 114, pp. 343–359.

Mohseni, K. (2001), "Statistical equilibrium theory for axisymmetric flows: Kelvins variational principle and an explanation for the vortex ring pinch-off process", Physics of Fluids, Vol. 13, p. 1924.

Mohseni, K. and Gharib, M. (1998), "A model for universal time scale of vortex ring formation", Physics of Fluids, Vol. 10, p. 2436.

Mohseni, K., Ran, H. and Colonius, T. (2001), "Numerical experiments on vortex ring formation", Journal of Fluid Mechanics, Vol. 430, pp. 267–282.

Nitsche, M. (1996), "Scaling properties of vortex ring formation at a circular tube opening", Physics of Fluids, Vol. 8, No. 7, pp. 1848–1855.

Norbury, J. (1973), "A family of steady vortex rings", Journal of Fluid Mechanics, Vol. 57, No. 03, pp. 417–431.

O'Farrell, C. and Dabiri, J. (2010), "A Lagrangian approach to identifying vortex pinch-off", Chaos: An Interdisciplinary Journal of Nonlinear Science, Vol. 20, p. 017513.

Olcay, A. and Krueger, P. (2008), "Measurement of ambient fluid entrainment during laminar vortex ring formation", Experiments in Fluids, Vol. 44, No. 2, pp. 235–247.

Pawlak, G., Marugan Cruz, C., Martínez Bazán, C. and García Hrdy, P. (2007), "Experimental characterization of starting jet dynamics", Fluid Dynamics Research, Vol. 39, No. 11-12, pp. 711–730.

Prasad, A., Adrian, R., Landreth, C. and Offutt, P. (1992), "Effect of resolution on the speed and accuracy of particle image velocimetry interrogation", Experiments in Fluids, Vol. 13, No. 2, pp. 105–116.

Pullin, D. (1979), "Vortex ring formation at tube and orifice openings", Physics of Fluids, Vol. 22, p. 401.

Raffel, M., Willert, C. and Kompenhans, J. (1998), Particle Image Velocimetry- A Practical Guide, Springer-Verlag, Berlin.

Raffel, M., Willert, C. and Wereley, S. (2007), Particle image velocimetry: a practical guide, Springer Verlag.

Rayleigh, L. (1880), "On the stability, or instability, of certain fluid motions", Proceedings of the London Mathematical Society, Vol. 11, p. 5770.

Rayleigh, L. (1892), "On the question of the stability of the flow of fluids", Phil. Mag, Vol. 34, No. 5, pp. 59–70.

Riley, N. and Stevens, D. (1993), "A note on leapfrogging vortex rings", Fluid dynamics research, Vol. 11, No. 5, pp. 235–244.

Rosenfeld, M., Rambod, E. and Gharib, M. (1998), "Circulation and formation number of laminar vortex rings", Journal of Fluid Mechanics, Vol. 376, pp. 297–318.

Saffman, P. (1975), "On the formation of vortex rings", Studies in Applied Mathematics, Vol. 54, pp. 261–268.

Saffman, P. (1978), "The number of waves on unstable vortex rings", Journal of Fluid Mechanics, Vol. 84, No. 04, pp. 625–639.

Saffman, P. (1995), Vortex dynamics, Cambridge Univ Pr.

Sau, R. and Mahesh, K. (2007), "Passive scalar mixing in vortex rings", Journal of Fluid Mechanics, Vol. 582, pp. 449–461.

Schram, C. and Riethmuller, M. (2001), "Vortex ring evolution in an impulsively started jet using digital particle image velocimetry and continuous wavelet analysis", Measurement Science and Technology, Vol. 12, p. 1413.

Shariff, K. and Leonard, A. (1992), "Vortex rings", Annual Review of Fluid Mechanics, Vol. 24, No. 1, pp. 235–279.

Shusser, M. and Gharib, M. (2000a), "Energy and velocity of a forming vortex ring", Physics of Fluids, Vol. 12, p. 618.

Shusser, M. and Gharib, M. (2000b), "A model for vortex ring formation in a starting buoyant plume", Journal of Fluid Mechanics, Vol. 416, pp. 173–185.

Shusser, M., Gharib, M., Rosenfeld, M. and Mohseni, K. (2002), "On the effect of pipe boundary layer growth on the formation of a laminar vortex ring generated by a piston/cylinder arrangement", Theoretical and Computational Fluid Dynamics, Vol. 15, No. 5, pp. 303–316.

Shusser, M., Rosenfeld, M., Dabiri, J. and Gharib, M. (2006), "Effect of time-dependent piston velocity program on vortex ring formation in a piston/cylinder arrangement", Physics of Fluids, Vol. 18, p. 033601.

Tollmien, W. (1935), "Ein allgemeines Kriterium der Instabilitat laminarer Geschwindigkeitsverteilungen, Nachr. Ges. Wiss. Math", Phys. Klasse, Vol. 50, pp. 79–114.

Turner, J. (1962), "The starting plumein neutral surroundings", Journal of Fluid Mechanics, Vol. 13, No. 03, pp. 356–368.

Wang, R., Law, A., Adams, E. and Fringer, O. (2009), "Buoyant formation number of a starting buoyant jet", Physics of Fluids, Vol. 21, p. 125104.

Weigand, A. and Gharib, M. (1997), "On the evolution of laminar vortex rings", Experiments in fluids, Vol. 22, No. 6, pp. 447–457.

Willert, C. and Gharib, M. (1991), "Digital particle image velocimetry", Experiments in fluids, Vol. 10, No. 4, pp. 181–193.

Yu, S., Law, A. and Ai, J. (2007), "Vortex formation process in gravity-driven starting jets", Experiments in Fluids, Vol. 42, No. 5, pp. 783–797.

Zhao, W., Frankel, S. and Mongeau, L. (2000), "Effects of trailing jet instability on vortex ring formation", Physics of Fluids, Vol. 12, p. 589.